GRID INTEGRATION OF COMBINED SOLAR-WIND-BATTERY ENERGY SYSTEMS WITH ECONOMIC ANALYSIS

BY

BILAL METIN ALTINOZ

B.S. IN ELECTRICAL & ELECTRONICS ENGINEERING
ISTANBUL KEMERBURGAZ UNIVERSITY (2016)

SUBMITTED IN PARTIAL FULLFILMENT OF THE REQUIREMENTS FOR
THE DEGREE OF MASTER OF SCIENCE IN
ELECTRICAL ENGINEERING

DEPARTMENT OF ELECTRICAL AND COMPUTER ENGINEERING
UNIVERSITY OF MASSACHUSETTS LOWELL
2017

DECLARATION OF ORIGINALITY

*I declare that this thesis entitled "***GRID INTEGRATION OF COMBINED SOLAR-WIND-BATTERY ENERGY SYSTEMS WITH ECONOMIC ANALYSIS***" is my own work and to the best of my knowledge except as cited in the references. It contains no materials previously published or written by another person, nor material which to a substantial extent has been accepted for the award of any degree or diploma at UMass Lowell or any other education institute, except where due acknowledgment, is made in the thesis. Any contribution made to the research by others, with whom I have worked at UMass Lowell or elsewhere, is explicitly acknowledged in the thesis.*

Signature: Bilal Metin Altınöz

Name: Bilal Metin ALTINOZ

Date: December 6, 2017

GRID INTEGRATION OF COMBINED SOLAR-WIND-BATTERY ENERGY SYSTEMS WITH ECONOMIC ANALYSIS

BY

BILAL METIN ALTINOZ

B.S. IN ELECTRICAL & ELECTRONICS ENGINEERING
ISTANBUL KEMERBURGAZ UNIVERSITY (2016)

SUBMITTED IN PARTIAL FULLFILMENT OF THE REQUIREMENTS FOR THE DEGREE OF MASTER OF SCIENCE IN ELECTRICAL ENGINEERING

DEPARTMENT OF ELECTRICAL AND COMPUTER ENGINEERING
UNIVERSITY OF MASSACHUSETTS LOWELL
2017

Signature of Author: _____ Date: 12 / 06 / 2017

Bilal Metin Altinoz

Signature of Thesis Supervisor: _____

Prof. Mufeed Mahd

Signatures of Other Thesis Committee Members:

Committee Member Signature: _____

Prof. Frank Tredeau

Committee Member Signature: _____

Prof. Siavash Pakdelian

GRID INTEGRATION OF COMBINED SOLAR-WIND-BATTERY ENERGY SYSTEMS WITH ECONOMIC ANALYSIS

BY

BILAL METIN ALTINOZ

ABSTRACT OF A THESIS SUBMITTED TO THE FACULTY OF THE DEPARTMENT OF ELECTRICAL AND COMPUTER ENGINEERING

IN PARTIAL FULLFILMENT OF THE REQUIREMENTS FOR THE DEGREE OF MASTER OF SCIENCE

UNIVERSITY OF MASSACHUSETTS LOWELL

2017

Thesis Supervisor: Mufeed Mah'd, Ph.D.
Professor, Department of Electrical and Computer Engineering

ABSTRACT

The green energy is an indispensable factor in our planet, since there are environmental pollution and global warming which damage the human life. The most significant way is either adaptation or implementation of the renewable energy sources practically in order to decrease the harmful effects of the fossil fuels in a vast scale. Nowadays, the initial investment cost of the renewable resources is so high, however, they have many advantages such as free energy, clean environment, and high class human life in a long time.

This paper introduces the combined energy systems which include solar, wind and battery with their grid integration. A DC and AC loads are implemented in the designed system. The solar system, wind system, battery management system and converters are modeled in Matlab/Simulink individually. After that they become integrated with the grid and a residential load. The wind and solar systems are supported by MPPT (Maximum Power Point Tracking) controllers which are Perturb & Observe and Fuzzy Logic. They are compared with each other in terms of their performance and efficiency. Also, these algorithms are analyzed at the various weather conditions. The battery system control method is based on the Fuzzy Logic controller to increase system efficiency. On the other hand, the specific market products and a residence location (Istanbul, Turkey) are selected for the proposed system design by using SAM software. The weather data of that location and specification of the equipment which are wind, solar, battery, converter, grid and load are transferred into HOMER software. Accordingly, a system schematic diagram is designed and the economic analysis is actualized with the system optimization in HOMER.

ACKNOWLEDGMENTS

I would like to offer my thanks of gratitude to Professor Mufeed Mah'd. He encouraged me during, not only this research, but also my professional growth. He supported me throughout my course work and challenging research period. I cannot perform this research study without his outstanding guidance and interest, which I will keep in my heart forever.

I would like to state my appreciation to Professor Frank Tredeau and Professor Siavash Pakdelian for allocating their time in spite of their busy schedule, to be members of my thesis committee.

Finally, I would like to express my gratefulness and special thanks to all my family and Elif Caner for putting their unabated supports behind me during the completion of this thesis.

TABLE OF CONTENTS

LIST OF TABLES

LIST OF FIGURES

LIST OF ABBREVIATIONS

AC	Alternative Current
Ah	Ampere hour
Btu	British thermal unit
CPP	Clean Power Plan
COE	levelized cost of energy
DC	Direct Current
FLC	Fuzzy Logic Controller
GHI	Global Horizontal Irradiation
HOMER	Hybrid optimization model of renewable energy
I-V	Current-Voltage
IGBT	insulated-gate bipolar transistor
MOSFET	metal–oxide–semiconductor field-effect transistor
MPP	Maximum Power Point
MPPT	Maximum Power Point Tracking
NPC	Total net present cost
OECD	Organization for Economic Co-operation and Development
P&O	Perturb and Observe
PLL	Phase Locked Loop
PMSG	Permanent Magnet Synchronous Generator
PMSM	Permanent Magnet Synchronous Machine

PV	Photovoltaic
P-V	Power-Voltage
PWM	Pulse Width Modulation
SAM	System Advisor Model
SOC	State-Of-Charge
TEIAS	Turkish Electricity Transmission Corporation
VSC	Voltage Source Converter
WECS	Wind Energy Conversion System

CHAPTER 1

INTRODUCTION

1.1 Problem Statement

The climate has been affected by environmental pollution and global warming excessively in our planet. The detrimental factors are going up day by day because of human needs. While the world population is growing, the countries development is an inevitable situation in terms of economic, social and industrial aspects. Accordingly, the most powerful factor that damages to our world is the process of producing and consuming energy. There are several problems that should be solved by humans about the energy. First, the major energy resources that are the fossil fuels are depleted swiftly. These fuels have major harmful effects environmentally as well. At the present time, the realization of this problem is at a high level among the people. Therefore, the alternative energy sources are implemented by all countries. Renewable energy is becoming a prioritized option nowadays instead of the oil, gas and coal. In this way, the clean energy is provided all around the world. Figure 1.1 shows the world net electricity generation by energy source between 2012 and 2040. Because of the high energy demand and prices, countries are deciding to change their energy policies and investments. According to REN21's 2017 annual report, China, United States, United Kingdom, Japan, Germany, Brazil, Canada and India have increased their annual investment, net capacity additions and production rate [3]. Table 1.1 demonstrates the energy consumption by the countries between 2012 and 2040. It proves that their long-term investments will be meaningful to obtain the required energy as clean. The world energy

demand is going to grow from 549 quadrillion British thermal units (Btu) in 2012 to 629 quadrillion Btu in 2020 and then it reaches to 815 quadrillion Btu in 2040. Therefore, the implementation of the renewable energy sources plays a significant role to fulfil the Clean Power Plan (CPP) regulations all around the world. Renewable energy consumption is going up by an average 2.6%/year between 2012 and 2040. On the other hand, the consumption of the fossil fuels is envisioned to decrease, while the non-fossil fuels is growing [1, 2].

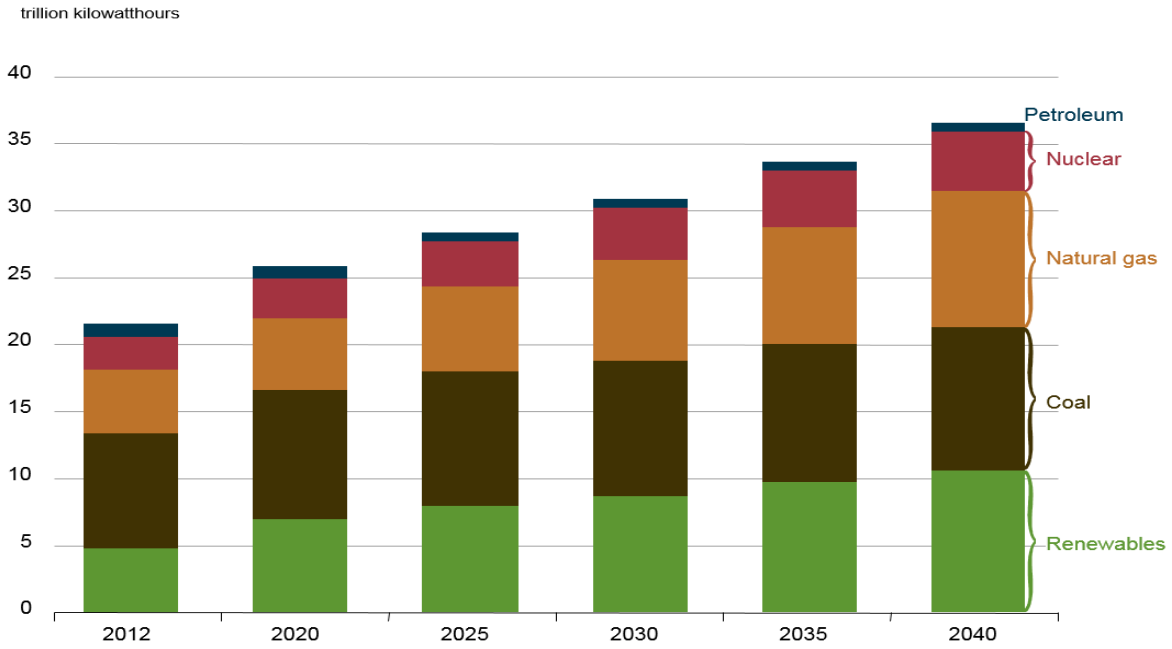

Figure 1.1 Electricity generation by energy sources in world 2012-40 [1]

The wind, solar, biogas, geothermal, hydro and nuclear energy sources represent the non-fossil fuels. The solar and wind energy are so valuable for our world since they provide the clean energy, low cost and safety. In order to use solar energy and wind energy, the radiation and wind speed have a key role in the individual power systems because, the weather condition has variability. It can affect the system's stability negatively, the reason being more efficient and stable power systems may be occurred by two or more renewable energy sources grouping with a battery system [4]. However, there are some inconveniences related to combined systems, since the wind and

solar energy have a low energy density. Also, the generated power by wind and solar does not fit the load requirements [5].

Therefore, the hybrid power systems which includes the solar, wind and battery were represented in this thesis. The system can be optimized efficiently by using the maximum power point tracking (MPPT) control methods. However, MPPT based renewables have high initial costs. Also, the state of charge (SOC) is controlled, thus, SOC of battery is regulated properly in the hybrid generation systems [6].

Table 1.1 Energy consumption based on country grouping, 2012-40 (quadrillion Btu) [2]

Region	2012	2020	2025	2030	2035	2040	Avg. Annual Percent Change
OECD	**238**	**254**	**261**	**267**	**274**	**282**	**0.6**
Americas	118	126	128	131	134	138	0.6
Europe	81	85	87	90	93	96	0.6
Asia	39	43	45	46	47	48	0.8
OECD with U.S. CPP	**238**	**252**	**258**	**265**	**272**	**280**	**0.6**
OECD Americans with U.S. CPP	118	124	125	128	132	136	0.5
Non-OECD	**311**	**375**	**413**	**451**	**491**	**533**	**1.9**
Europe/Eurasia	51	52	55	56	58	58	0.5
Asia	176	223	246	270	295	322	2.2
Middle East	32	41	45	51	57	62	2.4
Africa	22	26	30	34	38	44	2.6
Americas	31	33	37	40	43	47	1.5
Total World	**549**	**629**	**674**	**718**	**766**	**815**	**1.4**
Total World with CPP	**549**	**627**	**671**	**715**	**763**	**813**	**1.4**

1.2 Objectives

In this study, the main objective is to combine the renewables that are solar and wind as a hybrid power system with the grid. The variables of that renewables were used based on the specific market products to analyze and test the system. The steps are presented step by step below.

- Modeling the PV module by using mathematical expressions and Simulink to obtain the characteristic curves of temperature and irradiation.
- Modeling of wind power system by using mathematical expressions and wind turbine Simulink model to observe the characteristic curves such as torque, rotor speed, output power.
- The implementation of the different MPPT methods for the wind and PV array.
- To study the BOOST converter in terms of modeling and controllers.
- Building a battery system and bidirectional converter for this battery in order to design the hybrid system with the energy storage system.
- To study and design on the grid integration and its` controller part.
- To study on the market analysis and financial presentation of the proposed system.

1.3 Main Contributions

This thesis presents the solar-wind-battery energy system and their control mechanisms. Figure 1.2 demonstrates the energy generation system based on either AC or DC loads which are grid and residential by using the renewables.

There are three contributions in this thesis. The AC load and DC load were added separately in the system. The grid integration is introduced in the proposed design. In this way, the different kind of system loads can be implemented in that simulation.

Secondly, the power outputs and the system performance was analyzed owing to different kinds of the MPPT methods which are Perturb & Observe (PO) and Fuzzy Logic Controller (FLC). The output waveforms are tracked under the different weather conditions and different variables to observe the alteration of the system. In order to analyze which method is more productive and efficient, they implemented into the built system.

The designed system's elements are investigated in the market as well and the economic analysis is introduced in terms of the PV array, wind turbine, battery bank and converter. The weather data which belongs to Istanbul-Turkey is obtained by SAM software and HOMER software are used for the economic approach and design the proposed system according to that location data.

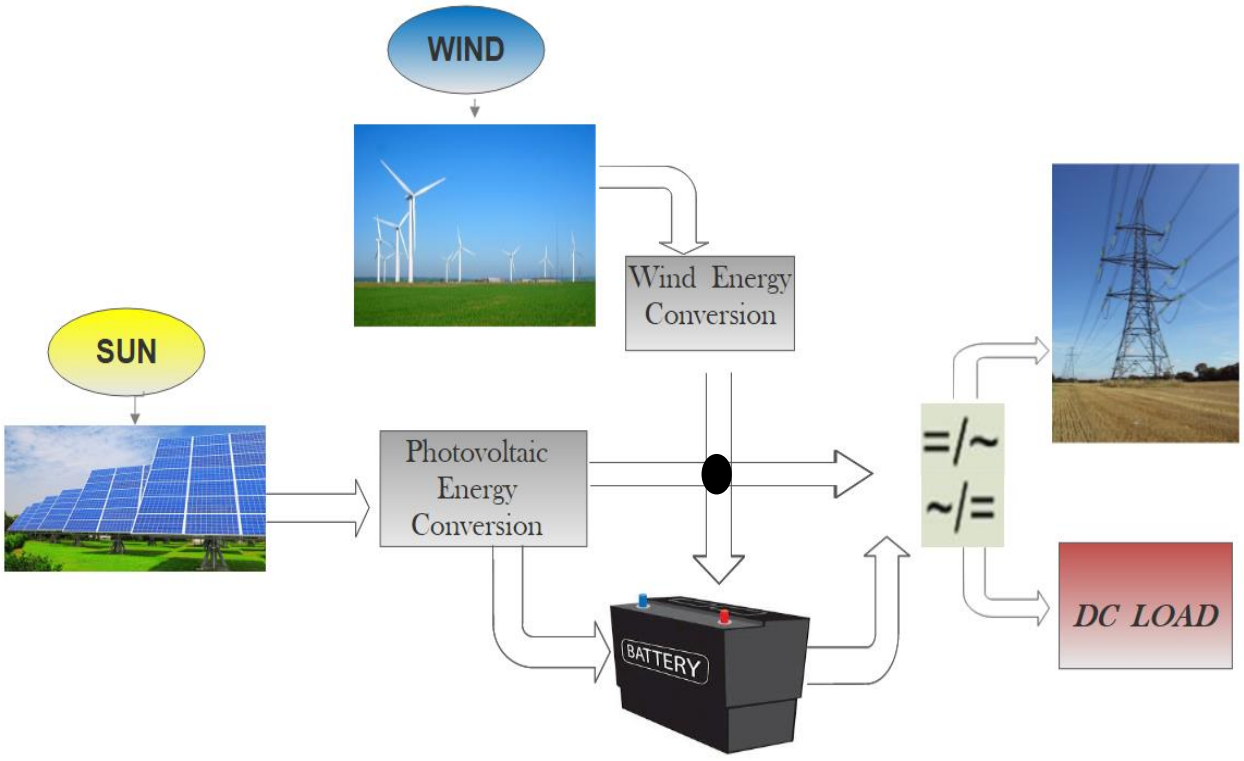

Figure 1.2 Proposed energy generation system with AC-DC microgrid

1.4 Structure of This Thesis

Chapter 1 introduces the problem statement about the renewable energy sources and hybrid power system that includes wind and solar. The objectives of this thesis are explained and the contributions are discussed. Lastly, the thesis outline is presented in this chapter.

Chapter 2 expresses the mathematical modeling of the combined power system that contains PV panel, wind turbine, converter, battery, bi-directional converter for the battery system, and permanent magnet synchronous machine (PMSM). The technical specifications are introduced by using SAM software.

Chapter 3 considers the Maximum power point tracking methods and their algorithms are explained with the flow charts. The Perturb observe (PO) method and Fuzzy Logic Controller method are compared, analyzed and discussed. Also, the Simulink design of all parts are introduced with their details. The other control mechanism and designs are explained in this chapter.

Chapter 4 demonstrates the simulation results. The comparisons, analysis and discussions on the results, are illustrated by this chapter. The MPPT outputs present in details under the different variables and weather conditions.

Chapter 5 approaches to this system in terms of the economic analysis. The market products and their economic sides are introduced depends on the proposed system.

Chapter 6 concludes the work as a summary. The outcomes and future works are expressed.

CHAPTER 2

MODELING OF PV-WIND-BATTERY HYBRID POWER SYSTEM

Chapter 2 explains the photovoltaic and wind energy conversion concepts and besides mathematical models of the hybrid power system that contains photovoltaic, wind, DC/DC, bi-directional converters, battery for the storage system and permanent magnet synchronous machine (PMSM), are introduced. The technical specifications are presented by using SAM software.

2.1 Photovoltaic Energy Conversion

Photovoltaic cells are produced according to increasing demand today. It is growing rapidly day by day, while the technological advancement is making real on the cells and other components. The important point is that development is providing the efficiency and low cost. The word of photovoltaic consists of two parts. “Photo” represents the light, and “Voltaic” represents the electricity, photovoltaic means obtaining electricity from sun-light [7]. A significant source of energy is solar energy for many years, due to the enormous amounts of energy. Solar energy is made easily available if it is connected by modern technology. Solar energy systems are used in places where it is difficult to set up electricity network but, there is a huge request for continuous electricity [7, 8].

PV cells are used to produce electricity and they are devices that turn into light energy directly into electrical energy. There are semiconductors (silicon alloys) in these cells. There is a connection that is provided by electrical contacts between the semiconductor material and the electrical load [8, 9]. Generally, sunlight shines on the photovoltaics and the surface of semiconductor material

is struck by photons. The electrons start to flow across the photovoltaic cell's surface like a current. There are bands which are over the photovoltaic cell to obtain that electrons. There are two connections, one of them is positive that is on the top and other one is negative that is at the bottom part of the photovoltaic cell [9].

There are two type junctions which are framed as n-type and p-type semiconductor materials. The n-type material has a high electron concentration and in spite of that p-type has a high hole which flow to n-type from the form of p-type. The power is delivered to load by photovoltaic cell. In this process, the electrons flows out of the n-side through the load and return to the p-side [9].

Producing solar energy is not complex. The rays or photons of the sun are connected. After that, cells transform them into electrical energy. In most instances, PV panels produce more than sufficient energy. The surplus electricity can be sold back to grid. Solar power system is not producing at evening, night-time or on overcast weathers. The electricity that goes back into the electrical grid, is used at that time. Much producing solar energy is achievable, the panels need the direct arrival to the rays of the sun for greater part of the 24 hours. However, shadowing effect on the solar system causes the generated power decrement. [8, 10].

PV module are different from PV cells. PV panels cannot produce electricity directly. There are many PV cells on the PV module. These PV cells help to absorb the solar energy. The produced energy by a PV cell is not enough to use in huge applications, due to less production than 1V. Therefore, the cells have to connect in series or parallel configurations to produce enough power. In this way, the module can be obtained. There can be different sizes of PV modules and the most used module is 36 to 72 solar cells connected in series to produce enough voltage. In order to get high power, the modules are interconnected as series or parallel to obtain form of arrays [8]. Figure 2.1 presents the cell, module and array structures. This system can supply all the electricity needs

of a typical household. Thousands of large system, that use PV array is built for power plants or industrial applications.

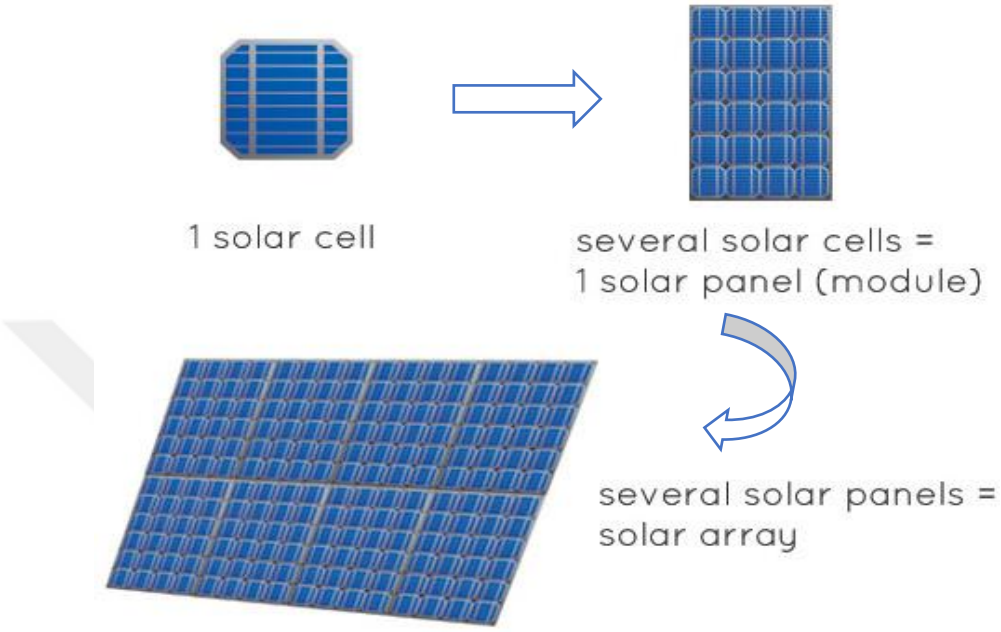

Figure 2.1 PV Cell, PV module, PV array Demonstration. [11]

2.1.1 Modeling of Solar Power System

In this part, the main aim is to present the modeling of the PV panel that is designed in Matlab/Simulink. Also, the mathematical equations, which are implemented in the Matlab code is explained. The PV cell circuit has a current source in parallel to the diode. That source symbolize the generated current by photons. The photocurrent I_{ph}, is directly proportional to this current source. The PV cell's I-V characteristic is determined by the diode. The circuit diagram of the PV module is illustrated in Figure 2.3.

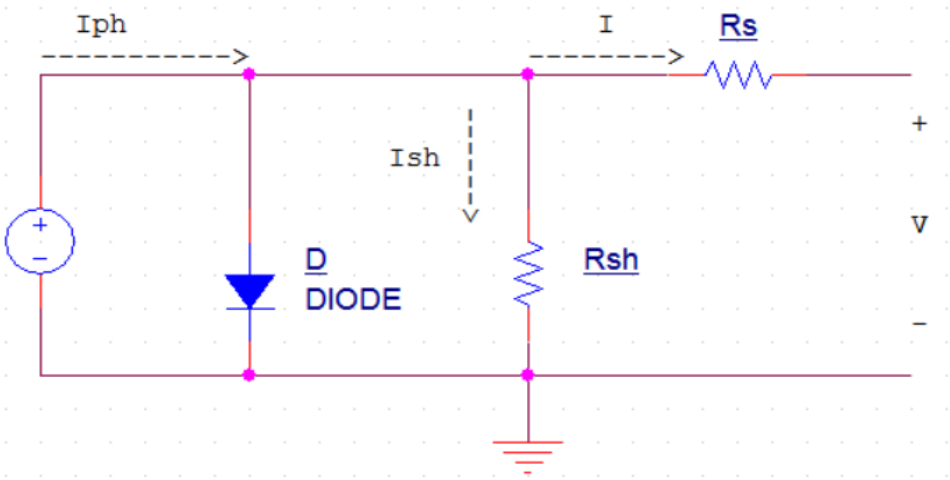

Figure 2.2 PV module equivalent circuit.

The accuracy and complexity of this circuit can be improved depends on the mathematical model. Where,

I_D – Diode internal diffusion current

I_{ph} – Photo Current

Rs – Series resistance (Ω); provides more accuracy between MPP and the losses.

Rsh – Shunt resistance (Ω) ; which is parallel to the diode.

The basic I-V characteristics of PV module is presented [12, 14].

$$I = Iph - I_D \tag{2.1}$$

$$I_D = Is\ (exp\left(\frac{q\ Vpv}{n\ k\ (Temp_K)}\right) - 1) \tag{2.2}$$

$$\text{Iph} = [\text{Isc} + \text{Kt}\ (Temp_K - \text{T}ref\ )]\ .\left(\frac{G}{G_{nominal}}\right) \tag{2.3}$$

$$Is = Ir\ x\ e^{\frac{(q\ Eq)}{nk\left(\frac{1}{Tref} - \frac{1}{TempK}\right)}} x\ \left(\frac{TempK}{Tref}\right)^{\frac{3}{n}} \tag{2.4}$$

$$Ir = \left(\frac{Isc}{exp\left(\frac{q\,Voc}{n\,k\,(Temp_K)}\right)-1} \right) \quad (2.5)$$

Where,

q — Electron charge, 1.602e-19 C.

k — Boltzmann's constant. Its value is 1.38e-23 (J/K).

Is — Cell's saturation current

Kt — Temperature coefficient (A/K)

$Temp_K$ — Operating temperature (K).

T_{ref} — 298 *K* (25 ^oC)

G — Solar insolation (W/m^2) and $G_{nominal}$ — Reference solar radiation (1000 W/m^2).

I*r* — Reverse saturation current in ampere at T_{ref}.

Eq — Band-gap energy (1.12 eV for Silicon).

n — Diode ideality factor (1 < n < 2).

Isc — Short circuit current at T_{ref} and $G_{nominal}$.

V_{OC} — Open-circuit voltage at T_{ref}.

In Figure 2.2, the general model is shown and is more accurate. The output current can be calculated by Equation (2.6) [13].

$$Ipv = Iph - Is \left(\left(exp\left(\frac{q\,(Vpv + Ipv\,Rs}{n\,k\,(Temp_K)}\right) - 1 \right) \right) \quad (2.6)$$

The series resistance Rs derives, when the Equation (2.6) differentiates. It is shown as below [14, 15].

$$\mathrm{Rs} = -\frac{\mathrm{d\,Vpv}}{\mathrm{d\,Ipv}} \Big| - \frac{n\,k\,(Temp_K)/q}{Is\,e^{\left(\frac{q\,Voc}{n\,k\,Temp_K}\right)}} \quad (2.7)$$

$$\mathrm{Rs} = \alpha, ref \ \frac{\ln\left(1-\frac{Im,ref}{Isc,ref}\right)+ Voc,ref - Vm,ref}{Im,ref} \tag{2.8}$$

The Equation (2.8) is applied by under the condition that Vpv = Voc and Ipv = 0. Also, α,*ref* is presented as below [16, 17].

$$\alpha, ref = \frac{2Vm,ref - Voc,ref}{\frac{Isc,ref}{Isc,ref - Im,ref}+\ln\left(1-\frac{Im,ref}{Isc,ref}\right)} \tag{2.9}$$

Where,

I*m,ref* – Maximum current at T*ref* and G*nominal*.

I*sc,ref* – Short circuit current at T*ref* and G*nominal*.

V*m,ref* – Maximum voltage at T*ref* and G*nominal*.

V*oc,ref* – Open circuit voltage at T*ref* and G*nominal*.

α,*ref* – The completion timing factor of thermal voltage at T*ref* and G*nominal*.

2.1.2 Technical Specifications and PV Characteristics by SAM and Simulink

The PV array is modeled and LG Electronics LG300N1W-G3 array is implemented in this design. Also, the module specification is validated by SAM [18]. I-V and P-V graphs of PV module are obtained by using SAM and Simulink in order to express the Photovoltaic panel characteristics under the different conditions in terms of variation of the temperature and solar irradiation. The equivalent circuit is used to get model characteristics and mathematical formulations are presented in the previous part.

The PV module consists of 60 cells and the module voltage can be calculated by multiplication of each cell voltage with total number of cells [13].

The model of PV panel is performed with Matlab/Simulink. The model parameters are given in Table 2.1.

Table 2.1 Simulation Model Parameters of PV Module

Maximum Power	Pm	(W)	302.72
Open Circuit Voltage	Voc	(V)	39.5
Voltage at maximum power point	Vm	(V)	32
Short Circuit Current	Isc	(A)	10.05
Current at maximum power point	Im	(A)	9.46
Temperature coefficient of Isc	-	(% / deg ^{0}C)	0.03
Diode ideality factor	n	-	0.96984
Shunt resistance	Rsh	(Ω)	212.8143
Series resistance	Rs	(Ω)	0.31448
Cells per module	N	-	60
Reference temperature of PV	T *ref*	(^{0}C)	25
Reference solar radiation of PV	G nominal	(W/m2)	1000

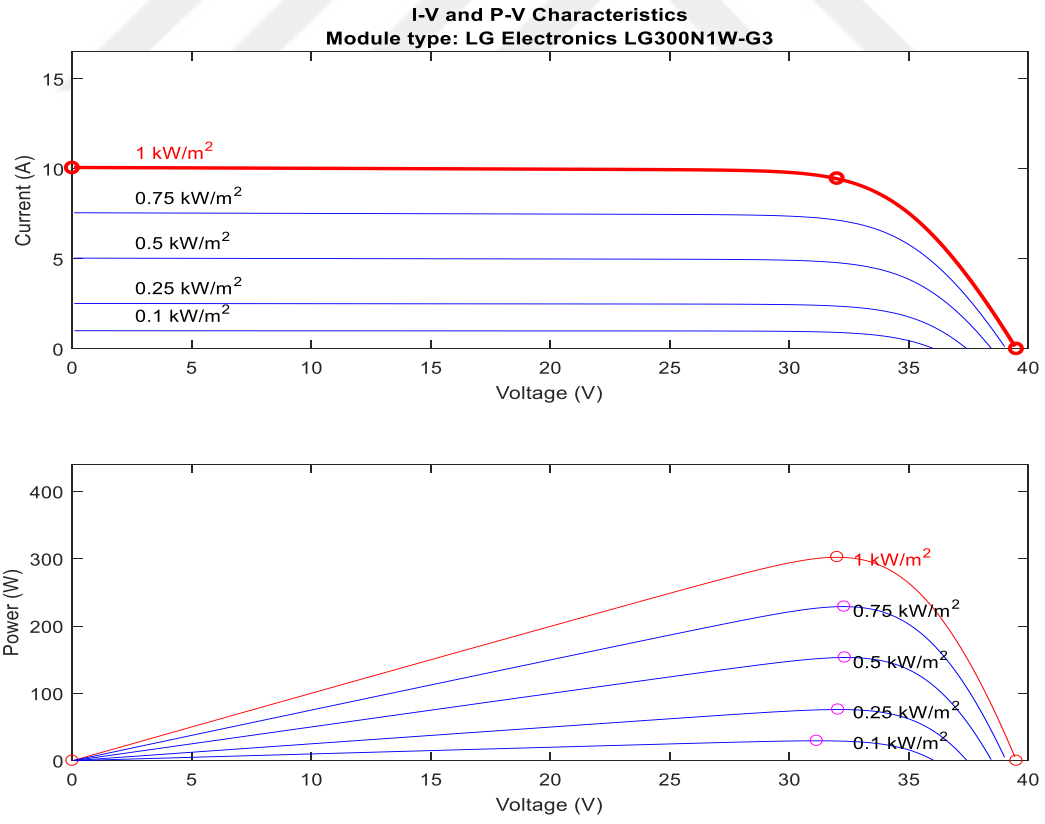

Figure 2.3 I-V and PV characteristics curve of PV model

Figure 2.3.a and Figure 2.3.b demonstrate the I-V and P-V curves of PV module at 25^{0}C temperature and specified solar irradiance values that are 100, 250, 500, 750 and 1000 W/m^2.

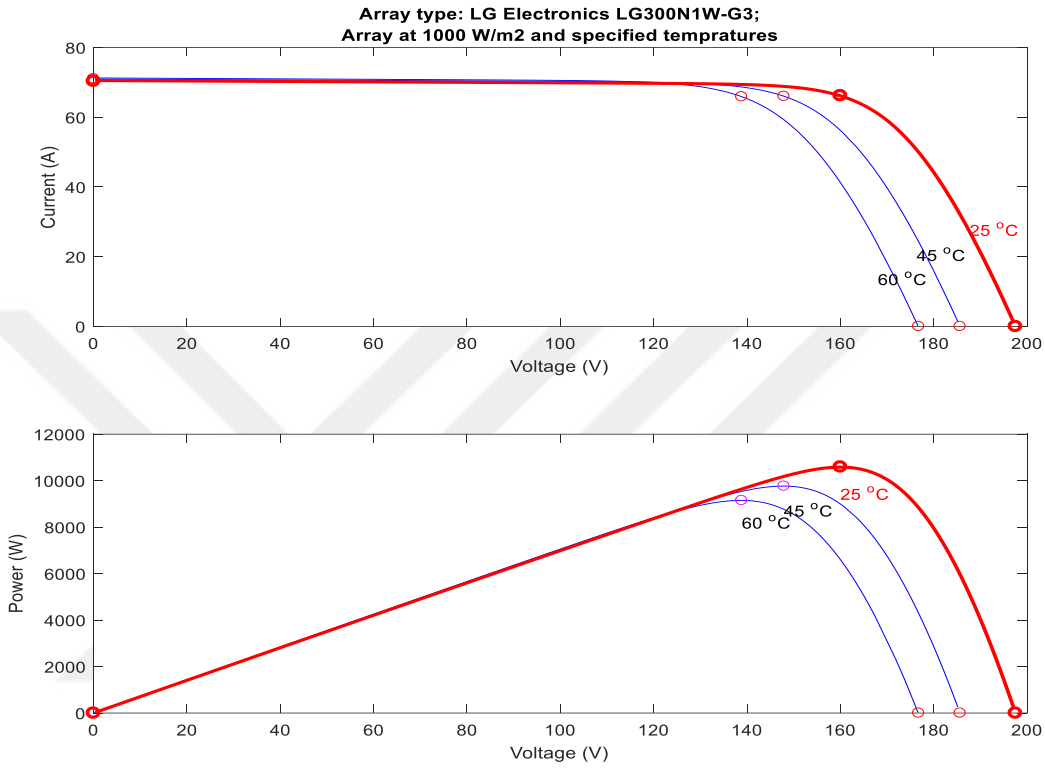

Figure 2.4 I-V and PV curves of PV array at various temperatures and 1000 W/m^2 irradiance.

Figure 2.4 illustrates I-V and P-V curves of PV array at the various temperatures which are 60, 45, 25 ^{0}C and the exact irradiance value which is 1000 W/m^2.

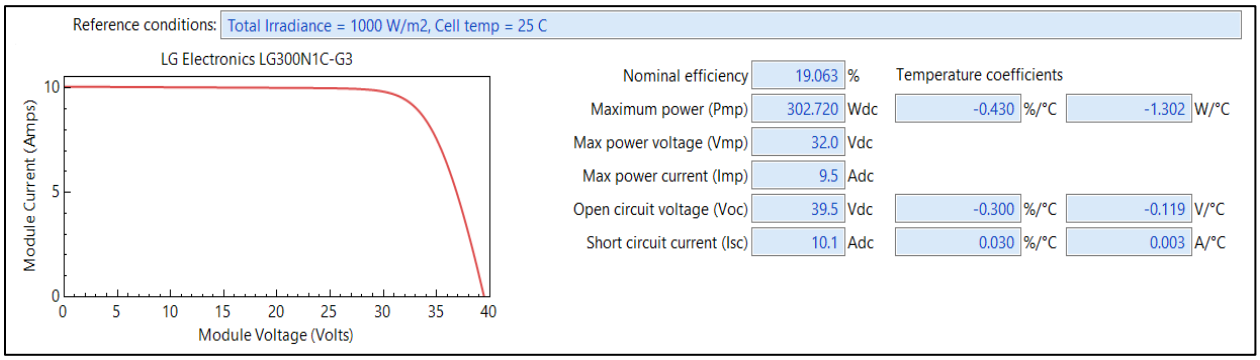

Figure 2.5 PV Module characteristic and parameters by SAM

Figure 2.5 presents the PV module parameters by SAM software [18]. The weather data which is in the SAM library, is used to analyze the module's performance. Figure 2.6 demonstrates the monthly solar irradiation level.

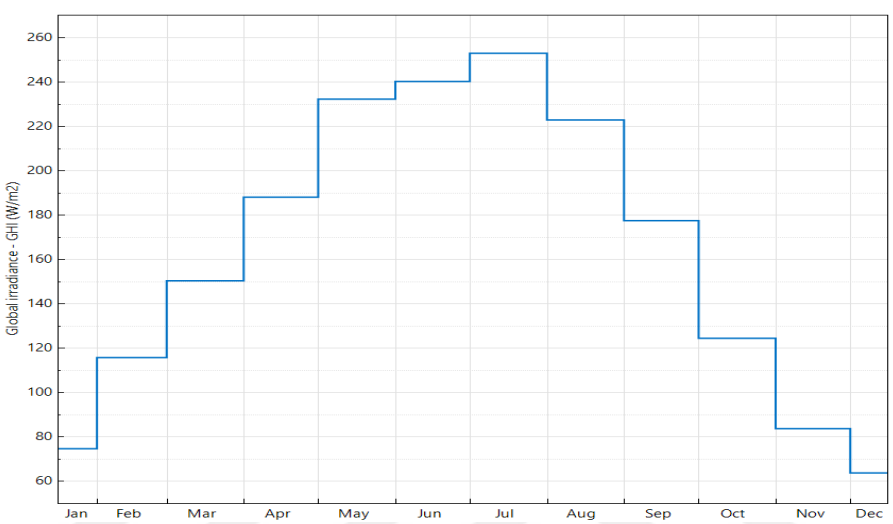

Figure 2.6 Monthly variation of solar irradiation levels

2.2 Wind Energy Conversion

The wind energy system is another component of the proposed hybrid power system. There are elements that built the wind generation system such as wind turbine, drive train, pitch angel control, generator and power converter. The permanent magnet synchronous generator (PMSG) is applied in that wind energy system. It provides the more system safety and nominal maintenance cost. Also, it can connect to the turbine directly [19].

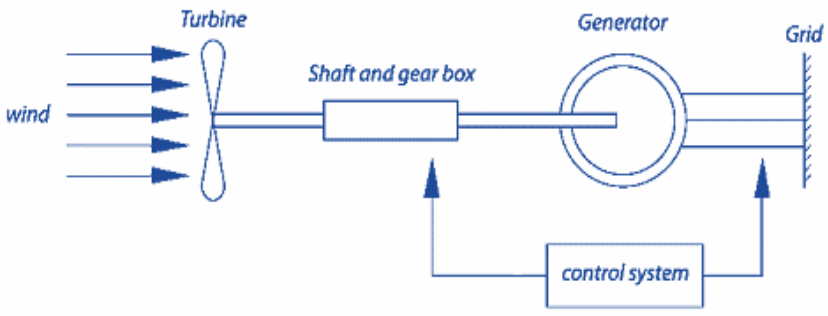

Figure 2.7 Wind system structure [21]

Figure 2.7 presents the components of the wind system. The wind turbine power curve is demonstrated by Figure 2.8. It presents the cut-in and cut-out speeds to observe the control area of wind speeds. The wind turbine is stopped, when the speed reaches out of this area [20].

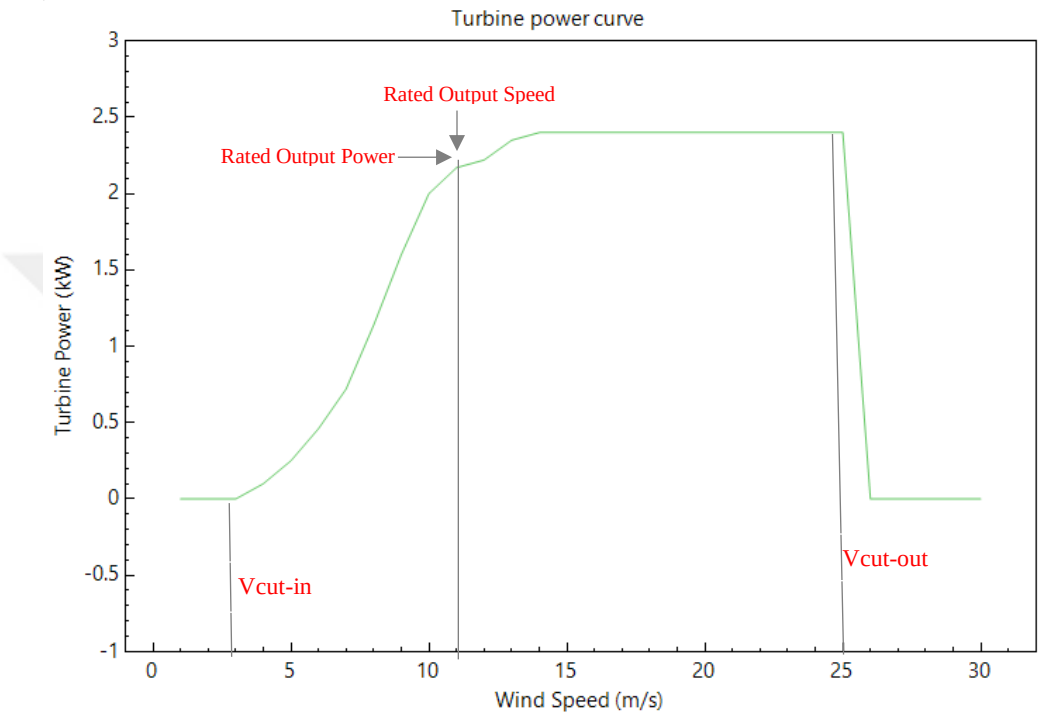

Figure 2.8 Power curve of wind turbine by SAM

2.2.1 Modeling of Wind Energy System

The wind energy system is modeled based on the characteristic of the wind turbine. The wind turbine output power is expressed by the given equation below [4, 21].

$$Pw = 0.5\ Cp\ (\rho A V^3) \tag{2.10}$$

Where,

ρ — Air density (kg/m^3)

Cp — Wind turbine performance coefficient

Pw — Wind turbine output power (W)

A – Turbine swept area by rotor blades (m^2)

Vw – Wind speed or air velocity (m/s)

The tip speed ratio of the rotor blade tip speed λ and performance coefficient of turbine Cp are expressed as below [4, 21].

$$\lambda = \frac{\omega R}{Vw} \tag{2.11}$$

$$Cp\ (\lambda, \beta) = C_1 \left(\frac{C2}{\lambda} - C_3\,\beta - C_4\right) e^{\frac{C5}{\lambda}} + C_6\,\lambda \tag{2.12}$$

$$\frac{1}{\lambda} = \frac{1}{\lambda + 0.08\beta} - \frac{0.035}{\beta^3 + 1} \tag{2.13}$$

Where,

λ – Tip speed ratio of the rotor blade tip speed to wind speed

β – Blade pitch angle (deg)

ω – Angular velocity of rotor (rad/s)

R – Turbine radius (m)

C_1= 0.5176, C_2 = 116, C_3= 0.4, C_4= 5, C_5= 21, C_6= 0.0068 [21].

The wind turbine is modeled in Matlab/Simulink and it is shown in Figure 2.9.

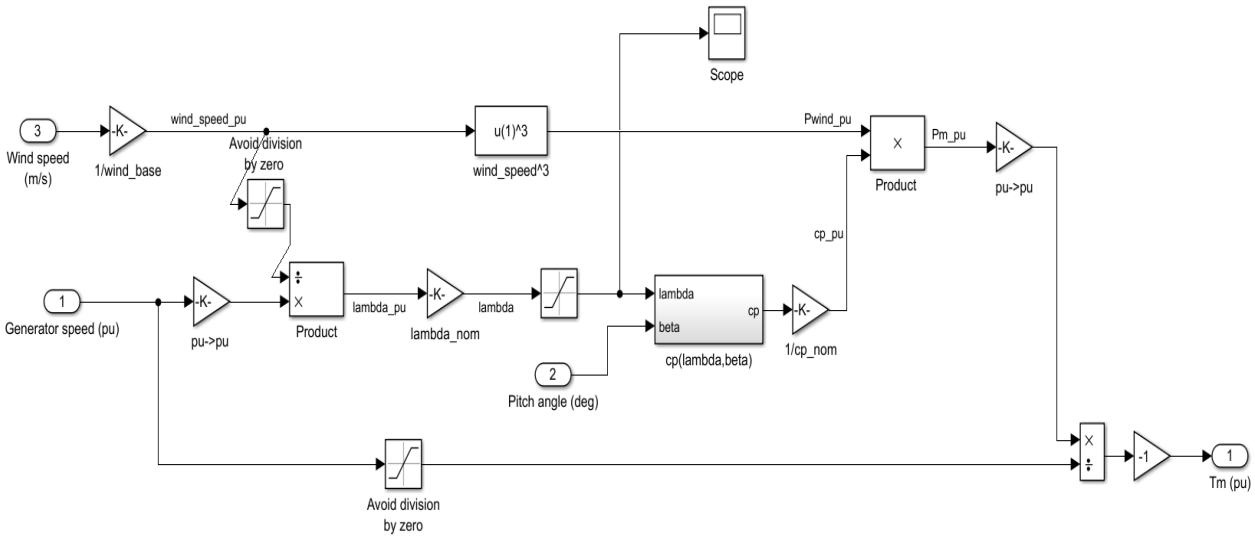

Figure 2.9 Wind Turbine Simulink model

The generator speed of the nominal speed, pitch angle and wind speed are the three inputs of this model. Figure 2.10 shows the either power of wind turbine output characteristics at the pitch angel= 0 or different turbine speeds.

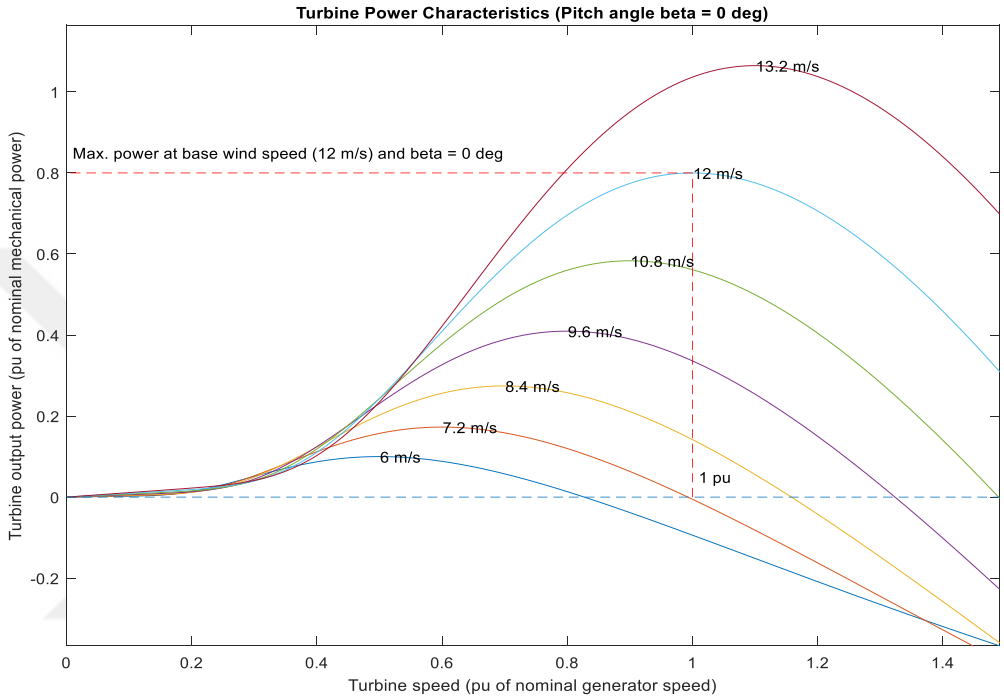

Figure 2.10 Wind turbine characteristics at β = 0 and different speeds

The wind turbine performance coefficient Cp reached to its maximum value at pitch angle = 0 and Cp declines, when the pitch angle increases. This variation is shown in Figure 2.11.

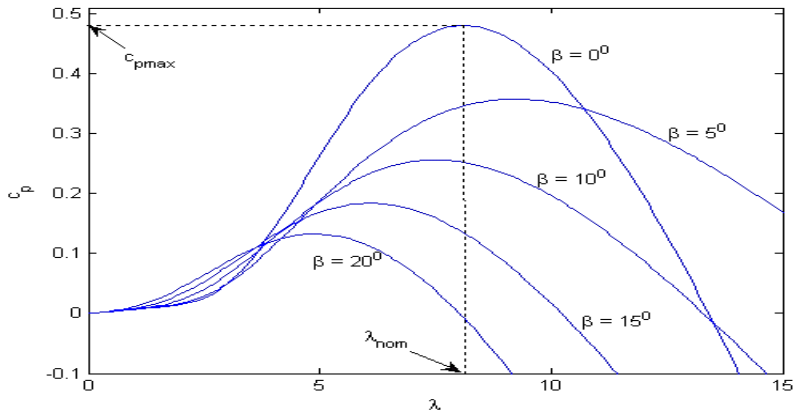

Figure 2.11 Cp value demonstrations at various pitch angles

The wind turbine power and torque can be obtained by using the equations below [21].

$$Pw = 0.5\,\rho A C p\,\left(\frac{\omega^3 R^3}{\lambda^3}\right) \tag{2.14}$$

$$Pw = T \tag{2.15}$$

Where, *T* is the wind turbine torque.

2.3 Modeling of BOOST and Bi-Directional Converter

In order to step up the input voltage, a boost converter can be designed. The most efficient method to get the expected voltage than buck and buck-boost converters. The usage aim of them can change depending on the system that is implemented. The source voltage is stepped up to produce an output voltage which is greater than the input voltage. The ideal circuit is presented in Figure 2.12. This circuit includes the elements which is a voltage source (*Vi*), an inductor (*L*), a diode (*D*), capacitor (*C*), resistor (*R*) and a switch that can be either IGBT or MOSFET based on the design [22]. The MOSFET is used in the Simulink design.

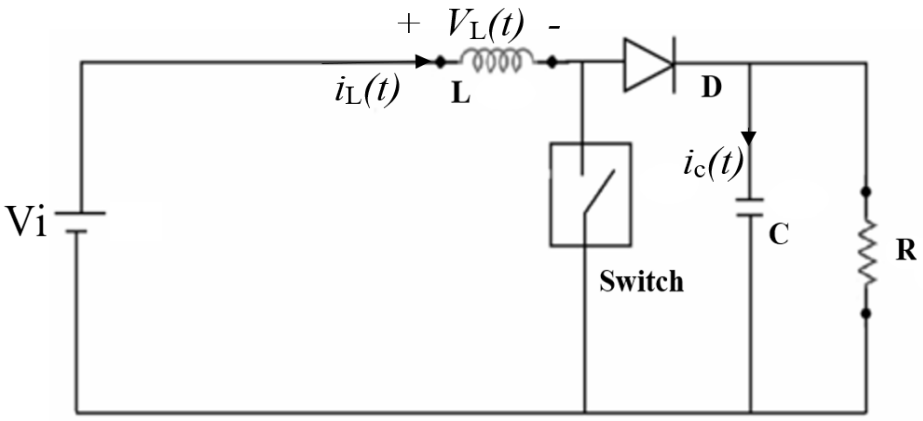

Figure 2.12 Circuit diagram of BOOST Converter [25]

The capacitors or inductors-resistors combination can be added to converter output in order to decrease the output voltage ripple, therefore, the converter's input current is higher than the output current [23].

BOOST converter works in two different modes. These modes depend on the switch status which is open or close. When the switch (S) is closed, the inductor can be charged by the supply and the diode (D) is reversed in this mode. When the switch (S) is opened, the inductor is discharged and the output voltage of the converter increases accordingly [24, 25]. The switching modes of the BOOST converter is illustrated in Figure 2.13.

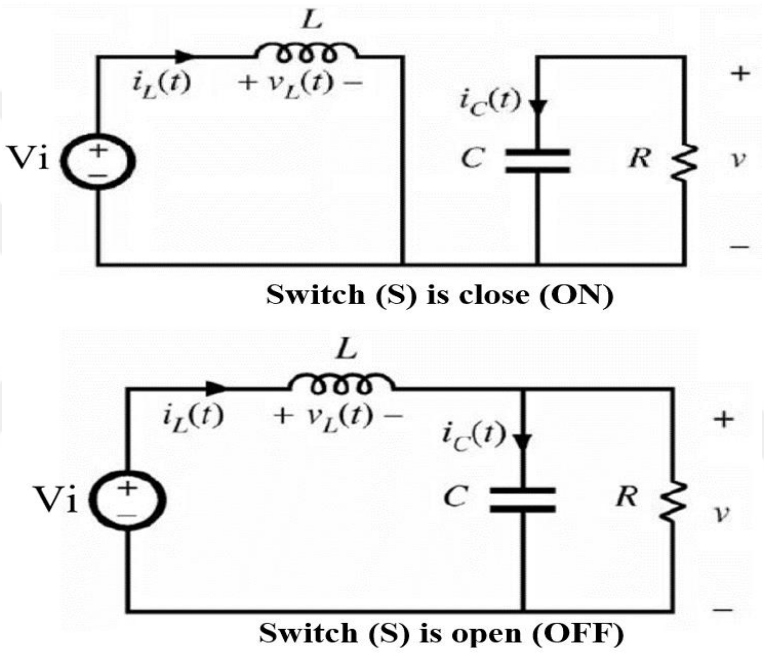

Figure 2.13 Switching modes of the BOOST converter circuit [24].

In the ON mode, the current flows through the inductor since it will be charged. The inductor voltage (v_L) and capacitor current (i_c) are presented as shown in Equations (2.16) and (2.17).

$$v_L = V_i \tag{2.16}$$

$$i_c = -\frac{v}{R} \tag{2.17}$$

In the OFF mode, the current is decreased and it flows through the resistor. Equations (2.18) and (2.19) demonstrates the inductor voltage (v_L), and capacitor current (i_c) below.

$$v_L = V_i - v \tag{2.18}$$

$$i_c = i_L - \frac{v}{R} \tag{2.19}$$

The modeled BOOST converter in Matlab/Simulink is illustrated with PV array connection in Figure below.

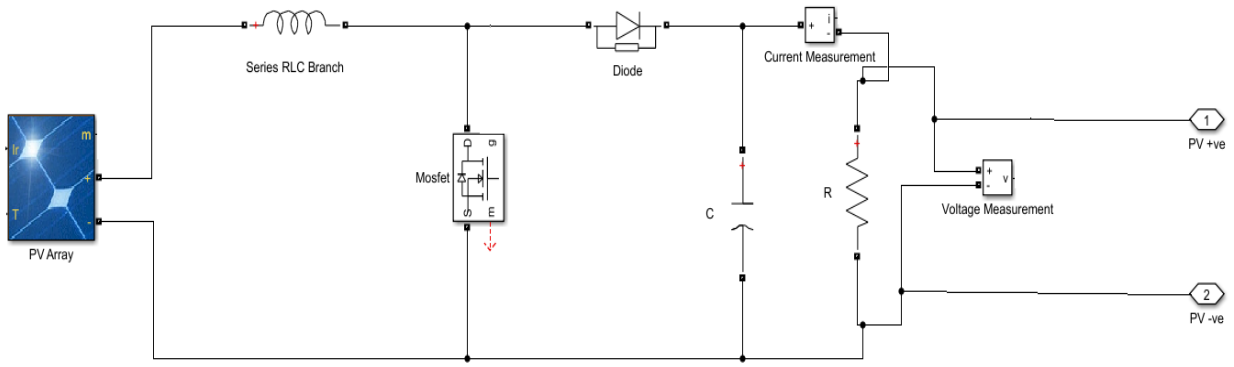

Figure 2.14 PV array connected BOOST Converter.

In the battery system, bidirectional converter is implemented, since it is a reassuring property in the power system and hybrid wind-solar applications especially. It makes the system efficient with the low cost [26]. The battery is designed with bidirectional converter in Matlab/Simulink and it is illustrated in Figure 2.15.

The solar energy can be transferred to battery to store this energy by using bidirectional battery as long as irradiation and wind speed are enough and also, energy carries to load. Either charge or discharge processes are performed by this type converter. There is not any transformers, current saturation and high switching losses. Also, it provides a large voltage diversity during the power flow [26, 27].

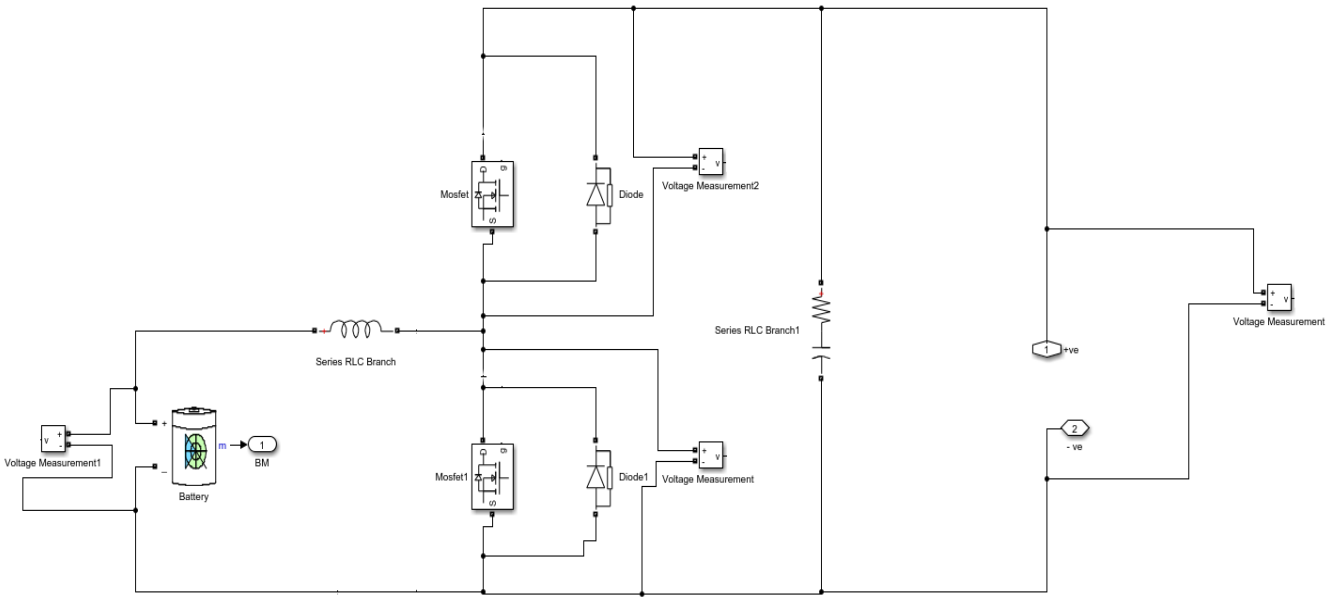

Figure 2.15 Bidirectional DC-DC converter circuit for Battery.

2.4 Modeling of Battery

The battery system has a key role for the wind-solar energy storage system. Lead-acid batteries are using commonly in this system, since it has a long lifetime and low cost. Also, it is a rechargeable battery. The battery consists of many electrochemical cells and they combine each other to get high voltage or current for operating mode. The cells should be connected as series to obtain high battery voltage. The capacity unit is Ah and the rates of discharge and charge are expressed with this unit [28, 29]. The State of Charge (SOC) of the battery is formulated as below [29].

$$\text{SOC} = \frac{\text{Ah capacity remaining in the battery}}{Rated\ Ah\ capacity} \tag{2.20}$$

The battery is directly implemented from Electric Drives/Extra Sources library which is in the Matlab/Simulink.

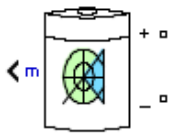

Figure 2.16 Simulink Battery

The battery has some parameters such as nominal voltage (V), rated capacity (Ah), initial State-Of-Charge, and charged voltage (V), nominal discharge current (A), internal Resistance (ohm) [29].

In this thesis, the battery is selected as lead-acid battery and it exists in the SimPowerSystems toolbox of Matlab/Simulink [30]. The battery's equivalent circuit is presented in Figure 2.17.

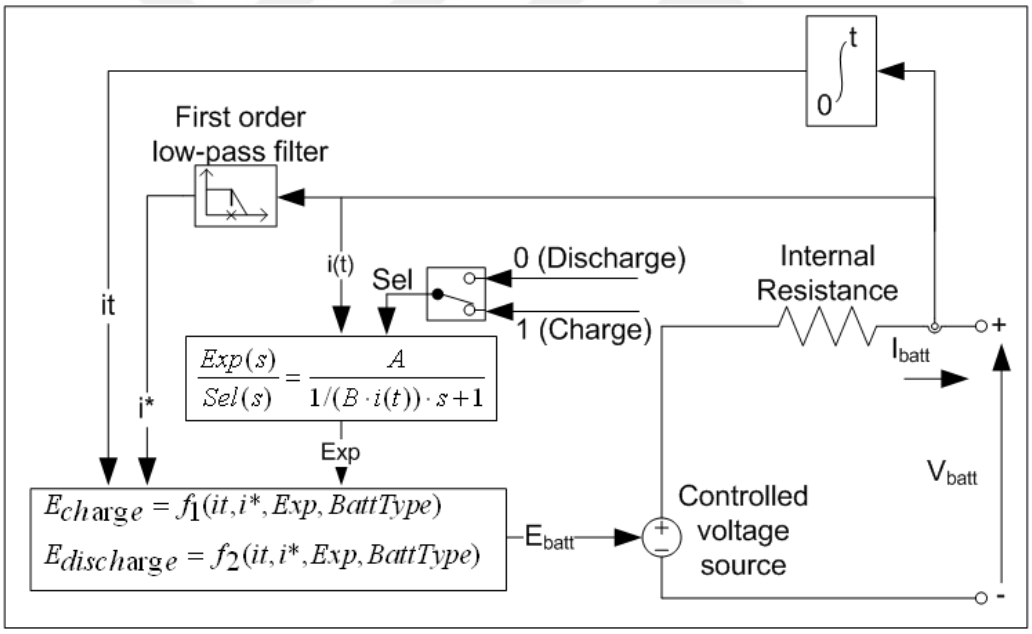

Figure 2.17 Battery equivalent circuit [30]

The mathematical model of the lead-acid battery is presented in Equations (2.21) and (2.22), depending on the charging and discharging conditions [30].

Discharge Model ($i^* > 0$)

$$f_1(it, i^*, i, Exp) = E_0 - K\frac{Q}{Q-it}i^* - K\frac{Q}{Q-it}it + Laplace^{-1}\left(\frac{Exp(s)}{Sel(s)}0\right) \quad (2.21)$$

Charge Model ($i^* < 0$)

$$f_2\,(it, i^*, i, Exp) = E_0 - K\,\frac{Q}{it + 0.1\,Q}\,i^* - K\,\frac{Q}{Q - it}\,it + Laplace^{-1}\left(\frac{Exp(s)}{Sel(s)}\,\frac{1}{s}\right) \quad (2.22)$$

Where,

E_{Batt} — Nonlinear voltage (V)

E_0 — Constant voltage (V)

Exp(s) — Exponential zone dynamics (V)

Sel(s) — Represents the battery mode. Sel(s) = 0 during battery discharge, Sel(s) = 1 during battery charging.

K — Polarization constant (Ah^{-1}).

i* — Low frequency current dynamics (A)

i — Battery current (A).

it — Extracted capacity (Ah)

Q — Maximum battery capacity (Ah)

A — Exponential voltage (V)

B — Exponential capacity (Ah^{-1})

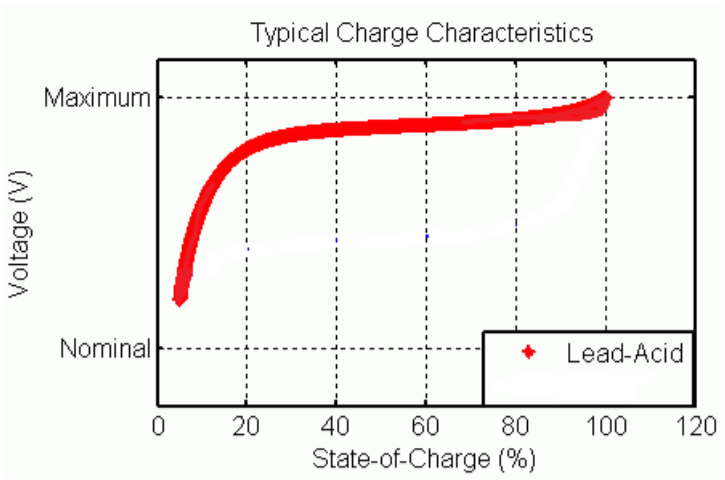

Figure 2.18 SOC of Lead-Acid Battery [30]

2.5 Modeling of Permanent Magnet Synchronous Machine (PMSM)

The permanent magnet synchronous machine is implemented into wind power system model. It provides the system efficiency during the generation process. This model depends on the

d and q synchronous reference frame that rotates synchronously. In this way, torque, flux and power control can be validated in the three phase systems. The two phase (d-q) reference frame includes the three phase a-b-c. The Figure 2.18 demonstrates the equivalent circuit of PMSG with its d-axis and q-axis.

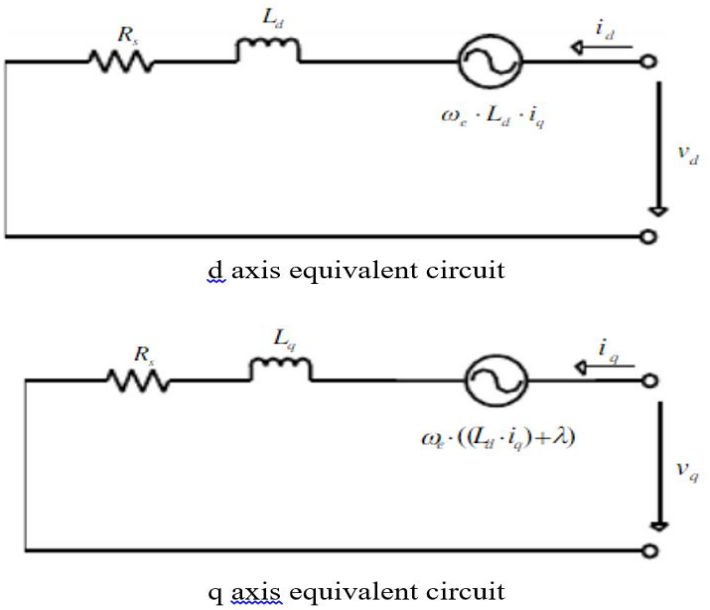

Figure 2.19 Equivalent circuit of PMSM [31]

The mathematical model is presented in Equations (2.23), (2.24), (2.25) based on the equivalent circuit [31, 32]. In this thesis, the mathematical model of PMSM is presented by using Matlab/Simulink SimPowerSystems library. The PMSM model which is designed in Simulink, is illustrated in Figure 2.19.

$$\frac{d}{dt} i_d = \frac{1}{L_d} v_d - \frac{R}{L_d} i_d + \frac{L_q}{L_d} p\, w_r i_d \tag{2.23}$$

$$\frac{d}{dt} i_q = \frac{1}{L_q} v_q - \frac{R}{L_q} i_q + \frac{L_d}{L_q} p\, w_r i_d \; - \frac{\lambda\, p\, w_r}{L_q} \tag{2.24}$$

$$T_e = 1.5\, p\, [\lambda\, i_q \, + (L_d - L_q) i_q\, i_d\,] \tag{2.25}$$

L_q and L_d — q and d axis inductances

R — Resistance of stator windings

i_q and i_d — q and d axis currents

v_q and v_d — q and d axis voltages

w_r — Angular velocity of rotor

λ — Amplitude of the flux induced by the permanent magnets of rotor in stator phases

p — Number of pole pairs

T_e — Electromagnetic torque

If $L_q = L_d$ (in surface-mounted PMSG), electromagnetic torque is formulated as below [32].

$$T_e = 1.5\, p\, \lambda\, i_q \tag{2.26}$$

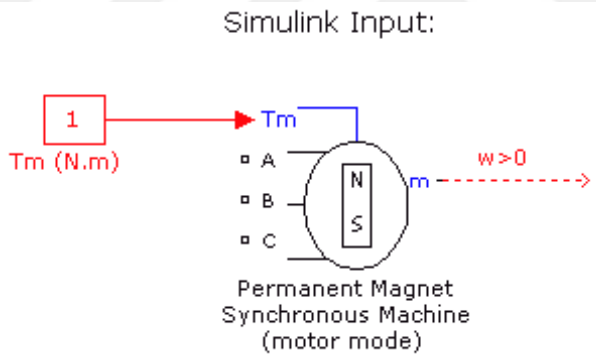

Figure 2.20 Simulink PMSM model

CHAPTER 3

CONTROL OF WIND-SOLAR-BATTERY HYBRID POWER SYSTEM

This chapter considers the Maximum power point tracking control methods and presents their algorithms with the flow charts. The Perturb and Observe (PO) method and Fuzzy Logic controller method are analyzed and discussed. Also, the Simulink design of all parts are introduced with their details. The other control mechanism for the battery and grid integration are explained in this chapter.

3.1 Maximum Power Point Tracking Controls for Solar Power System

The MPPT methods provide more energy production for PV sources. MPP of the PV panel can change based on the different temperature and irradiation level, therefore, MPPT algorithms are used. The voltage and current are controlled by the MPPT for finding their MPP which are in the I-V characteristic curve. Figure 4.1 demonstrates the PV array output characteristics and the maximum power points as theoretically. In the proposed design, the MPPT algorithms which are Perturb and Observe and Fuzz Logic Controller, are implemented and they compared each other in terms of their performance such as converge speed, effectiveness and correct tracking. There are about 19 MPPT algorithms which are stated in [33]. The P&O algorithm is an easy method to implement among them. In spite of that the implementation of Fuzzy Logic Controller is harder than P&O, however, it gives better performance than P&O. Both of them are used in this thesis.

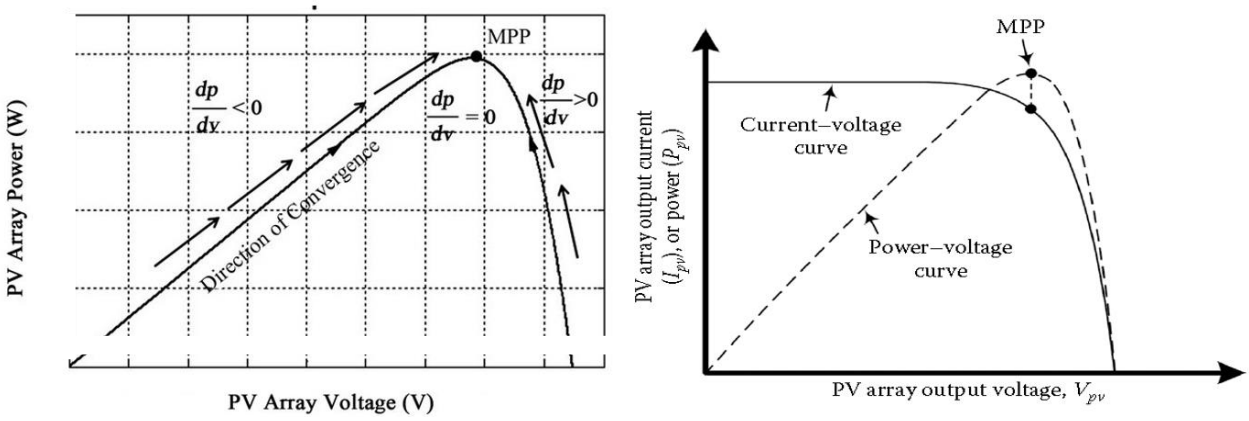

Figure 3.1 PV array output characteristic curves [34]

3.1.1 Perturb and Observe Control Method

The P&O algorithm is preferred commonly among other MPPT methods due to easy implementation and simplicity. There are two inputs which are current of the PV, I_{pv} and voltage of the PV, V_{pv} in this algorithm. The block diagram with the embedded MATLAB function is demonstrated in Figure 3.2.

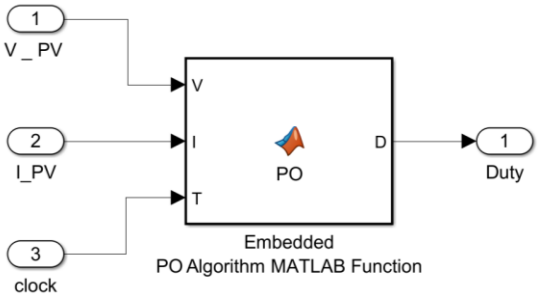

Figure 3.2 Block diagram of P&O

Perturb means the increasing or decreasing, therefore, the PV array terminal voltage and current are perturbed periodically by the algorithm and the PV output power is compared with the previous one. *P(k+1)* represents the PV output power and it is compared with the *P(k)* which represents the previous perturbation. Also, *V(k-1)* represents the operating voltage of the algorithm. *P(k - 1)-P(k)* and *V(k-1)-V(k)* can be called as ΔP and ΔV respectively. When ΔP and ΔV are less than 0, the

point of operation is going to move towards the MPP from the left side of MPP. Accordingly, the output voltage is increased by next perturbation of duty cycle. When ΔP and ΔV are greater than 0, the point of operation is distant from the MPP, hence the output voltage is increased by next perturbation of duty cycle again. On the other hand, when the ΔP is greater than 0 (PV panel power output is declining) and ΔV is less than 0 (PV panel output voltage is increasing), the point of operation is at the right side of MPP. Hence, the output voltage is decreased by next perturbation of duty cycle. Other case is that when the ΔV is greater than 0 (PV panel output voltage is declining) and ΔP is less than 0 (PV panel output power is increasing), the point of operation is going to be at the right side of MPP. Thus, the output voltage is decreased by next perturbation of duty cycle [4, 36, 37]. The P&O control algorithm flow chart [35] is illustrated in Figure 3.3.

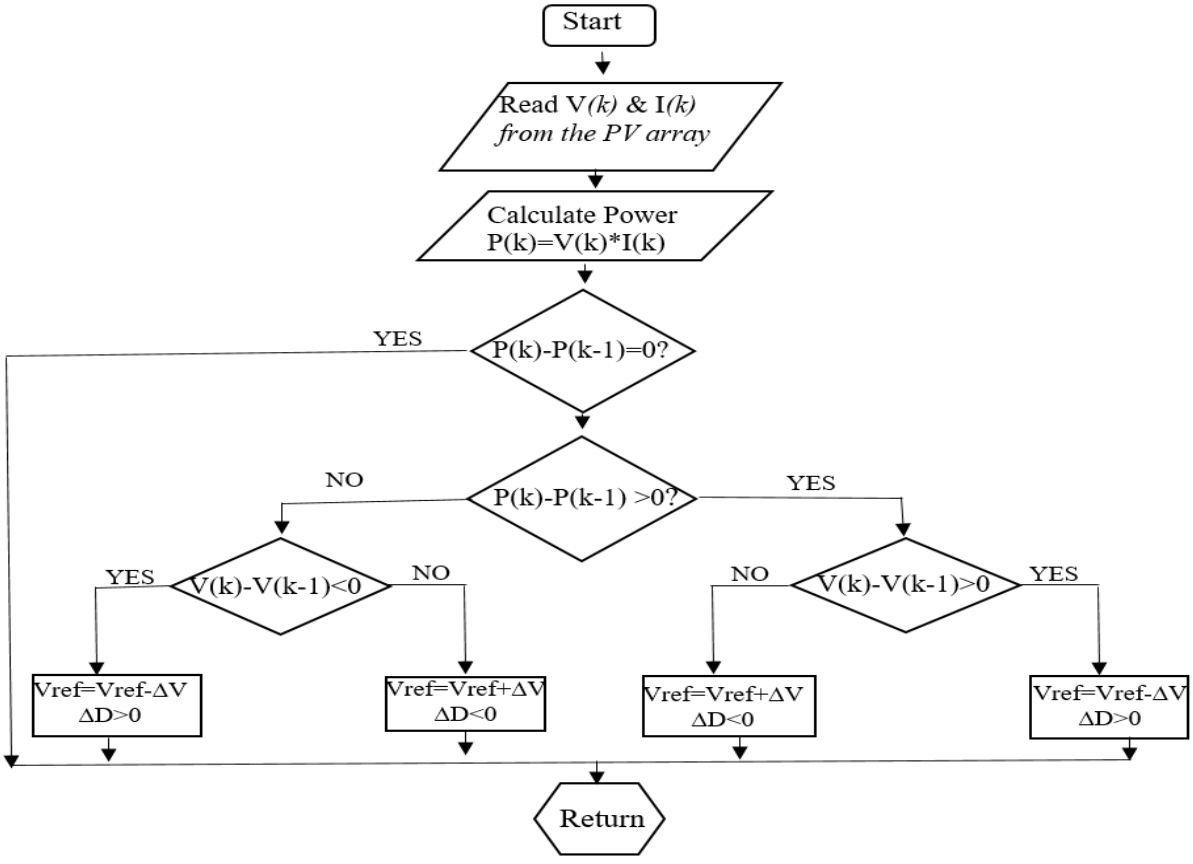

Figure 3.3 Flow chart of P&O algorithm

In this thesis, P&O method is implemented owing to PWM (pulse width modulation) cycles which measure the power. In this way, the duty ratio is perturbed directly [35]. Simulink design which includes all block, is presented in Figure 3.4.

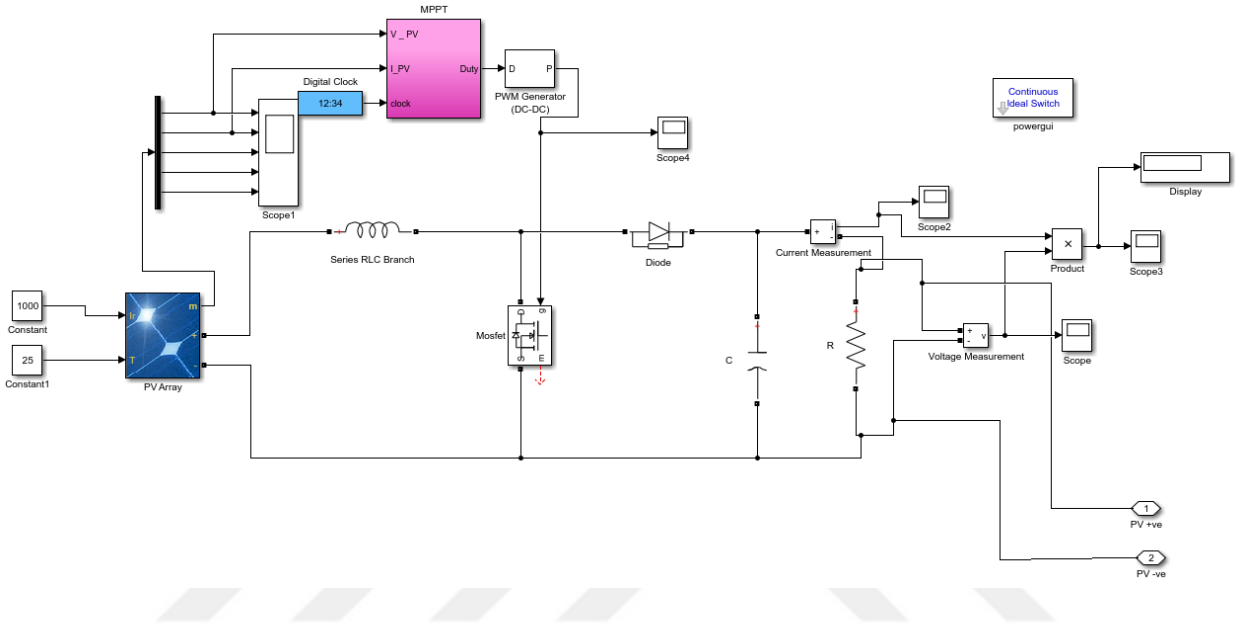

Figure 3.4 Simulink design of solar system with P&O (MPPT) control

3.1.2 Fuzzy Logic Control Method

The FLC based on a mathematical model which is easy to understand. It is flexible and easy to layer on more functionality. The controller is working with imprecise inputs. Also, it is the basis for human communication [38]. This control system compares an input signal in order to determine the fuzzy sets (logic variable membership function) in the range 0 and 1. The duty cycle, D is the output of FLC. There are two main inputs that are the error, E and error variation, ΔE in the fuzzy logic based MPPT controller. The following equations (3.1) and (3.2) are used to calculate them [27, 39].

$$E(k) = \frac{P(k)-P(k-1)}{V(k)-V(k-1)} \tag{3.1}$$

$$\Delta E(k) = E(k) - E(k-1) \tag{3.2}$$

In the control process, there are three levels that are fuzzification, rule based and defuzzification. In the rule base level, the membership functions' shape can change and this effects on the FLC. The power converter is controlled due to analog signal procurement by FLC and it is converted to digital signal. In the fuzzification stage, the input variables are transformed into linguistic variables. This process depends on the membership function which has different levels that are NB (negative big), NS (negative small), ZE (zero), PB (positive big) and PS (positive small) [27, 40, 41] which is illustrated in Figure 3.5.

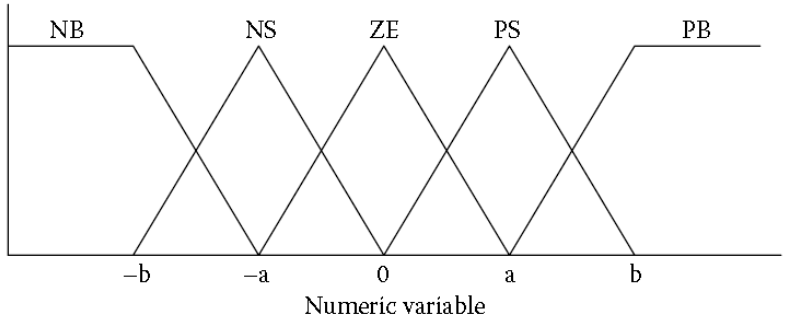

Figure 3.5 Membership function for inputs and outputs of FLC [27]

The FLC rule base table is given in Table 3.1.

Table 3.1 Rule Base of FLC

ΔE → E	NB	NS	ZE	PS	PB
NB	ZE	ZE	NB	NB	NB
NS	ZE	ZE	NS	NS	NS
ZE	NS	ZE	ZE	ZE	PS
PS	PS	PS	PS	ZE	ZE

There are four main parts which build up the FLC. These are the fuzzification, inference, rule based and defuzzification as shown in Figure 3.6.

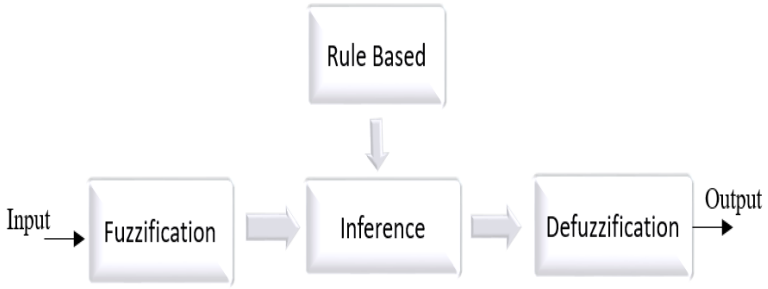

Figure 3.6 Fuzzy Logic Controller Structure

There are different kind of membership functions in terms of the shapes that can be triangular, trapezoidal, Gaussian, bell-shaped, etc. [35]. The controlled system has the system information and fuzzy rule is based on that information. If the number of memberships increase, the system has better performance, however, the system complexity is increased [35]. The used fuzzy interface method in this thesis, is Mamdani [42] and it depends on the if-then rules. Mostly, the triangular and trapezoidal shapes are used by Mamdani. In this thesis, FLC is implemented for solar system and Simulink design with all block is presented in Figure 3.7.

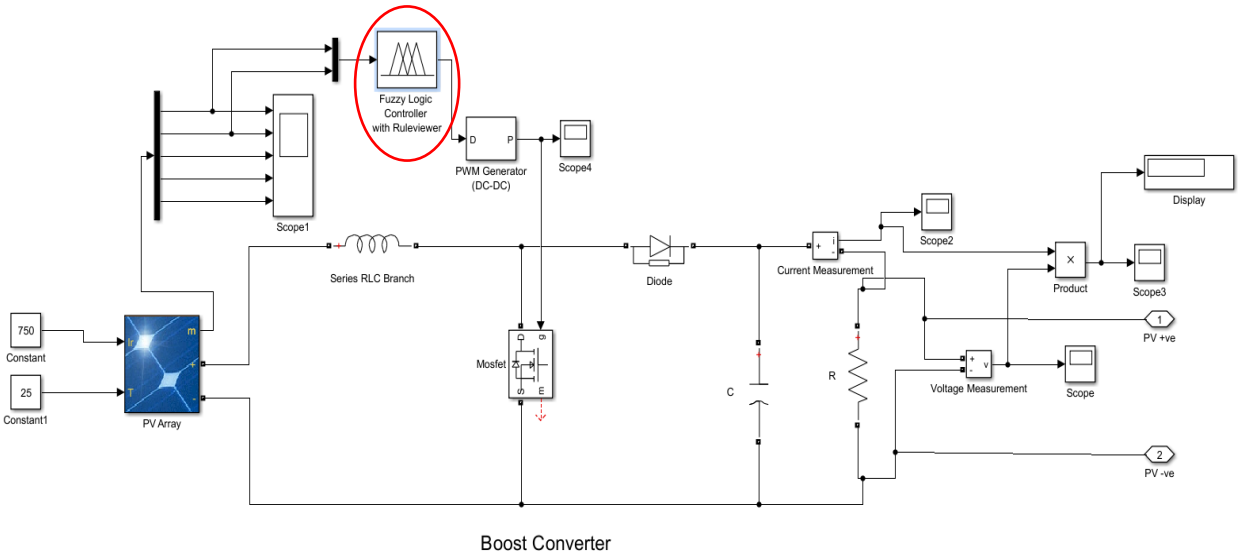

Figure 3.7 Simulink design of solar system with FLC

3.2 Maximum Power Point Controls for Wind Power System

The power generation process by using wind, depends on various factors. Therefore, the maximum power can be obtained by using MPPT control methods under the different conditions. The wind speed is the most important factor due to its variations. The MPPT algorithms are applied for obtainment the MPP at any wind speed. Wind Energy Conversion Systems (WECS) can be affected by different weather conditions and locations. The Perturb and Observe and Fuzzy Logic based MPPT algorithms are applied for proposed WECS in this chapter.

3.2.1 Perturb and Observe Control Method

The change in output power is observed by P&O control algorithm in order to reach the MPP. Also, the rotor speed perturbation is generated. Generally, when the rotor speed is increased, the energy consumption declines and the output power is decreased [4, 37]. In the wind MPPT, either the rotor speed is changed or maximum utilization factor, Cp is kept by the duty cycle adjustment. The system voltage can be increased with the increment in the duty cycle [37]. The algorithm has different control methods. It demonstrates in the Figure 3.8.

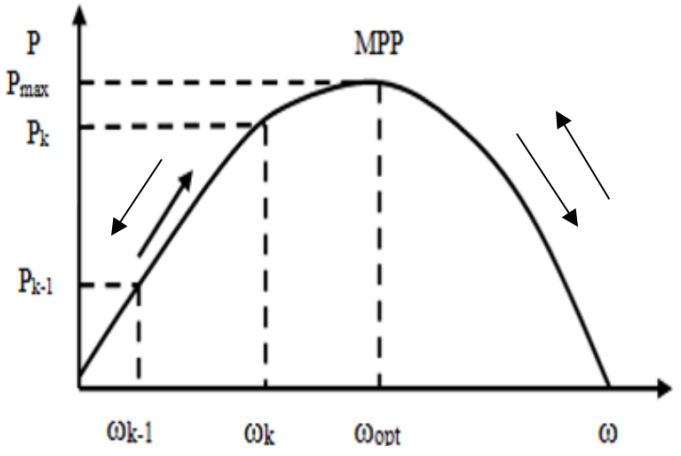

Figure 3.8 MPP demonstration for wind power system [37]

$P_k - P_{k-1}$ and $\omega_k - \omega_{k-1}$ can be called as ΔP and $\Delta\omega$ respectively. When ΔP and $\Delta\omega$ are greater than 0, the point of operation is going to move towards the MPP from the left side of MPP. The rotor speed increases, when the $\omega_k > \omega_{k-1}$ and the duty cycle and next perturbations become negative. When ΔP and $\Delta\omega$ are less than 0, the point of operation is distant from the MPP at left side and the rotor speed declines ($\omega_k < \omega_{k-1}$). Thus, the duty cycle and next perturbations become positive [4, 37]. Other case is that when the $\Delta\omega$ is greater than 0 (the rotor speed increases, $\omega_k > \omega_{k-1}$) and ΔP is less than 0, the working point is at the right side. Thus, the last perturbation of duty cycle is negative, while the next one becomes positive [37]. Last case is that when the $\Delta\omega$ is less than 0 (the rotor speed decreases, $\omega_k < \omega_{k-1}$) and ΔP is greater than 0, the working point is at the right side. Thus, the next perturbation of duty cycle is positive, while the last one becomes positive [37]. The control method of P&O can be stated as follow in Equation (3.3).

$$D(k) = D(k-1) \pm (\Delta P) \pm (\Delta\omega)\, D_{step} \tag{3.3}$$

$D(k)$ represents the control signal for the converter and $\Delta\omega$ and ΔP are the change in rotor speed and output power respectively. D_{step} is the step size which belongs the control signal [37].

On the other hand, this algorithm cannot be effective in the large systems since the power generation is increased. In the residential use, it can be applicable method like in this thesis.

In this thesis, P&O algorithm is implemented owing to PWM (pulse width modulation) cycles and the duty ratio is perturbed directly [35]. Simulink design which includes all block, is presented in Figure 3.9.

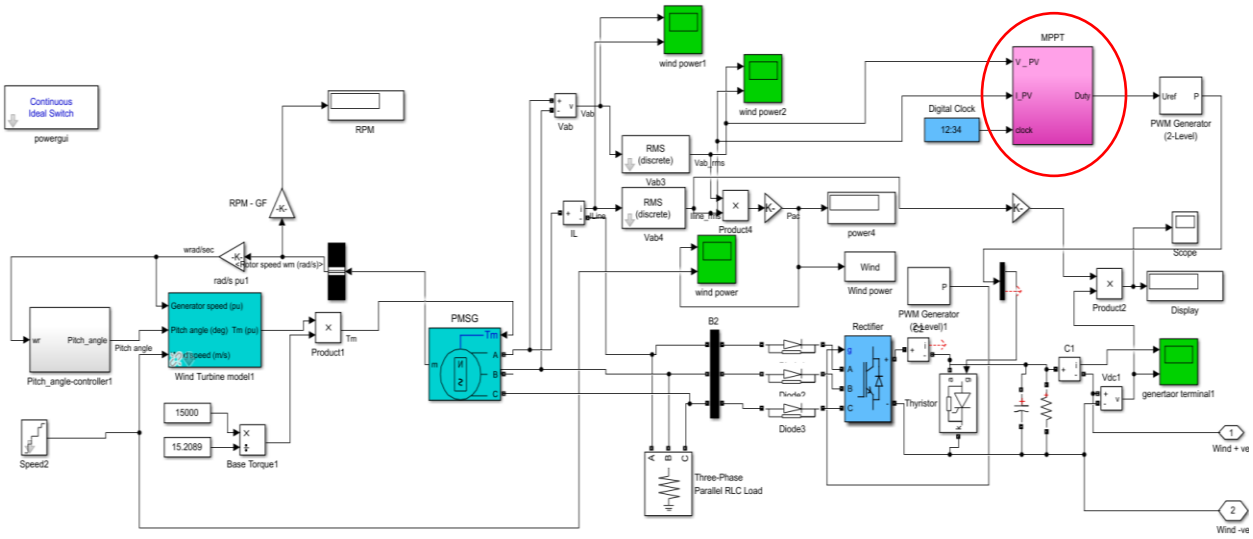

Figure 3.9 Simulink design of wind system with P&O control

3.2.2 Fuzzy Logic Control Method

The Fuzzy Logic Control mechanism is combined with wind energy conversion system in this thesis. The electrical power is obtained by the PMSG. Also, the bridge rectifier provides the ad-dc conversion for the wind generator. On the other hand, The BOOST converter controls that rectifier's voltage. The measured current and voltage values of the rectifier are directly sent to controller part. FLC achieves the maximum power point after it has the measured voltage, current and power values [36]. The control mechanism of the FLC is shown in Figure 3.10 in details. FLC membership functions (0 and 1) [38] convert the input variables to membership values for controllers. The change in the output power and duty cycle of converter are the inputs of the FLC as shown in Figure 3.10 and they can be calculated as expressed in Equations (3.4) and (3.5) below.

$$\Delta P_k = P_k - P(k-1) \tag{3.4}$$

$$\Delta D_k = D_{k-1} - D_{k-2} \tag{3.5}$$

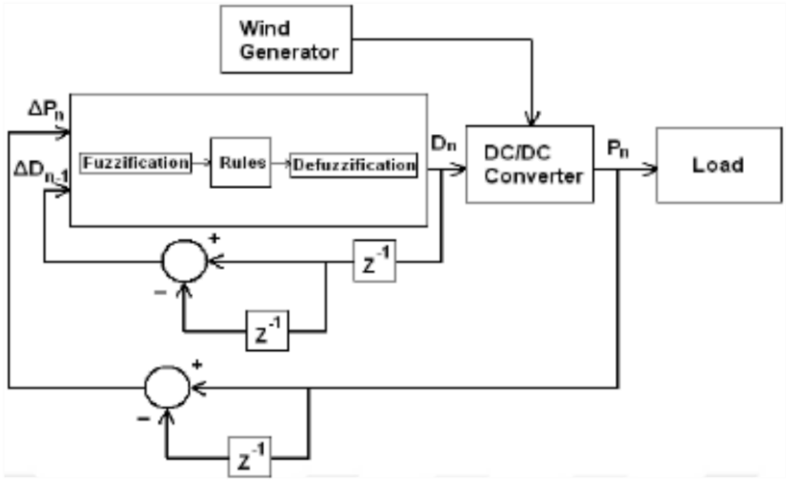

Figure 3.10 FLC based wind MPPT control mechanism [36]

This control system measures the change in output power, ΔP_k and also, duty cycle, D is adjusted at the same time in order to find the MPP [43]. All wind energy system blocks with FLC is shown in Figure 3.11 below.

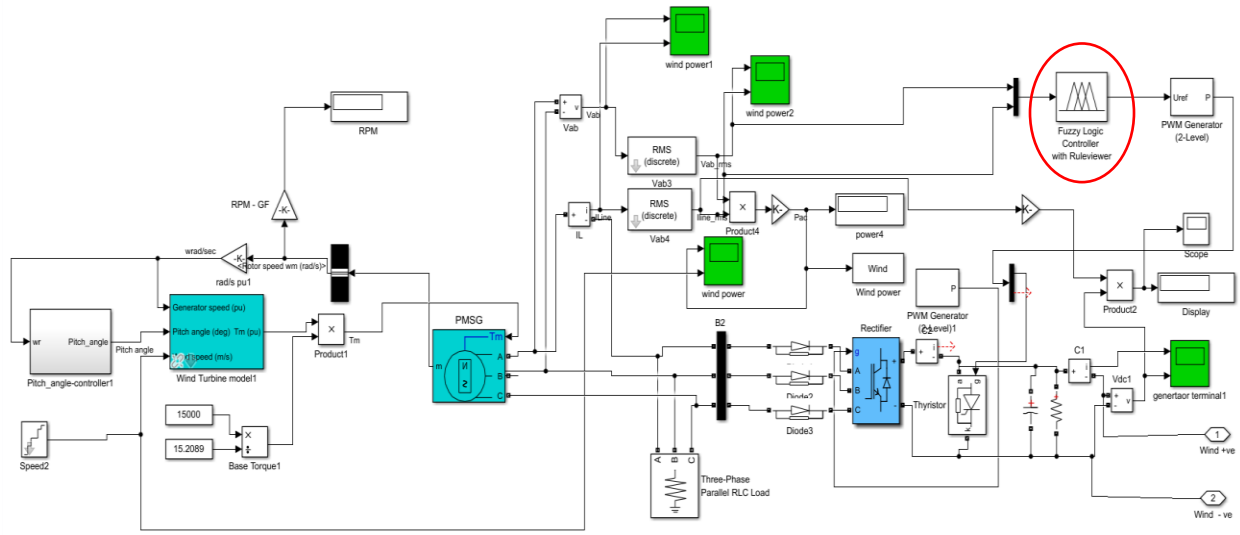

Figure 3.11 Simulink design of wind system with FLC

3.3 Fuzzy Logic based Control for Battery

In the proposed model, the battery system is adopted to enhance the system efficiency. The battery system is controlled by the FLC to track the SOC status with high efficiency. The produced energy by wind-solar system combination can be stored by the battery system in order to save that energy. When the generation of energy decreases, the system load or grid can be fed by the battery. The fuzzy logic controller is used to increase either energy efficiency or battery life. This controller establishes the parameters of the battery state-of-charge and also, it provides the energy optimization. Accordingly, the battery life time and SOC are directly proportional each other and the fuzzy logic controller improves the Lead-Acid battery's life significantly [44].

There are two modes that are applied by controller; charging and discharging for the wind-solar power system. ΔSOC and ΔP are the inputs and ΔI is the fuzzy logic controller's output. The fuzzy control diagram for the SOC of battery is illustrated in Figure 3.12.

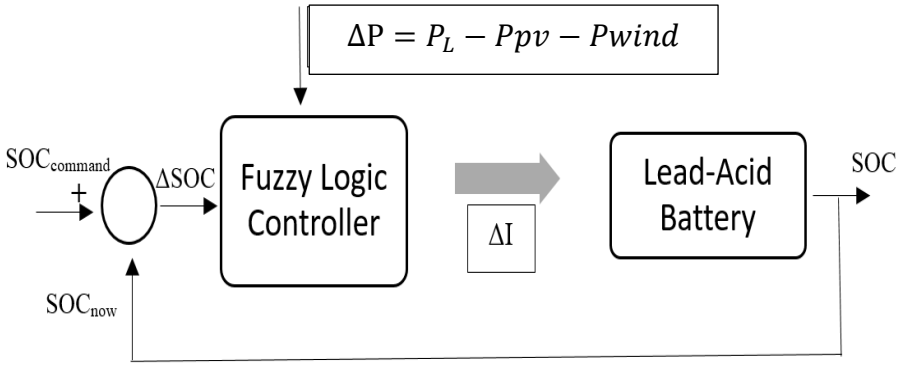

Figure 3.12 Fuzzy control diagram for SOC of battery

The input variables can be calculated as followed in Equations (3.6) and (3.7) [44, 45].

$$\Delta SOC = SOC_{COMMAND} - SOC_{NOW} \tag{3.6}$$

$$\Delta P = P_L - Ppv - Pwind \tag{3.7}$$

ΔP expresses the difference between total power which is produced by wind-solar and the system load requirement. P_L is the required load power and P_{pv} and P_{wind} are the generated powers by solar and wind systems respectively [44, 27]. The input-output variables of membership functions for FLC, are presented in the Figure 3.5 and the rule table of FLC is given in 3.1 (section 3.1.2). According to this rule, the output current of Lead-Acid battery which demonstrates the variety of charge-discharge (ΔI), is obtained. There is no enough generated energy for the system load by wind-solar system, when the ΔP < 0. In this case, the battery is going to be charging (ON) mode. On the other hand, when the ΔSOC < 0 which means that SOC of battery supplies with the demand of SOC, the battery is going to be discharging (OFF) mode [45, 46].

The proposed system of battery system is designed in Matlab/Simulink and it is presented in the Figure 3.13 below.

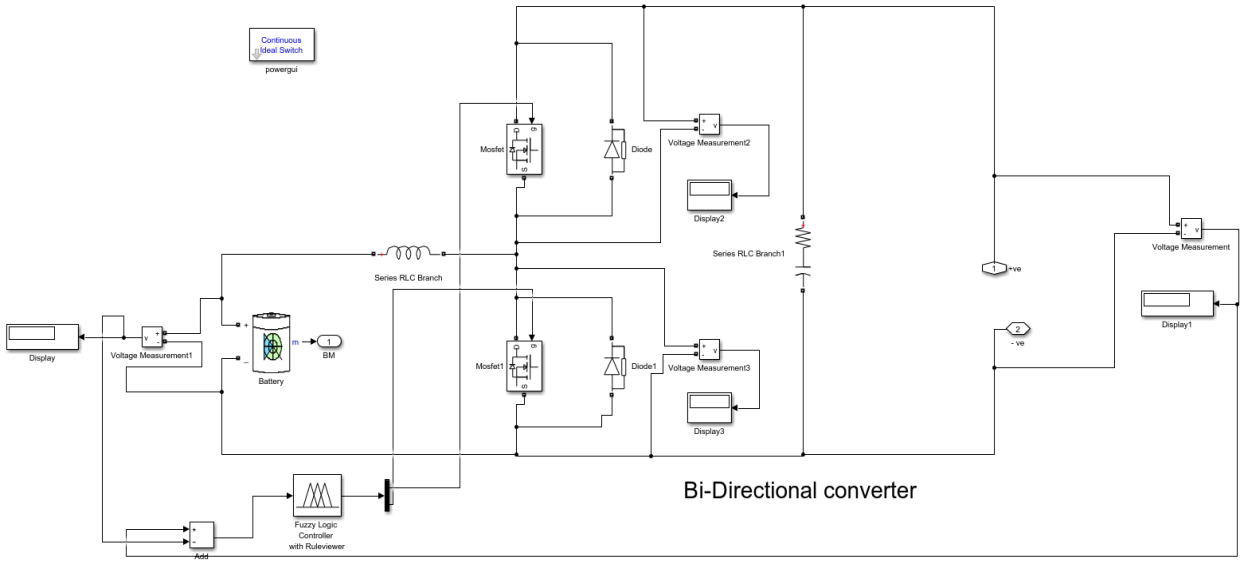

Figure 3.13 Fuzzy logic controller based battery system Simulink design

3.4 Voltage Source Converter Controller

The grid integration of the system can be completed by using the Voltage source controller. The controller is simulated in the Matlab/Simulink and it consists of phase locked loop, voltage regulator and signal generator. Figure 3.14 demonstrates the Simulink model of voltage source controller.

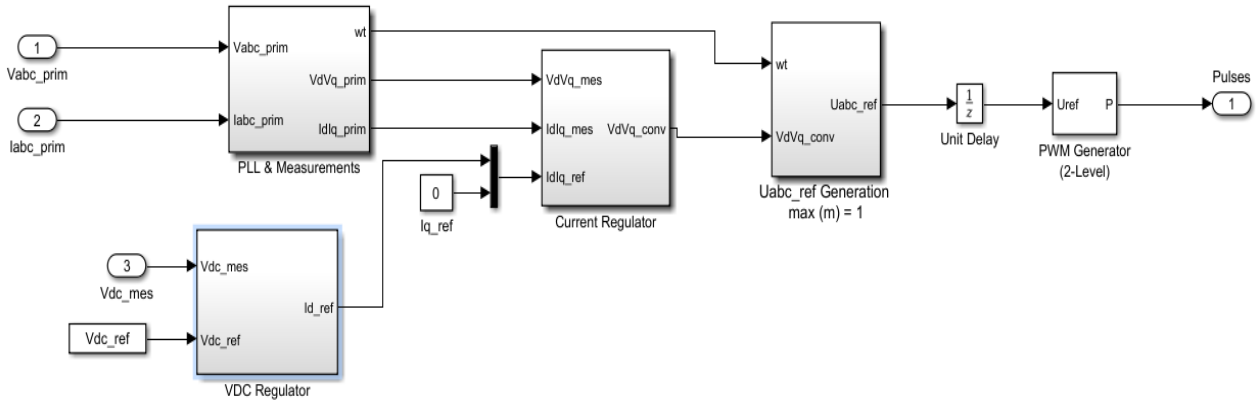

Figure 3.14 Simulink model of Voltage source converter controller

The voltage regulator has two inputs which are the reference voltage, Vdc_ref and the measured voltage Vdc_ref. The output of the regulator is d-phase current, Id_ref which is calculated in the given equation below [48, 49].

$$I_{d\_ref} = K_p \left(V_{dc_{ref}} - V_{ref}\right) + K_i \int \left(V_{dc_{ref}} - V_{ref}\right) dt \qquad (3.8)$$

On the other hand, the Iq_ref is equal to zero. The d and q currents are represented by Id_ref and Iq_ref. The integral constants are the Kp and Ki. The current regulator has the same constants which are Kp_cr and Ki_cr. In this way, the voltage values Vd and Vq can be obtained by using Equations (3.9) and (3.10).

$$V'_d = V_d\left[K_{p\_cr}\left(I_{d\_ref} - I_d\right) + K_{i\_cr} \int \left(I_{d\_ref} - I_d\right) dt\right] + LIq \qquad (3.9)$$

Id and Iq represent the currents of d and q which are transformed from 3-phase (abc). The difference between the reference voltage and actual voltage gives the error voltage which moves through to PI controller [50].

The system's real and reactive powers can be controlled by the current regulator, therefore, it plays a key role for that controller. There are two operation mode which are inverter and inductive modes. When the active power is generated, it operates as inverter. If the reactive power is drawn by the converter, the regulator works in inductive mode [49]. When the current flows out of the converter, it is called as positive current and Id and Iq are positive in both mode [48].

The other component is the phase locked loop and it operates for controlling of the inverter and also, the system's power phase can be tracked by PLL [49]. The Simulink model is given in the Figure 3.15.

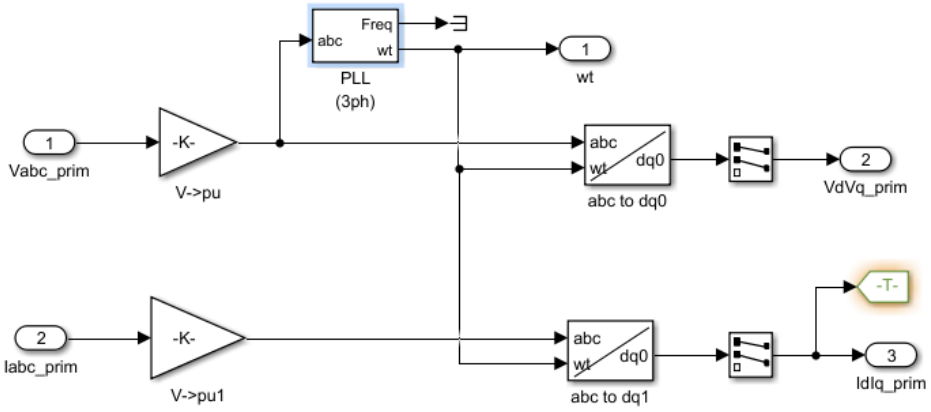

Figure 3.15 Phase Locked Loop Simulink model

CHAPTER 4

SIMULATION RESULTS & ANALYSIS

In this chapter, the results of simulated system which is the grid connected wind-solar power system with the battery, is presented and analyzed in detail. The MATLAB simulation results are discussed and compared. Also, they are tabulated as numerical in this part.

4.1 Maximum Power Point Tracking (MPPT) for Solar Power System

The wind-solar-battery power system is at a price and the constant efficiency cannot be obtained during either all day or under different weather conditions. Accordingly, MPPT methods provide the produce of maximum power effectively, while the general produce is pretty weak with approximately 8-16% efficiency.

4.1.1 Perturb and Observe Algorithm for MPPT of 10kW PV system

The voltage and current of PV are measured livingly depends on the conditions. Then, the power of PV is calculated by using the product of the measured values. This is the first power which is calculated depends on the minor changes in duty cycle. The second calculated power and the first one are compared each other. If the second calculated power is more than first one, the perturbation can be accepted as correct. P&O algorithm based MPPT is developed in Simulink under the various conditions in terms of irradiation and temperature. The obtained results of the

simulation and efficiency of PV system waveform are illustrated in Figure 4.1 and the numerical results are given in Table 4.1.

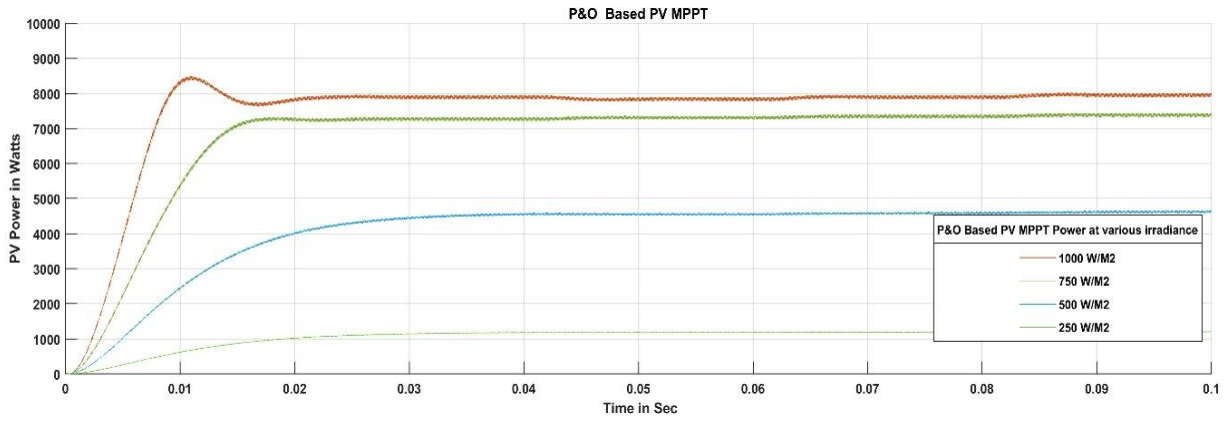

Figure 4.1 P&O Algorithm based MPPT of 10kW PV system output waveform

Table 4.1 Efficiency of P&O Algorithm

#	Irradiance W /M^2	PV Output in Watts	Efficiency %
1	1000	8450	84.50
2	750	7250	96.66
3	500	4550	91
4	250	1350	54

4.1.2 MPPT of 10kW PV system based on Fuzzy Logic Controller

The FLC method is used in the proposed solar system and it is demonstrated in Figure 4.2. The voltage and current are the inputs for that controller method. The trapezoidal shape is preferred among the presented membership functions [44] and the inputs are converted to fuzzy set by this method. This rule based controller system is compared with the observed value and the if-then rule that is for the duty cycle selection is applied based on the error. The center of gravity method is implemented in this part in order to convert the fuzzy set value to crisp set. The obtained signal by PWM generator, produces the pulse which conveys to DC-DC converter.

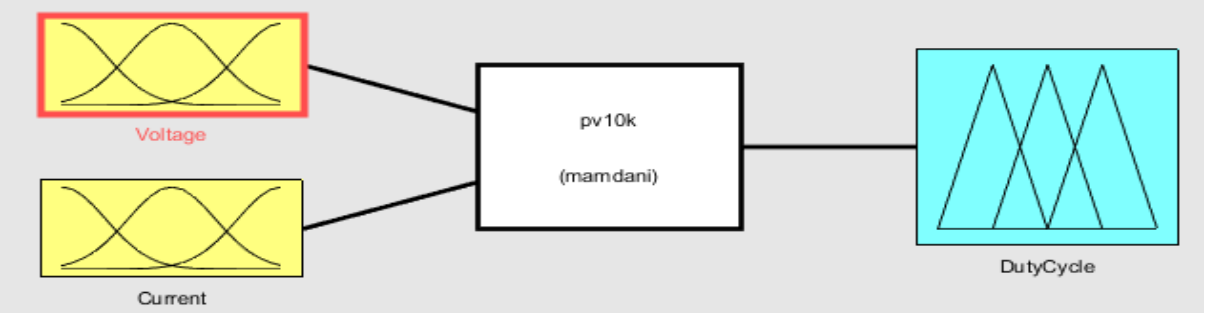

Figure 4.2 Fuzzy controller based MPPT of PV System design

The Fuzzy input membership function (PV Voltage) has been develop in Matlab/Simulink. The membership ranges selected based on PV system as shown in Figure 4.3. The Fuzzy input membership function (PV Current) has been develop in Matlab/Simulink. The membership ranges selected based on PV system as shown in Figure 4.4. The output membership function of FLC is duty cycle and it is developed in Matlab/Simulink as demonstrated in Figure 4.5. Finally, the developed fuzzy rules base which depends on inputs and outputs, are illustrated in Figure 4.6 and Figure 4.7.

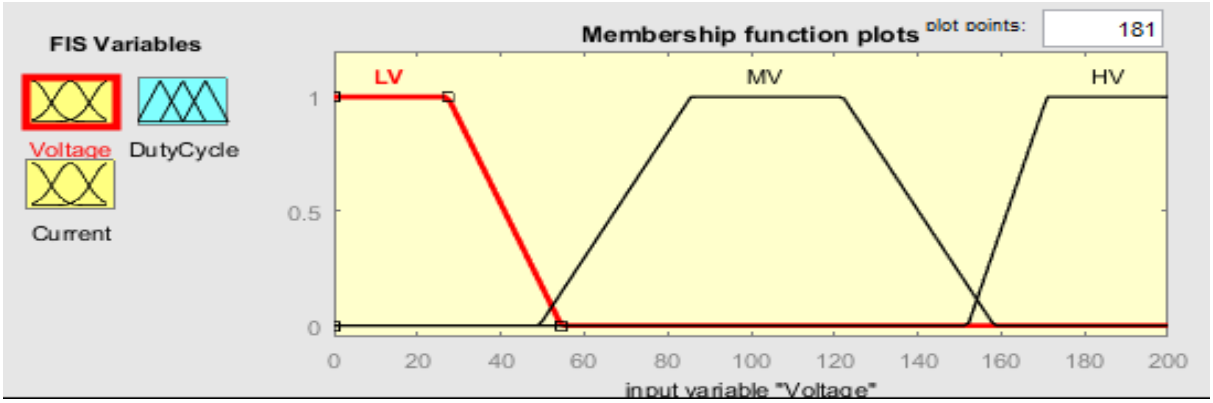

Figure 4.3 Fuzzy Input membership function (PV Voltage)

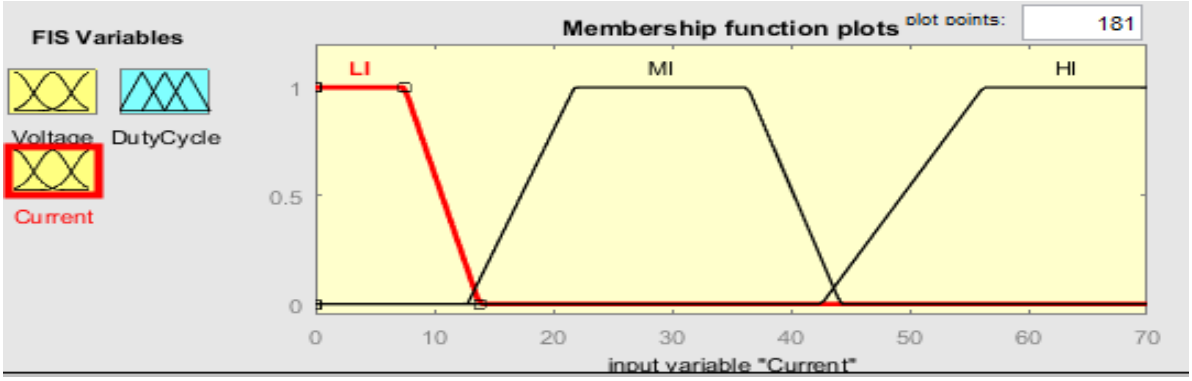

Figure 4.4 Fuzzy Input membership function (PV Current)

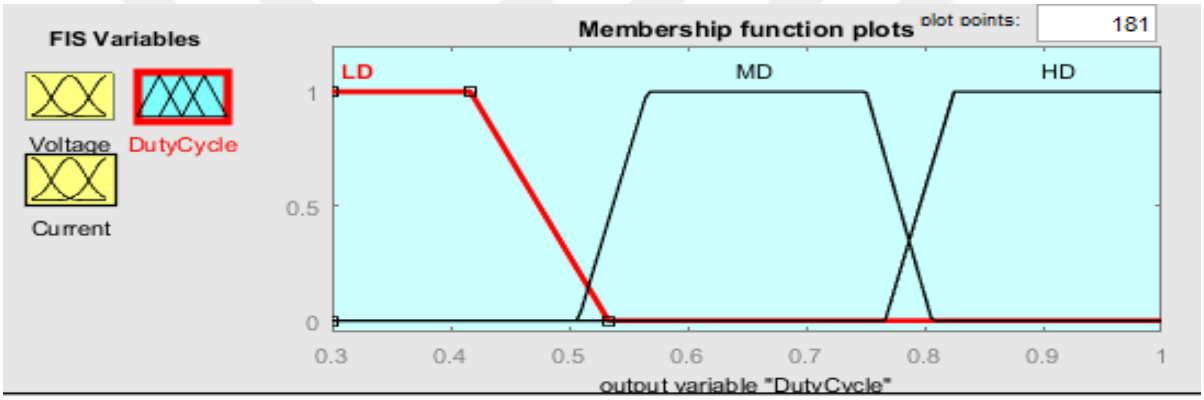

Figure 4.5 Fuzzy output membership function (Duty Cycle)

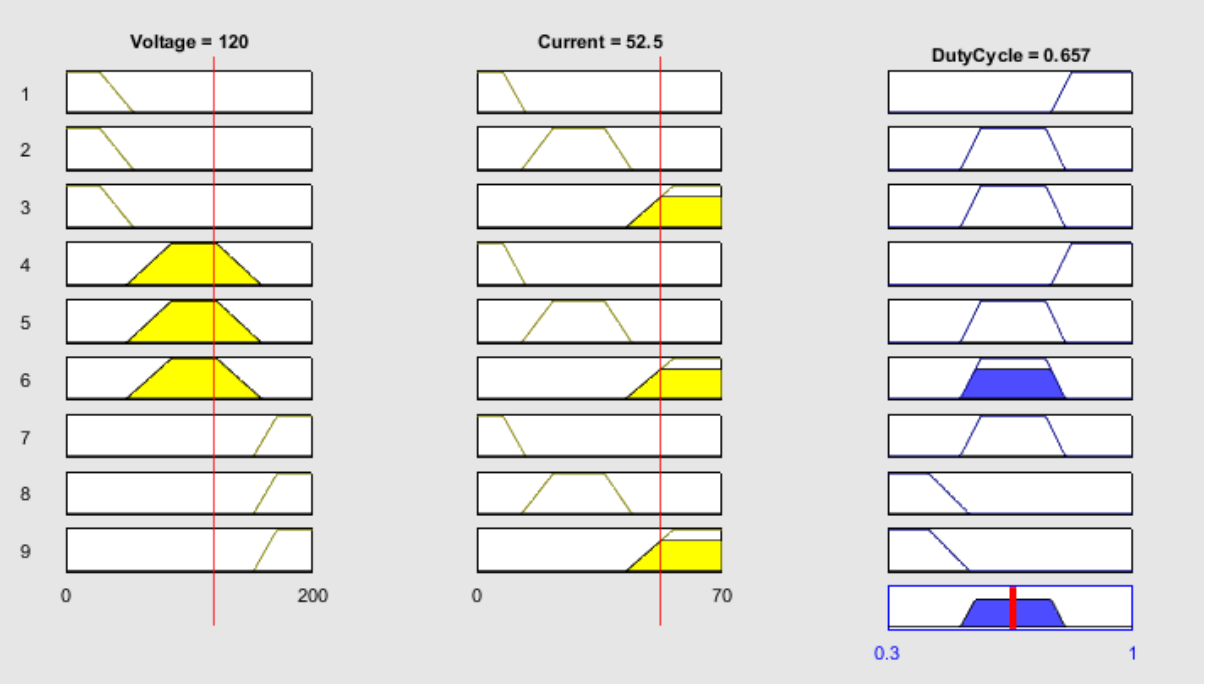

Figure 4.6 Fuzzy Rules for MPPT Controller of PV System

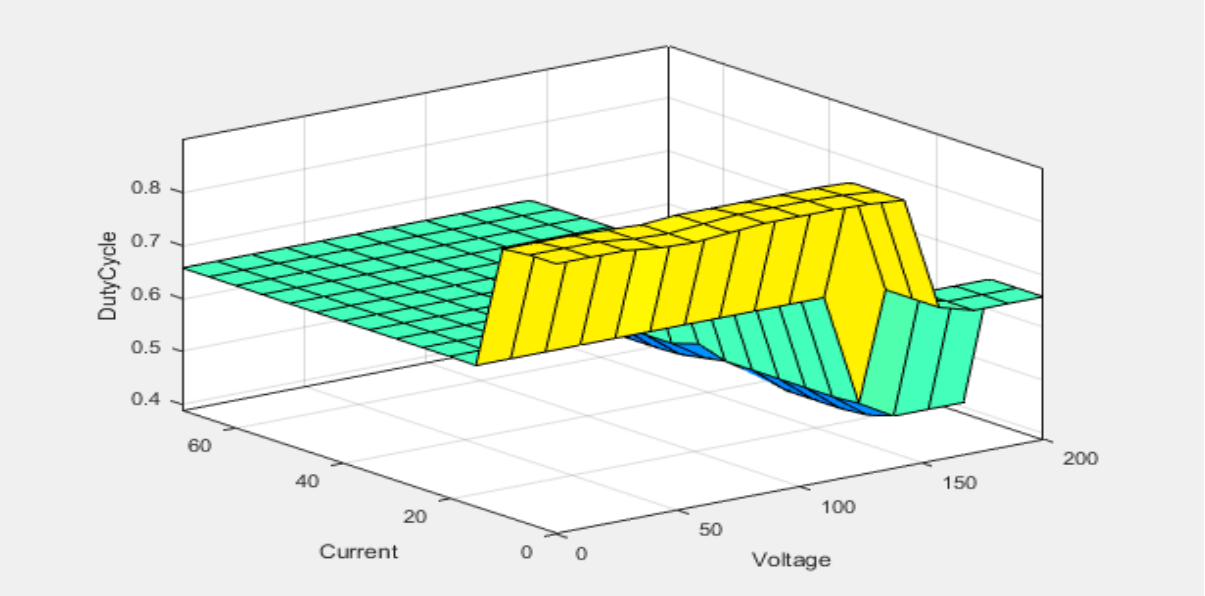

Figure 4.7 Fuzzy Surface view for MPPT Controller of PV System

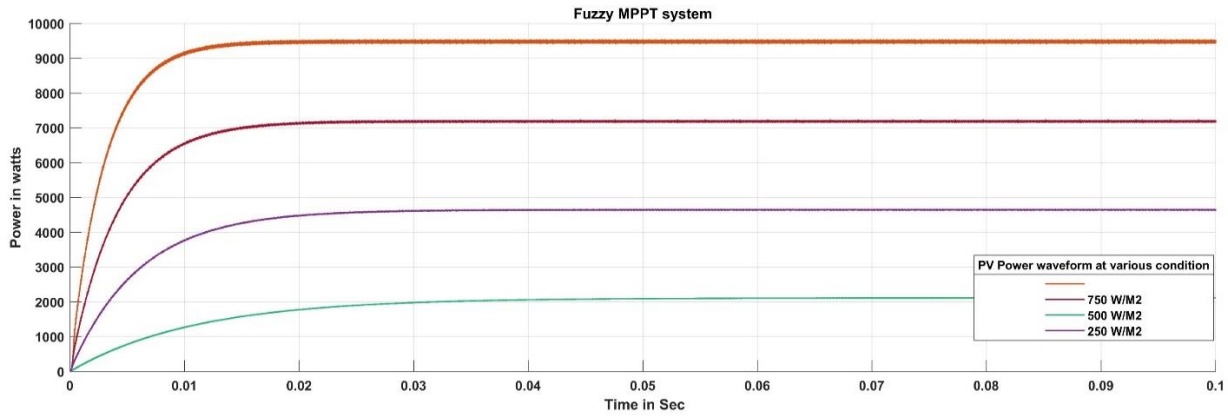

Figure 4.8 Fuzzy based 10 kW PV System Output Power Waveform at various irradiance

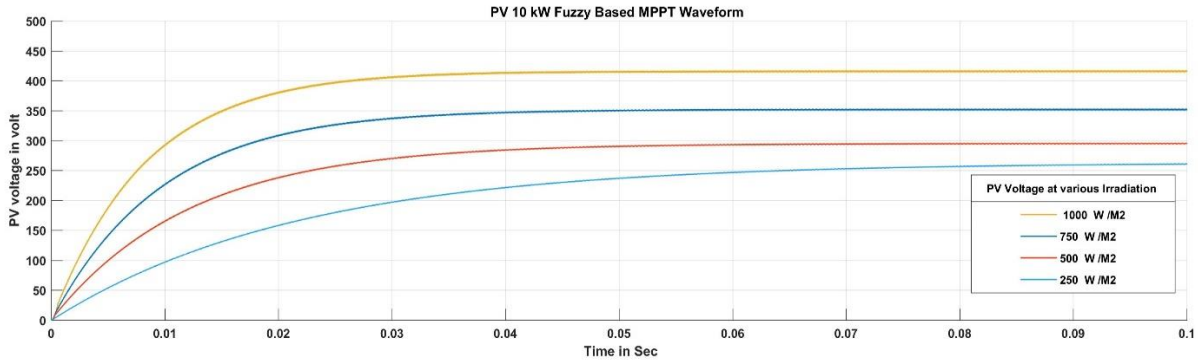

Figure 4.9 Fuzzy based 10 kW PV System Output Voltage Waveform at various irradiance

4.1.3 Result Discussion and Comparison

The proposed Fuzzy based MPPT of 10 kW PV power system has been developed in Matlab/Simulink and simulated at various weather conditions. The proposed system has been simulated at irradiance of 250 W/M^2 , 500 W/M^2 , 750 W/M^2 and 1000 W/M^2 respectively. The simulated results such as PV power and BOOST Converter voltage are presented in Figure 4.8 and Figure 4.9 respectively. Finally, the results from the simulation and efficiency of the system are tabulated in Table 4.2. In order to prove the performance effectiveness of the proposed Fuzzy controller based MPPT system is compared with P&O based MPPT system as shown in Table 4.3.

Table 4.2 Efficiency of Fuzzy Algorithm

#	Irradiance W /M^2	PV Output in Watts	Efficiency %
1	1000	9529	95
2	750	7220	96
3	500	4670	93
4	250	2150	86

Table 4.3 Comparison of Efficiency of P&O and Fuzzy Algorithm

#	P&O	Fuzzy	Improved %
1	84	95	10
2	96	96	0
3	91	93	2%
4	54	86	32%

4.2 Maximum Power Point Tracking (MPPT) for Wind Power System

The wind energy conversion systems have not any constant generation process like in the solar systems, therefore, the system is tracking by the P&O and Fuzzy control methods based on MPPT. In this way, the generated wind energy is reached to maximum power. The proposed systems are compared and kindly tabulated.

4.2.1 Perturb and Observe Algorithm based MPPT of Wind Power System

The voltage and current of wind are measured depends on the weather conditions. Then, the power of wind is calculated by using the product of the measured values. This is the first power which is calculated depends on the minor changes in duty cycle. The second calculated power and the first one are compared each other. If the second calculated power is more than first one, the perturbation can be accepted as correct. P&O algorithm based MPPT is developed in Simulink

under the various conditions. The voltage and current waveforms of the wind system RMS are presented in Figure 4.10. The simulation results of wind energy system, power output versus wind speed waveform is illustrated in Figure 4.11. Also, another simulation results that generator RPM and Duty Cycle waveforms are presented in Figure 4.12. Finally, the various weather condition such 5 m/s, 7 m/s, 9 m/s, 11 m/s and 12 m/s are simulated and MPPT of wind power system waveforms are demonstrated in Figure 4.13 and Figure 4.14. The results of simulation are tabulated in Table 4.4.

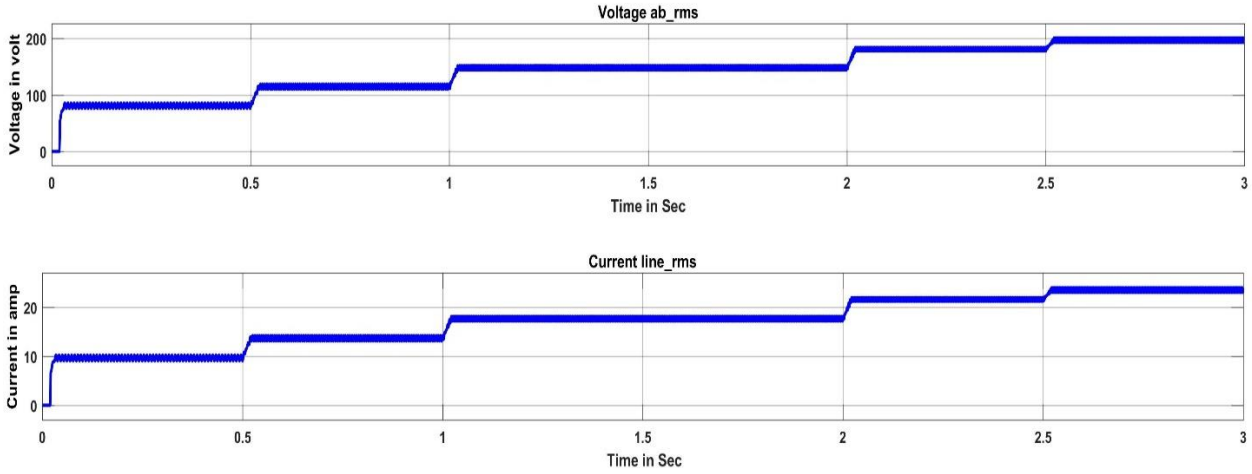

Figure 4.10 WECS Voltage and Current RMS waveform

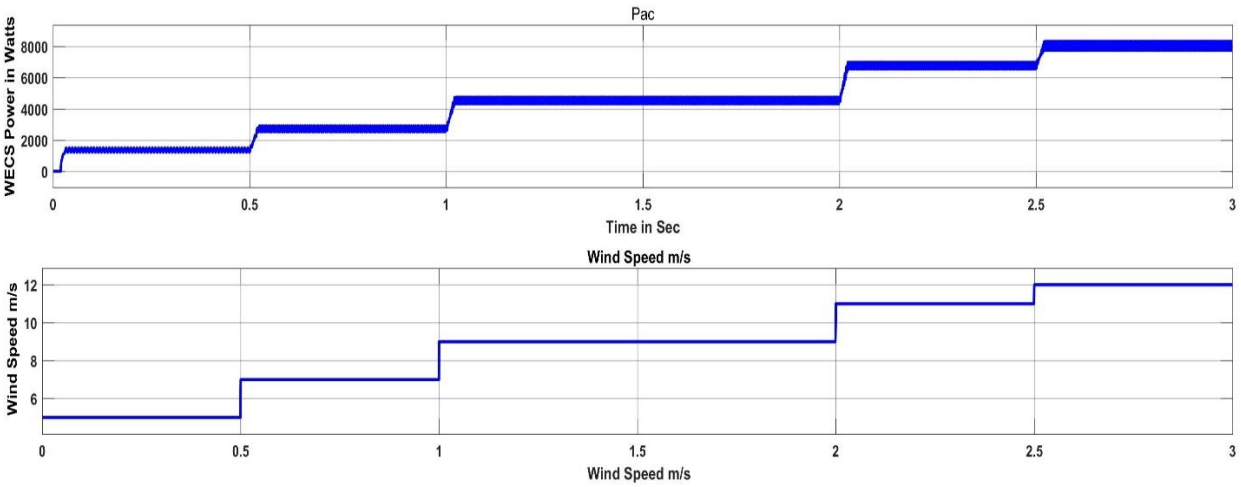

Figure 4.11 WECS Power output and Wind Speed waveform

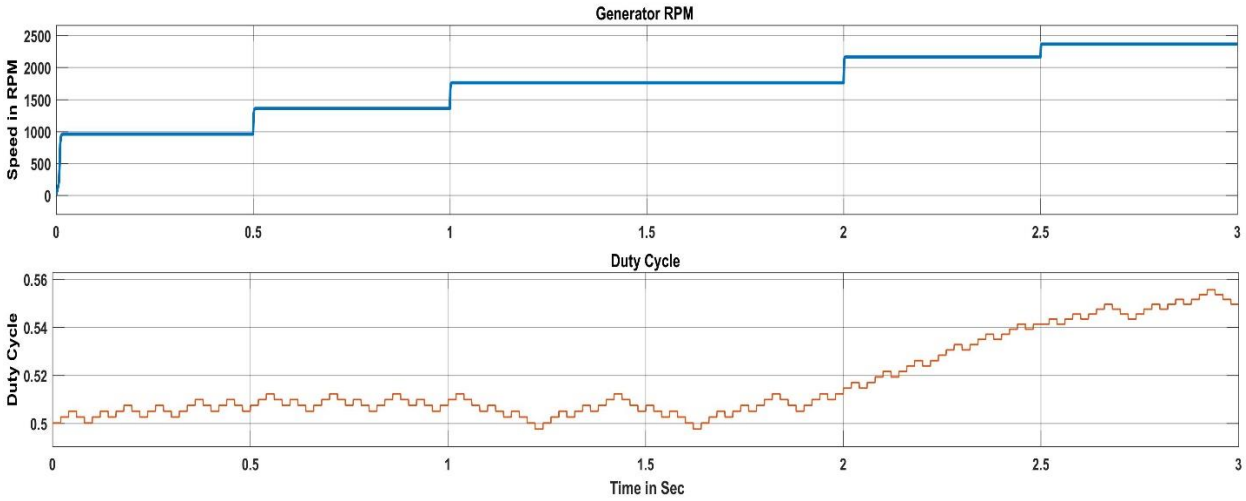

Figure 4.12 WECS generator RPM and Duty Cycle waveform

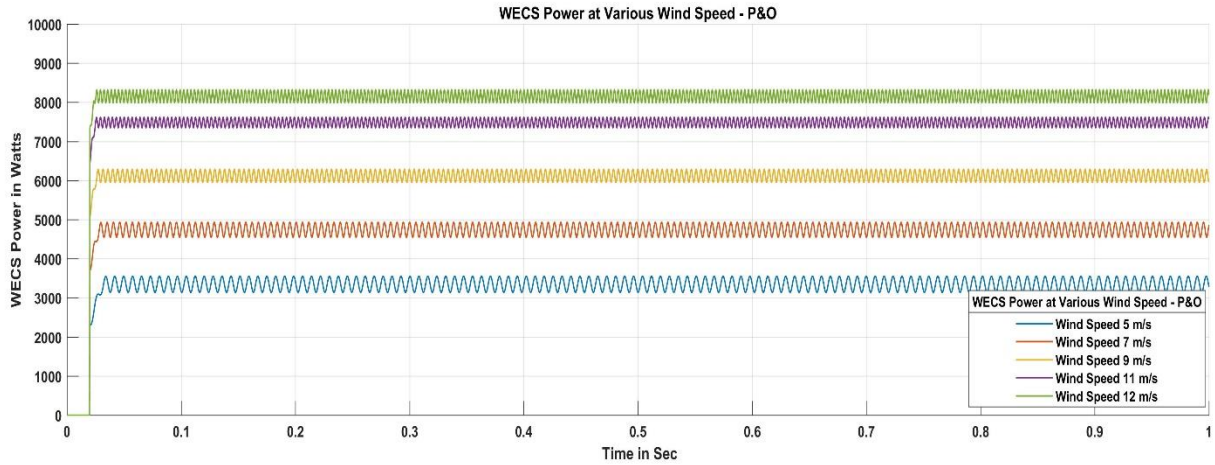

Figure 4.13 WECS Power output waveform at various Wind Speed

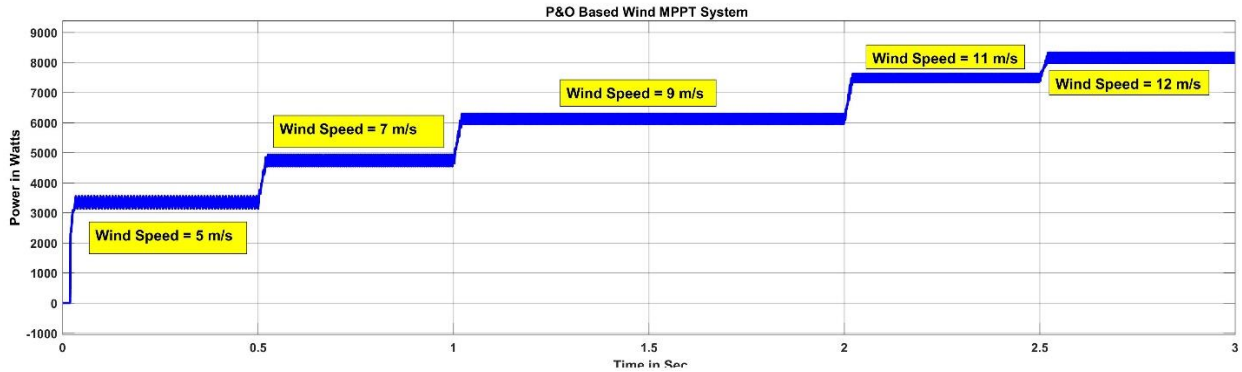

Figure 4.14 WECS Power output waveform at various Wind Speed

Table 4.4 Efficiency of P&O Algorithm

#	Wind Speed m/s	WECS Output in Watts	Efficiency %
1	12	8324	83.2
2	11	7618	83.1
3	9	6253	83.3
4	7	4923	84.3
5	5	3543	85

4.2.2 Fuzzy Logic Controller for MPPT of Wind Power System

The fuzzy logic controller is designed for MPPT controller of wind energy system as presented in Figure 4.15. The proposed system is developed in Simulink. Its performance analyze is made under different weather condition. The proposed fuzzy MPPT controller has two inputs which are the voltage and current of wind energy system and they implemented by using trapezoidal membership function as illustrated in Figure 4.16 and Figure 4.17. The output of fuzzy control is trapezoidal membership function, namely duty cycle is demonstrated in Figure 4.18. The input 1 and input 2 has three different membership functions that are Low, Medium and High as well as the output has three membership functions that are Low, Medium and High. The proposed fuzzy based controller is developed by trapezoidal type for fuzzification and center of gravity method for Defuzzification. The Fuzzy rules are developed based on input and output parameters of wind energy system are presented in Figure 4.19 and Figure 4.20.

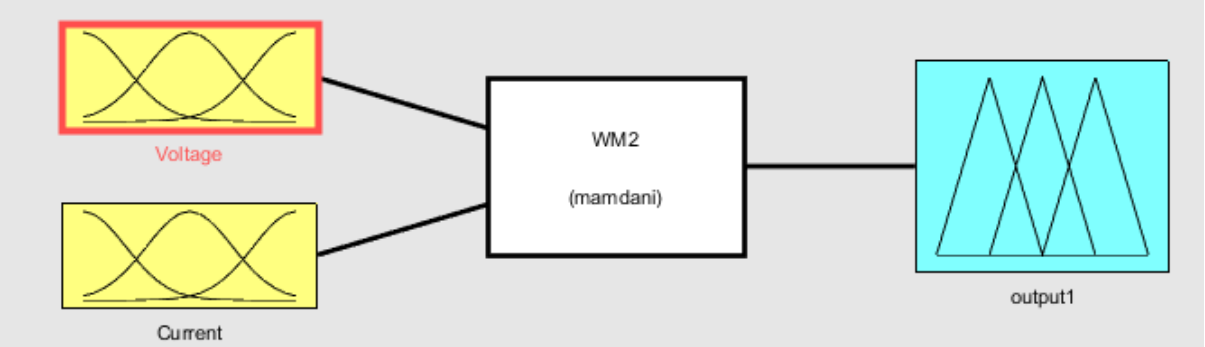

Figure 4.15 Fuzzy based WECS MPPT design

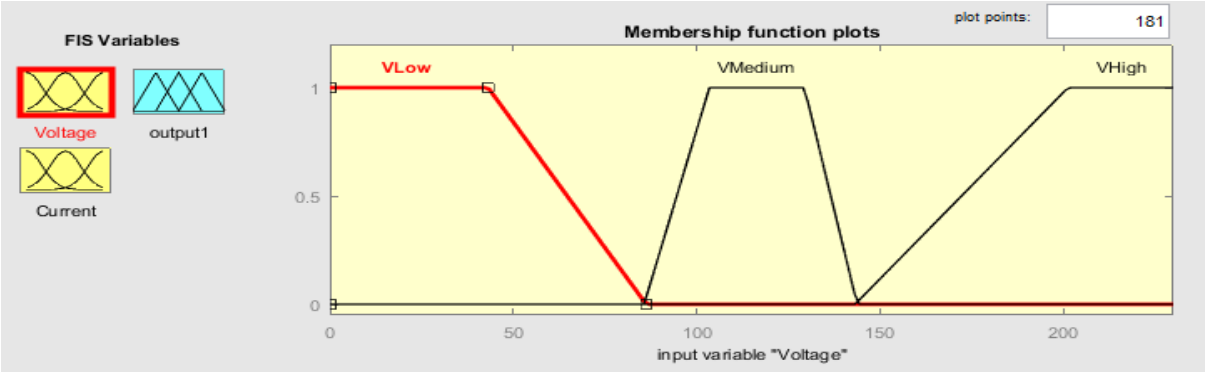

Figure 4.16 Fuzzy input membership function for WECS (Wind Voltage)

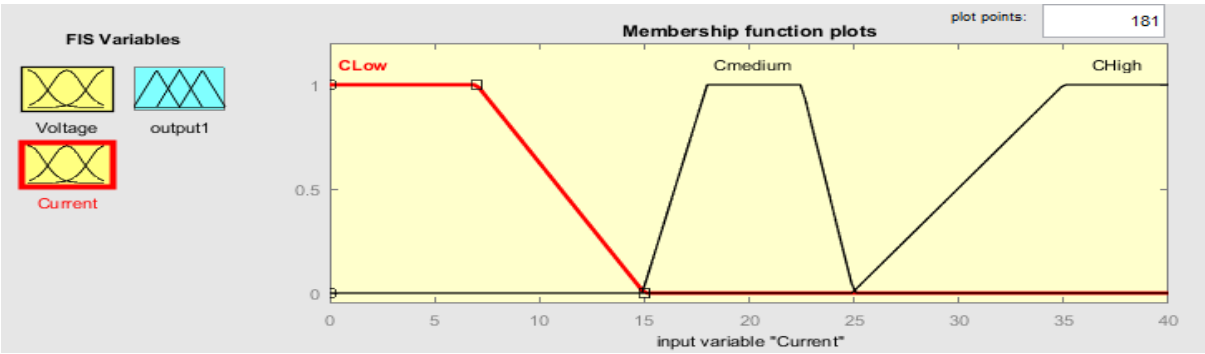

Figure 4.17 Fuzzy input membership function for WECS (Wind Current)

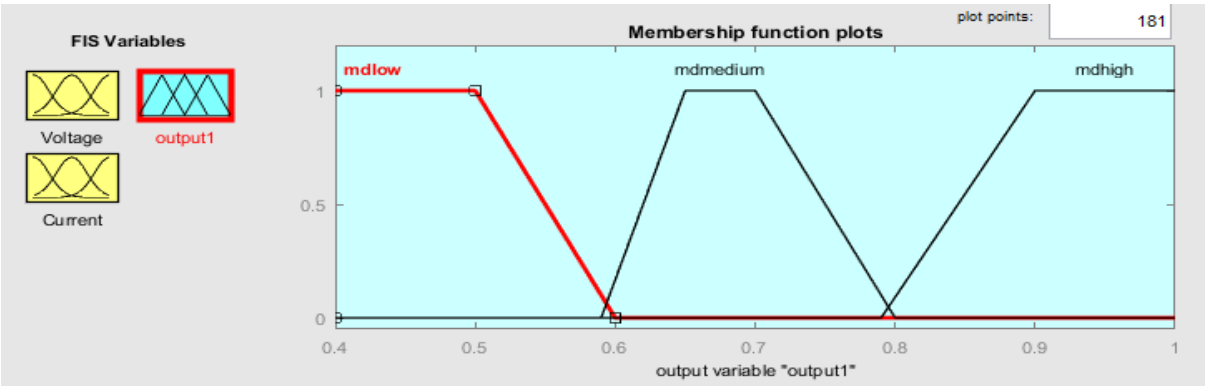

Figure 4.18 Fuzzy output membership function for WECS (Duty Cycle)

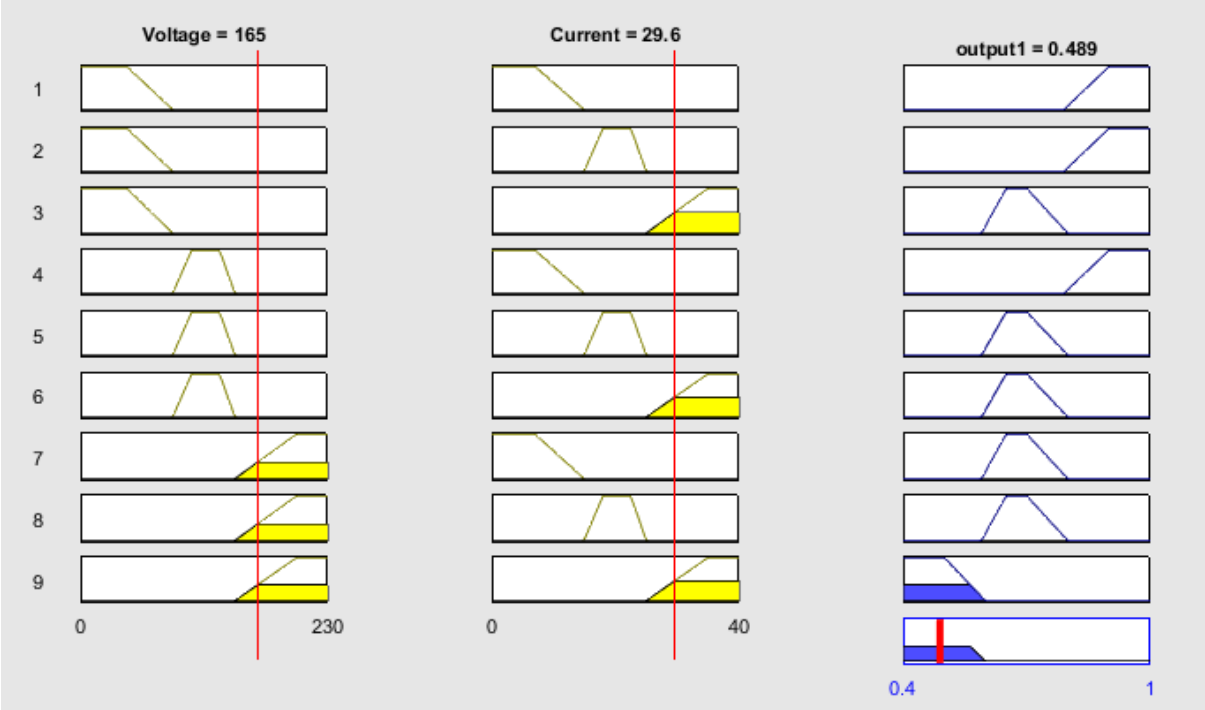

Figure 4.19 Fuzzy controller Rules for WECS MPPT

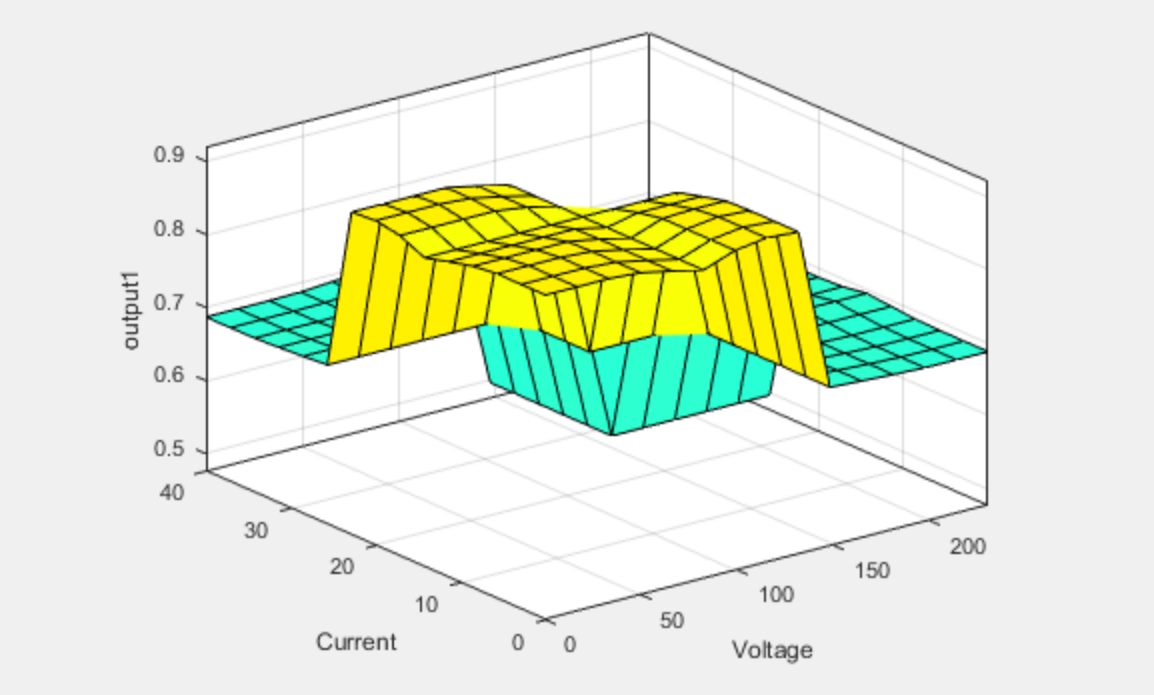

Figure 4.20 Fuzzy controller surface view for WECS MPPT

4.2.3 Result Discussion and Comparison

The Fuzzy based MPPT of WECS is developed in Matlab/Simulink and simulated at various weather conditions such as 5 m/s, 7 m/s, 9 m/s, 11 m/s and 12 m/s. The wind energy system's RMS voltage and current waveforms at under various weather condition are presented in Figure 4.21. Figure 4.22 illustrates the wind energy system power output versus wind speed waveform. The generator speed and duty cycle simulation results are demonstrated in Figure 4.23. The wind energy conversion system is simulated at various wind speed and presented the Fuzzy based MPPT of WECS output waveform as illustrated in Figure 4.24 to Figure 4.30 respectively. Finally, the results from simulation and efficiency of system are tabulated in Table 4.5. In order to prove the performance effectiveness of proposed Fuzzy controller based MPPT system is compared with P&O based MPPT system for the wind energy system, as shown in Table 4.6.

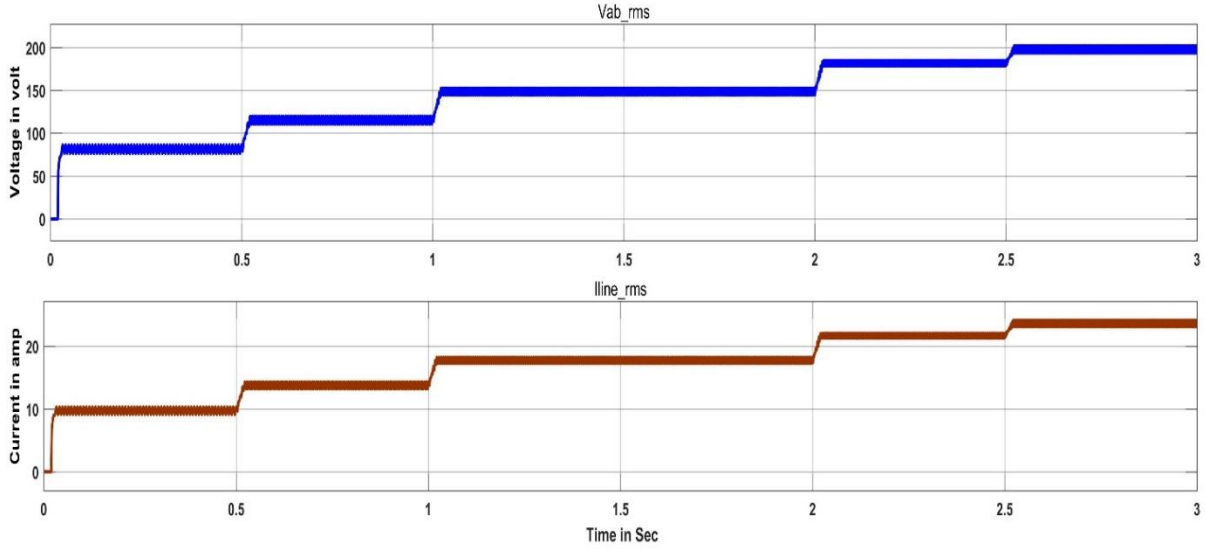

Figure 4.21 WECS Voltage and Current RMS waveform (Fuzzy)

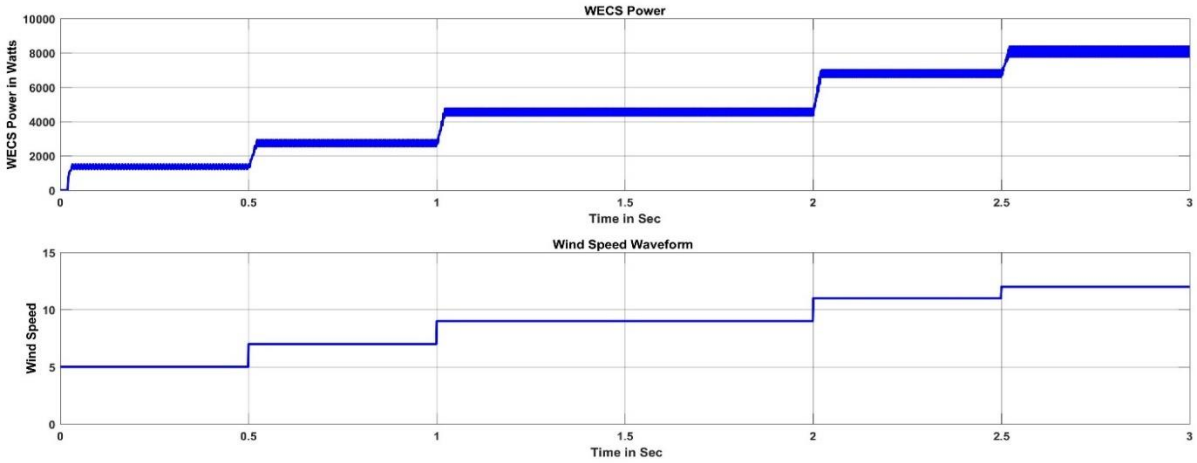

Figure 4.22 WECS Output Power and Wind Speed waveform (Fuzzy)

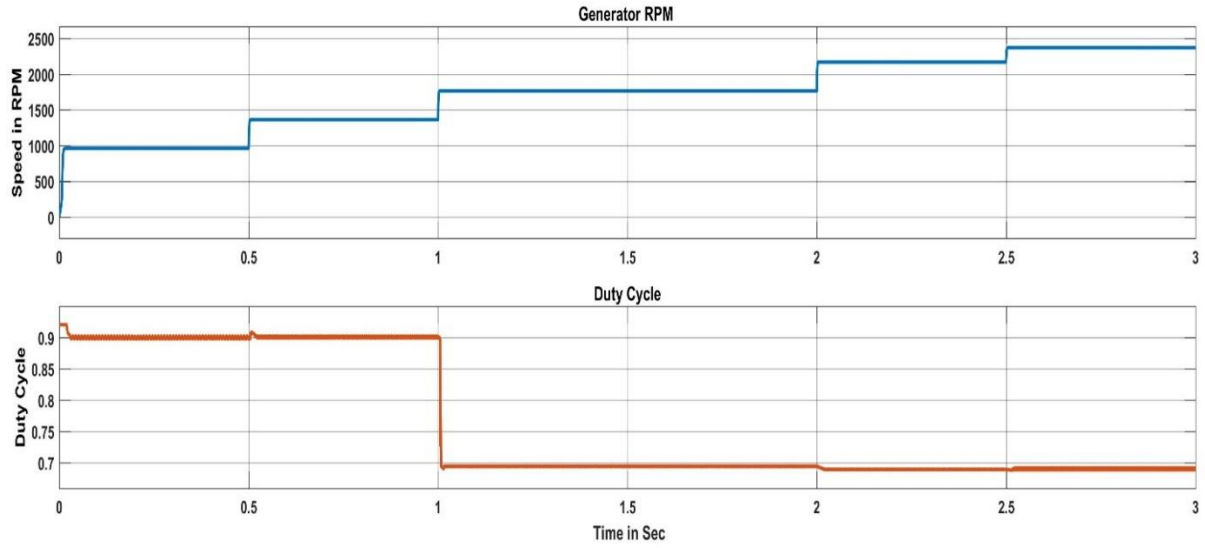

Figure 4.23 WECS generator RPM and Duty Cycle waveform (Fuzzy)

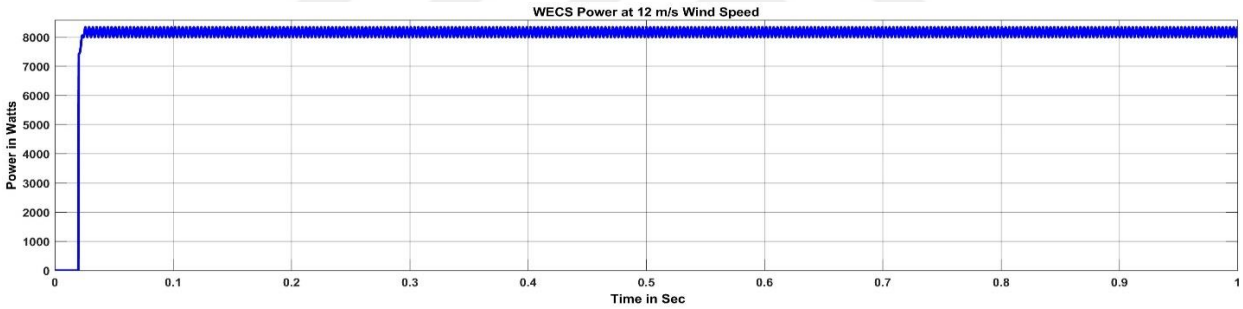

Figure 4.24 WECS Output Power waveform at 12 m/s Wind Speed (Fuzzy)

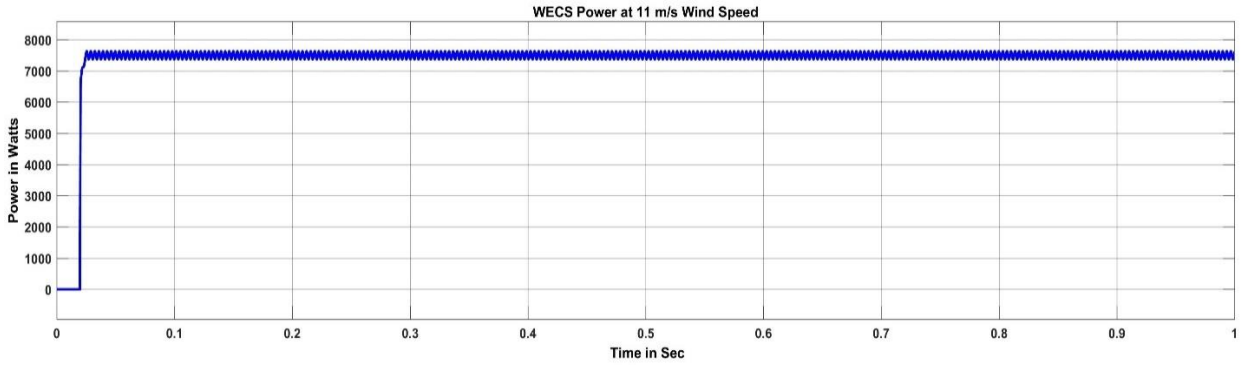

Figure 4.25 WECS Output Power waveform at 11 m/s Wind Speed (Fuzzy)

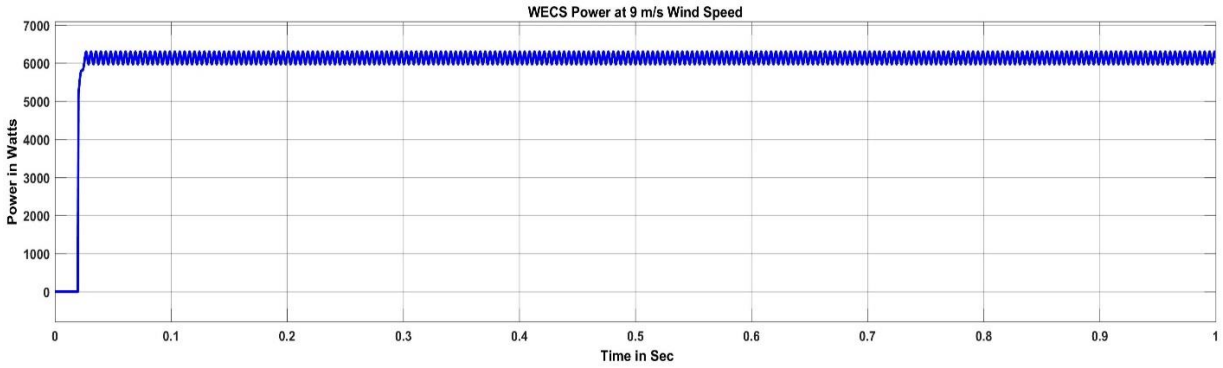

Figure 4.26 WECS Output Power waveform at 9 m/s Wind Speed (Fuzzy)

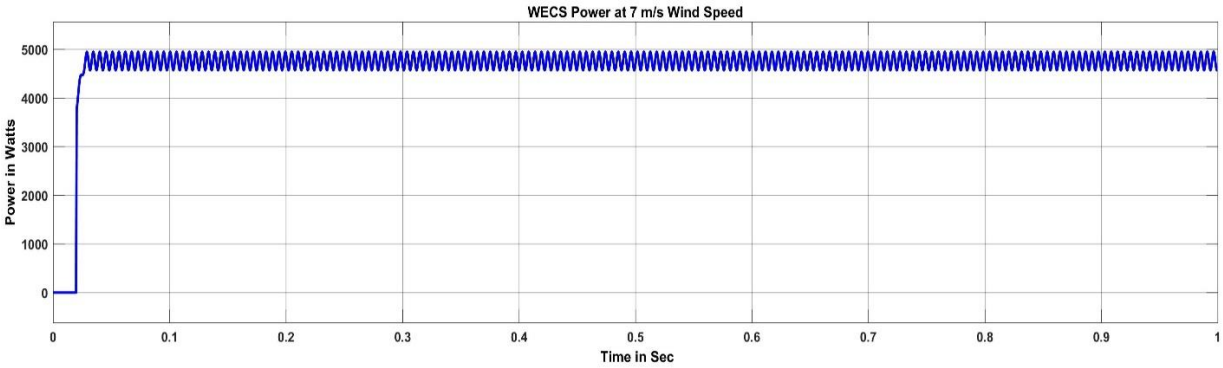

Figure 4.27 WECS Output Power waveform at 7 m/s Wind Speed (Fuzzy)

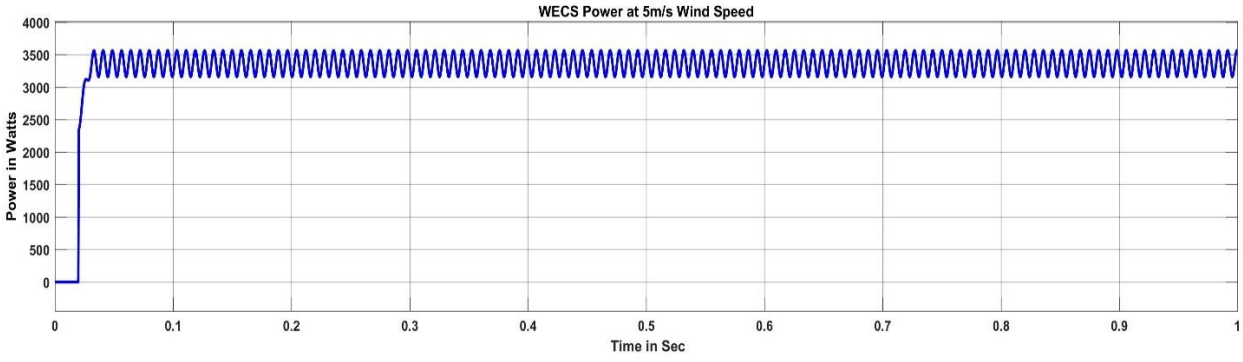

Figure 4.28 WECS Output Power waveform at 5 m/s Wind Speed (Fuzzy)

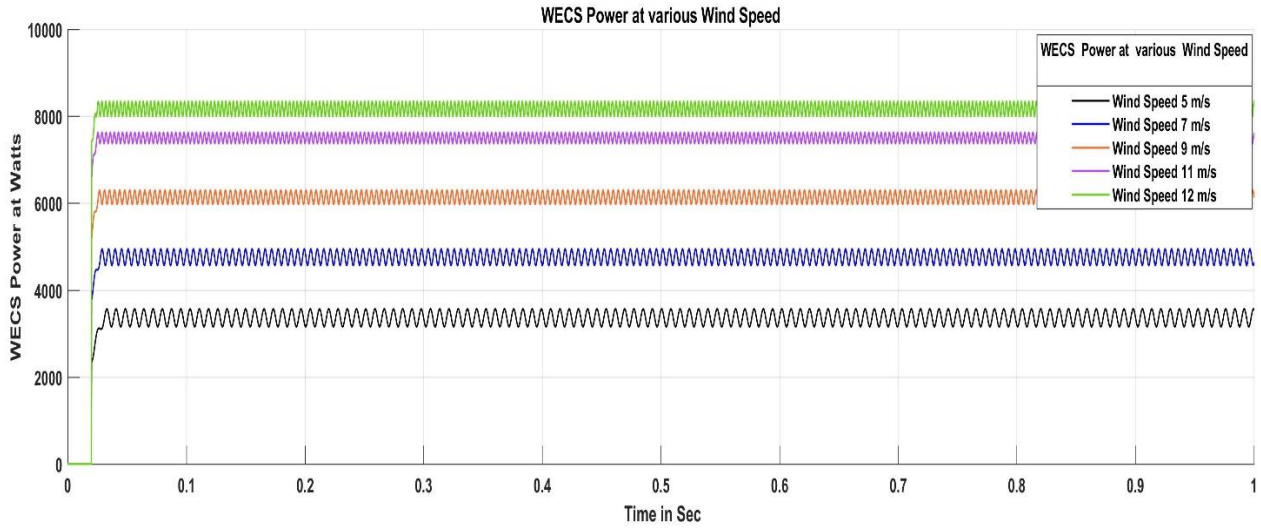

Figure 4.29 WECS Power output waveform at various Wind Speed (Fuzzy)

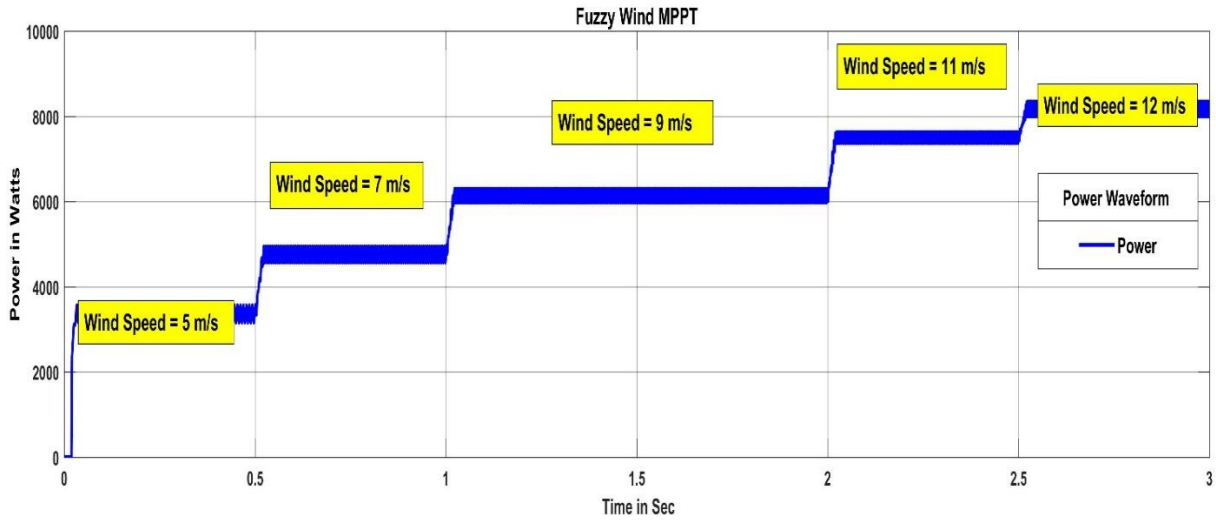

Figure 4.30 WECS Power output waveform at various Wind Speed (Fuzzy)

Table 4.5 Efficiency of MPPT Fuzzy Algorithm

#	Wind Speed m/s	WECS Output in Watts	Efficiency %
1	12	8345	83.45
2	11	7620	83.13
3	9	6302	84.02
4	7	4929	84.5
5	5	3561	85.4

Table 4.6 Comparison of Efficiency of MPPT Fuzzy and P&O Algorithm

#	P&O - Efficiency %	Fuzzy - Efficiency %
1	83.2	83.45
2	83.1	83.13
3	83.3	84.02
4	84.3	84.5
5	85	85.4

4.3 Battery management system

In the wind-solar power systems, the battery is the important part to store the generated energy. The Lead-Acid battery and its controller parts are designed in order to increase the performance of that hybrid system, since they are not producing at a constant rate. In this thesis, the battery system can operate on the battery modes which are charging and discharging. Also, the system output can be managed by battery.

4.3.1 Fuzzy Based Battery management system

The battery system is developed as the fuzzy logic controller based in the Matlab/Simulink. Figure 4.31 shows the fuzzy design of battery system. The battery system is combined with bi-directional converter for the battery charging or discharging through this converter. This converter has two power electronics switches; Q1 and Q2. The proposed fuzzy controller's operation depends on the status of that switches. The Fuzzy controller has one input membership function which is the value of difference between load power and renewable energy power as illustrated in Figure 4.32. Two output of the membership function are developed to operate on the power electronics switches (Q1 and Q2) based on input value as expressed in Figure 4.33 and Figure 4.34. Finally, the fuzzy rules are applied depends on the input and output parameters. The proposed

grid integration of solar and wind power systems are simulated in Matlab/Simulink with the battery system. In these studies, there are two cases which are considered; case 1: Load demand is less than power of renewables and case 2: Load demand is greater than power of renewables. For case 1, the simulation results are, such as PV power, wind power, load demand and battery power presented in Figure 4.36. The load voltage and load current are given in Figure 4.37. For case 2, the simulation results are, such as PV power, wind power, load demand and battery power presented in Figure 4.38. The load voltage and load current are given in Figure 4.39. The grid voltage waveform of the power distributed grid is presented in Figure 4.40. Finally, the THD values of the current and voltage are presented in Figure 4.41 and Figure 4.42 respectively.

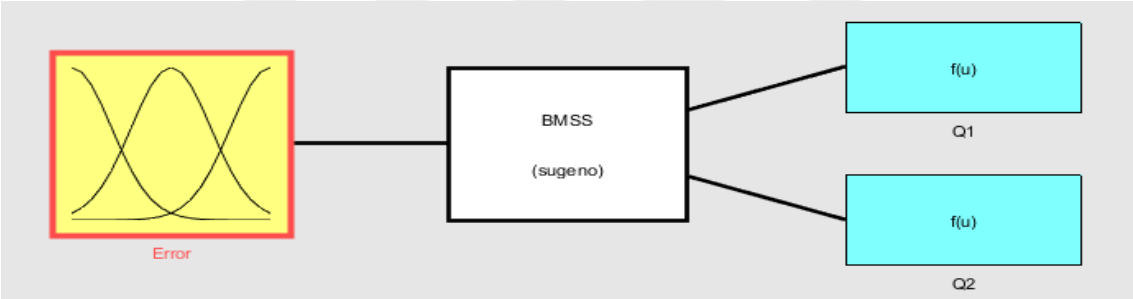

Figure 4.31 Fuzzy Design for Battery Management System

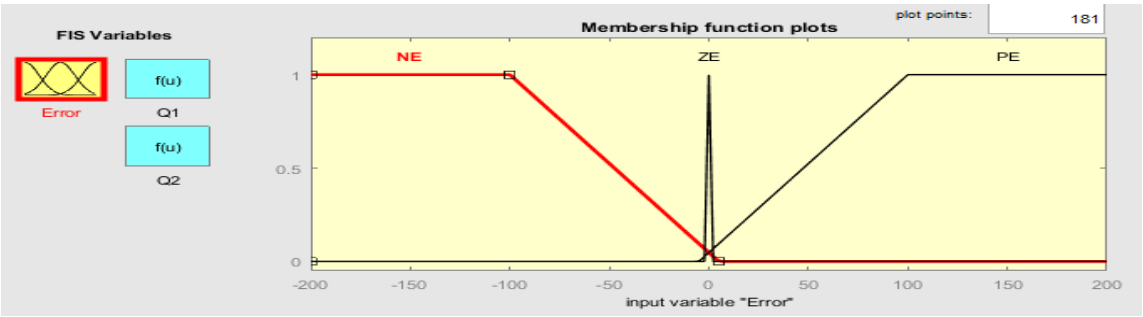

Figure 4.32 Fuzzy input membership function for Battery Management System

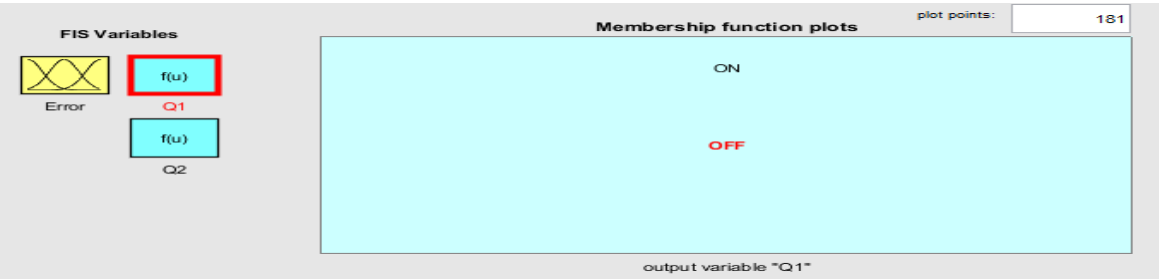

Figure 4.33 Fuzzy output membership function for Battery Management System

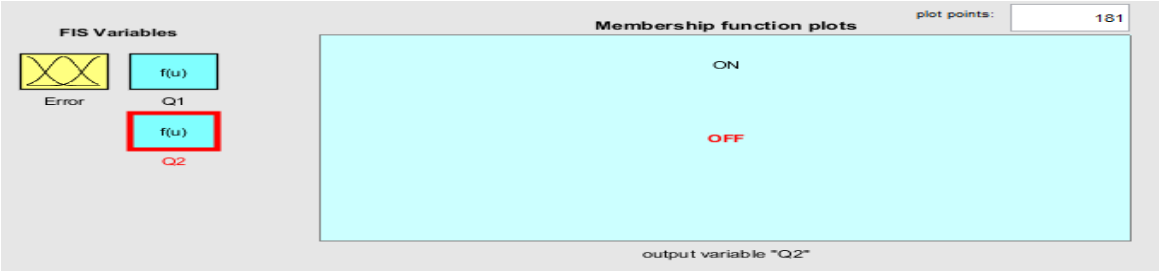

Figure 4.34 Fuzzy output membership function for Battery Management System

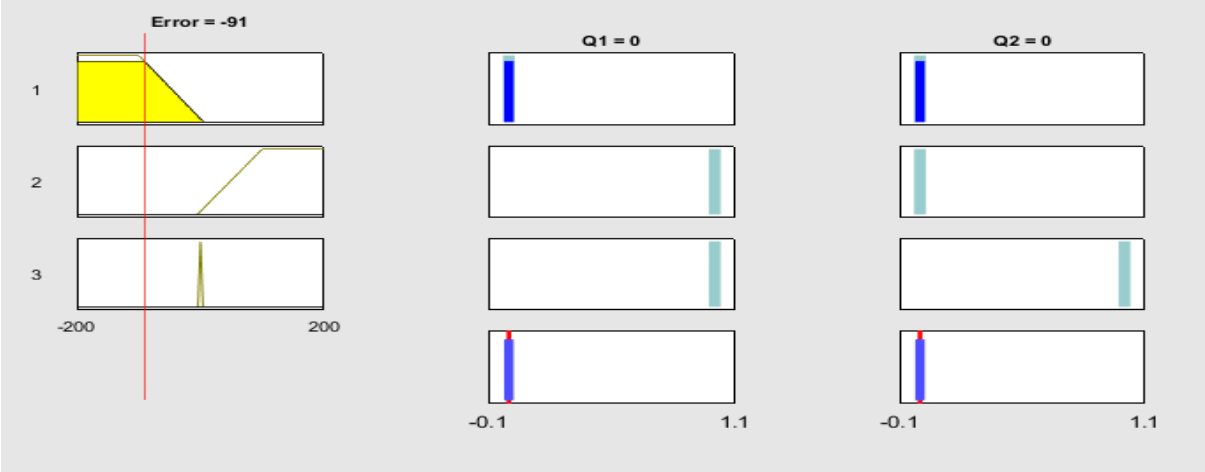

Figure 4.35 Fuzzy Controller rules for Battery Management System

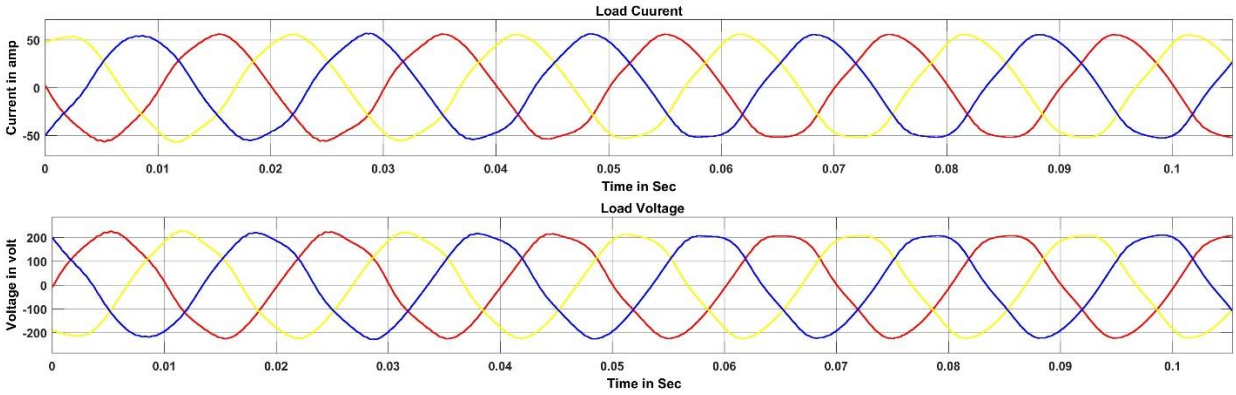

Figure 4.36 Voltage and Current waveform for smaller Load

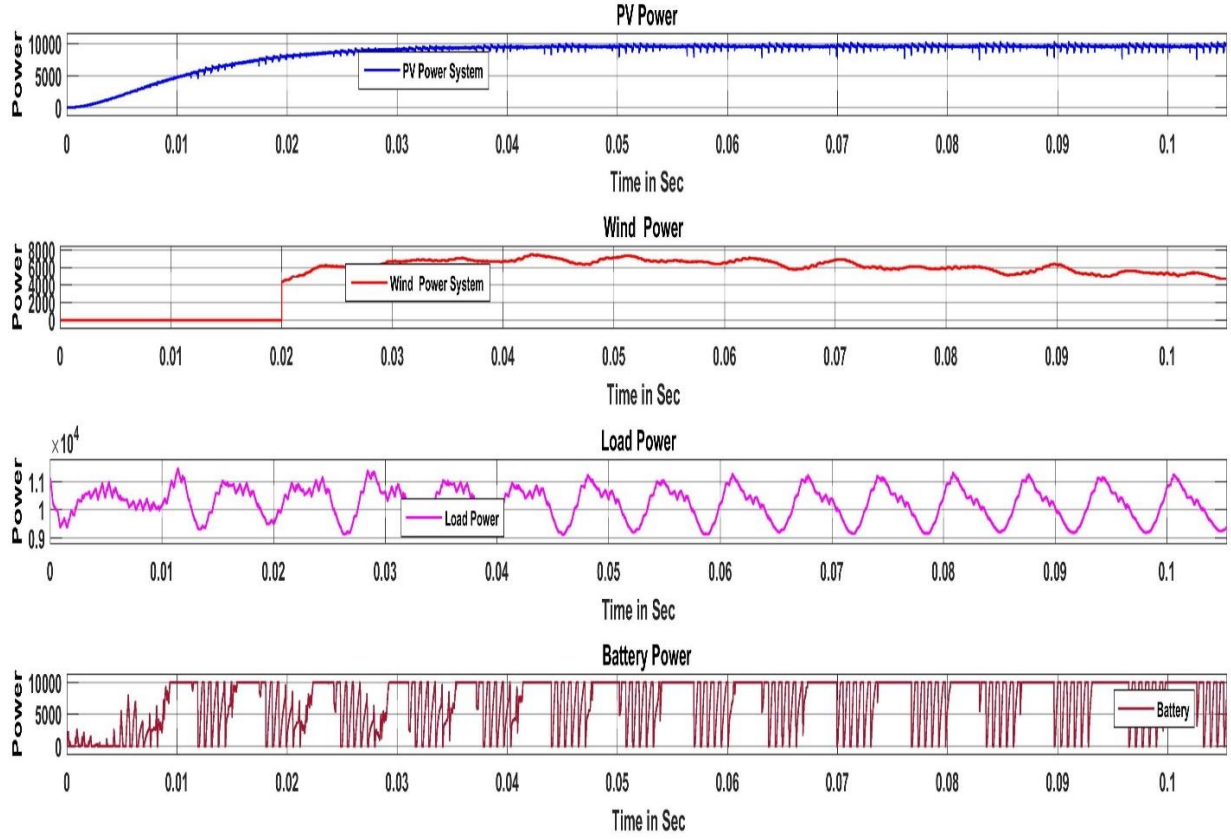

Figure 4.37 Power Waveform at various sources under different conditions for smaller load

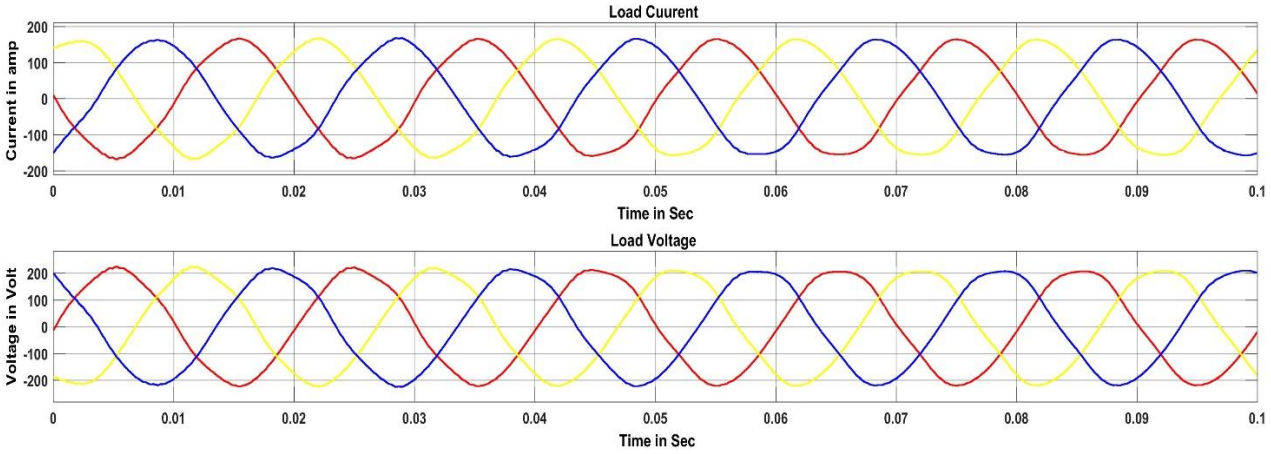

Figure 4.38 Voltage and Current waveform for large Load

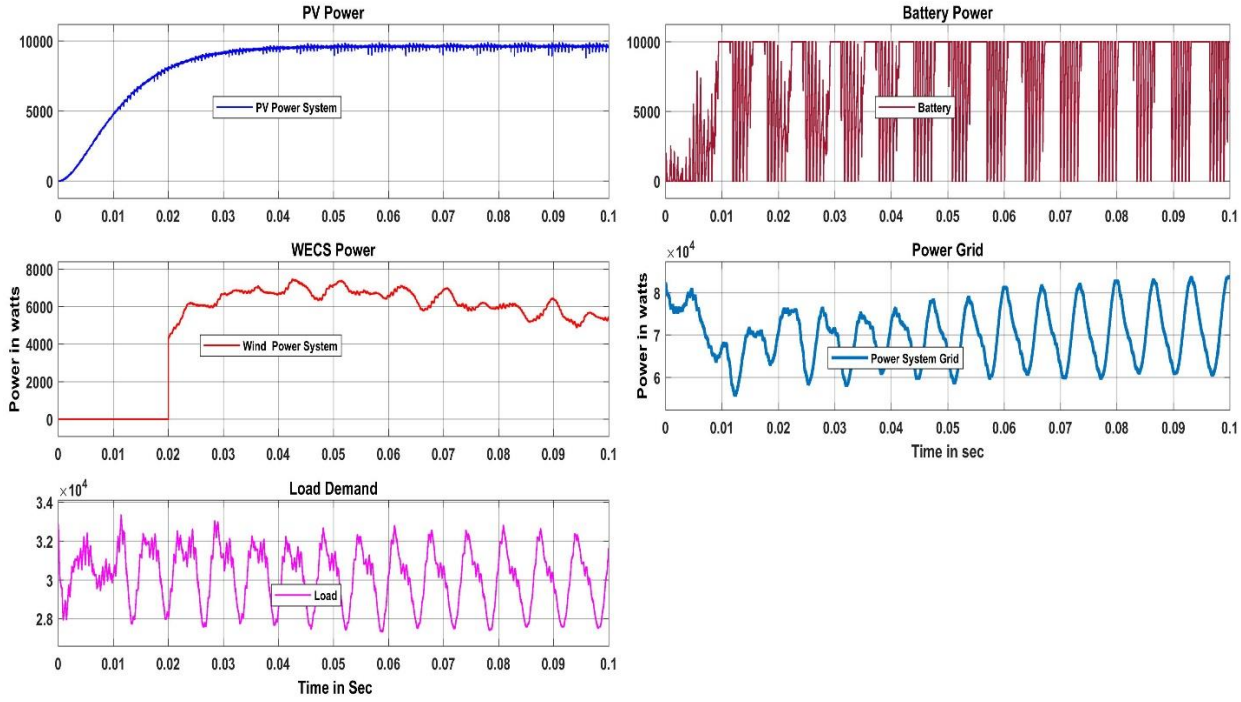

Figure 4.39 Power Waveform at various sources under different conditions

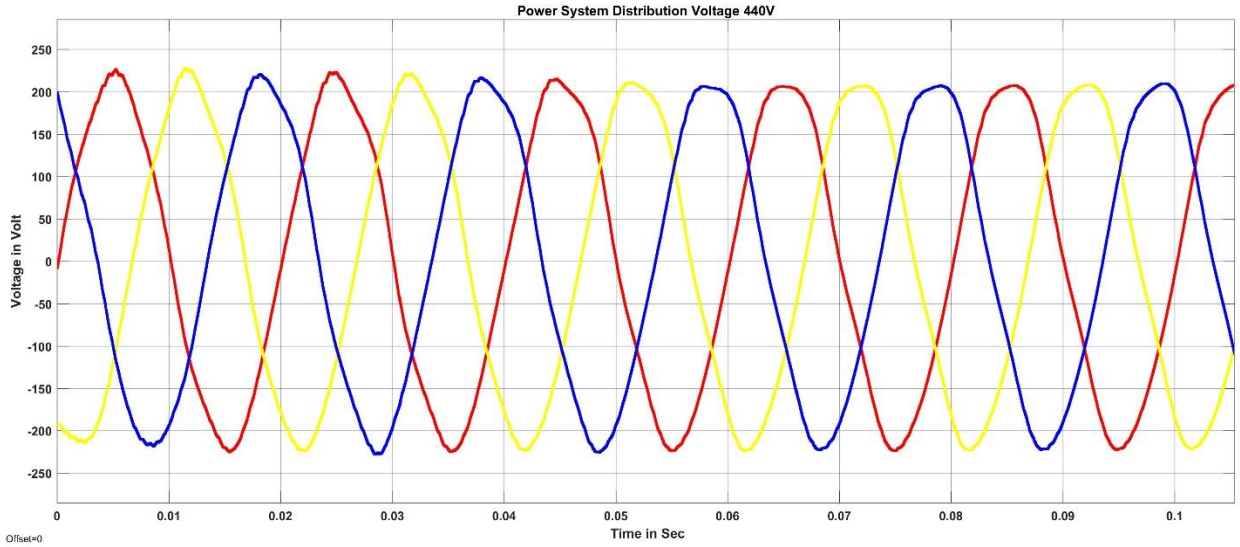

Figure 4.40 Distributed grid Voltage waveform

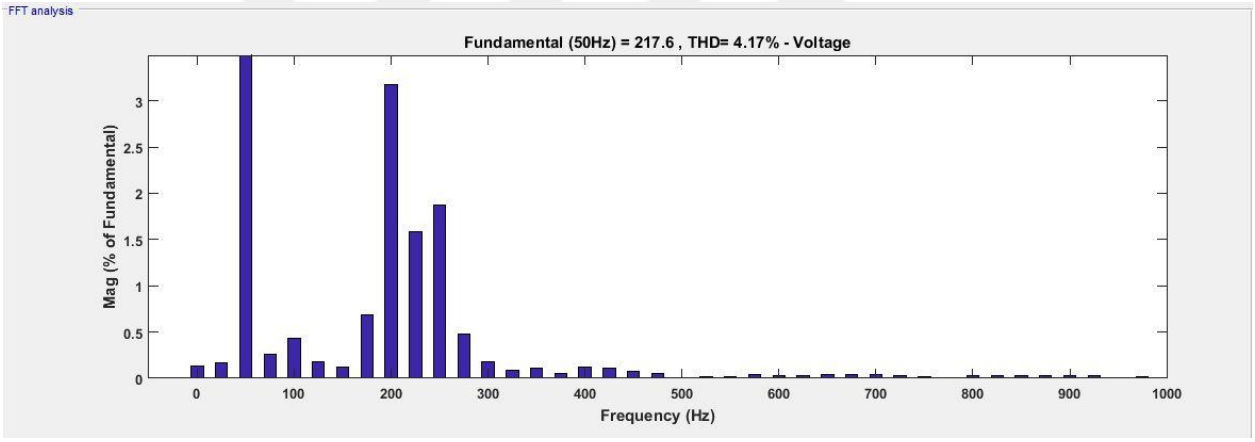

Figure 4.41 Load Voltage THD Waveform

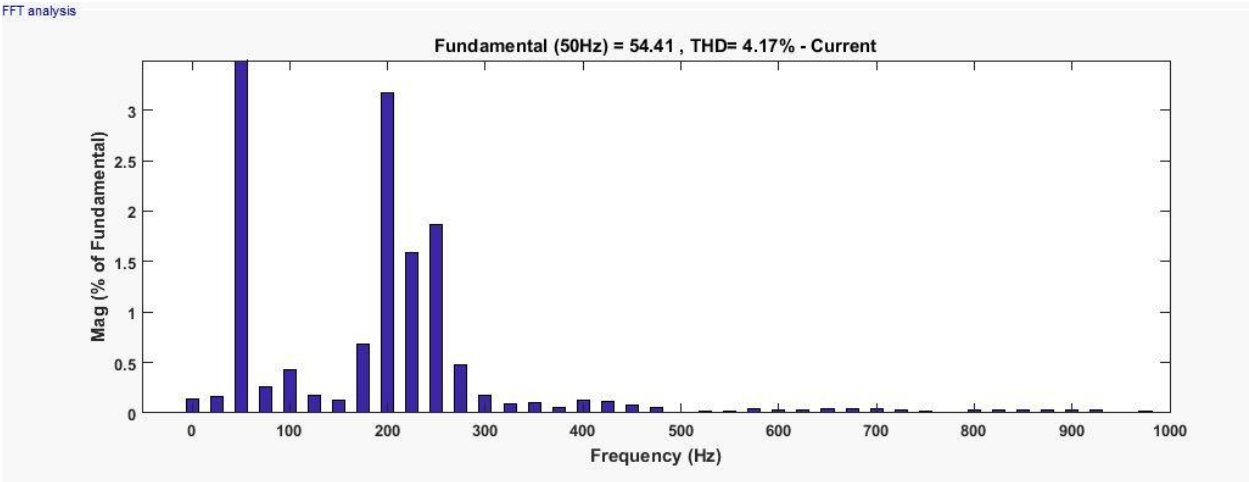

Figure 4.42 Load Current THD Waveform

In this chapter, the proposed hybrid grid integration of solar and wind power with battery system by using MPPT controllers, were simulated at Matlab/Simulink. The MPPT controller has been developed for wind and solar systems and analyzed system performance under various conditions. Fuzzy based battery system is developed and tested for the proposed system. The proposed system voltage and current THD values are calculated as evaluated based on IEEE 1547 standard.

CHAPTER 5

MARKET ANALYSIS & FINANCIAL PRESENTATION

In this chapter, the economic analysis of the proposed system is presented by using Hybrid optimization model of renewable energy (HOMER) [51] and System Advisor Model (SAM) [18] software. The installation of this system has been planned in Istanbul, Turkey. The schematic of the system which includes the market products and their costs are presented.

5.1 Solar and Wind Energy Potential of Turkey

The solar energy is most popular renewable source in Turkey due to high energy potential which is approximately 15,120 TW/h (terawatt (10^{12}) hours) by only natural resources [52] and the country is feeding by the sunlight during the 2.640 hours in a year as average. It can be calculated as 7.2 hours for daily duration. On the other hand, the daily pressure of radiation is about 3.6 kWh/m^2 [53]. In Figure 5.1 demonstrates the global horizontal irradiation (GHI) map of Turkey which location is better for solar energy installation.

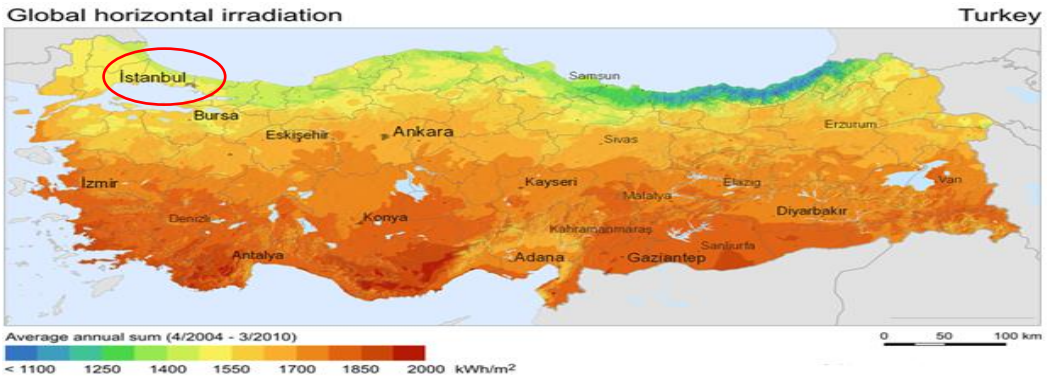

Figure 5.1 GHI level demonstration in Turkey map [54]

The selected residence is located in the latitude, 41^0 04’ 57.71” N and longitude, 28^0 39’ 21.18” E in Istanbul, Turkey. The solar GHI data of that location is obtained from NASA Surface meteorology and Solar Energy database in order to implement in the HOMER and SAM software [51, 18]. It is demonstrated in Figure 5.3. The annual average radiation is 3.94 kWh/m^2/day.

Month	Clearness Index	Daily Radiation (kWh/m²/day)
January	0.375	1.520
February	0.416	2.270
March	0.453	3.390
April	0.482	4.600
May	0.526	5.790
June	0.572	6.630
July	0.609	6.870
August	0.589	5.920
September	0.556	4.540
October	0.455	2.750
November	0.397	1.730
December	0.350	1.270

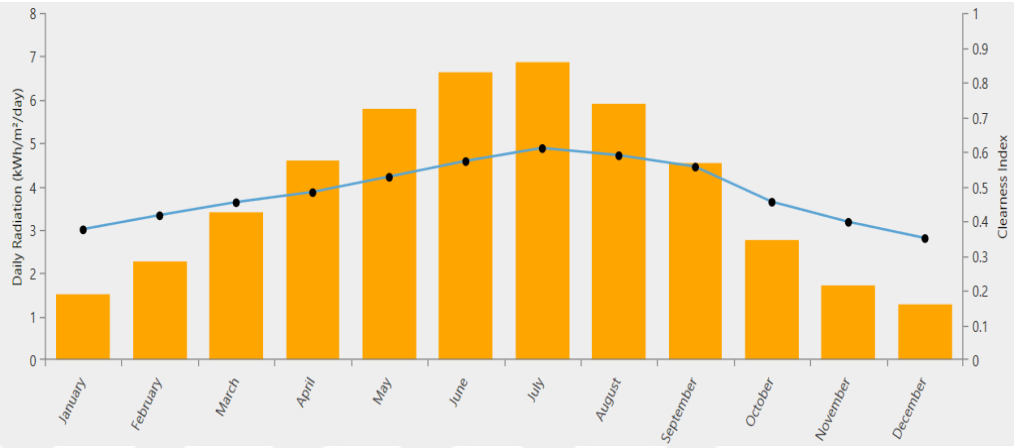

Figure 5.2 Monthly average solar irradiation levels at the selected location

The monthly average temperature of that location is presented in the Figure 5.3. The annual average temperature is measured as 14.46 ^{0}C.

Month	Daily Temperature (°C)
January	5.880
February	5.700
March	7.790
April	12.070
May	16.730
June	21.320
July	23.640
August	23.750
September	20.960
October	16.800
November	11.470
December	7.420

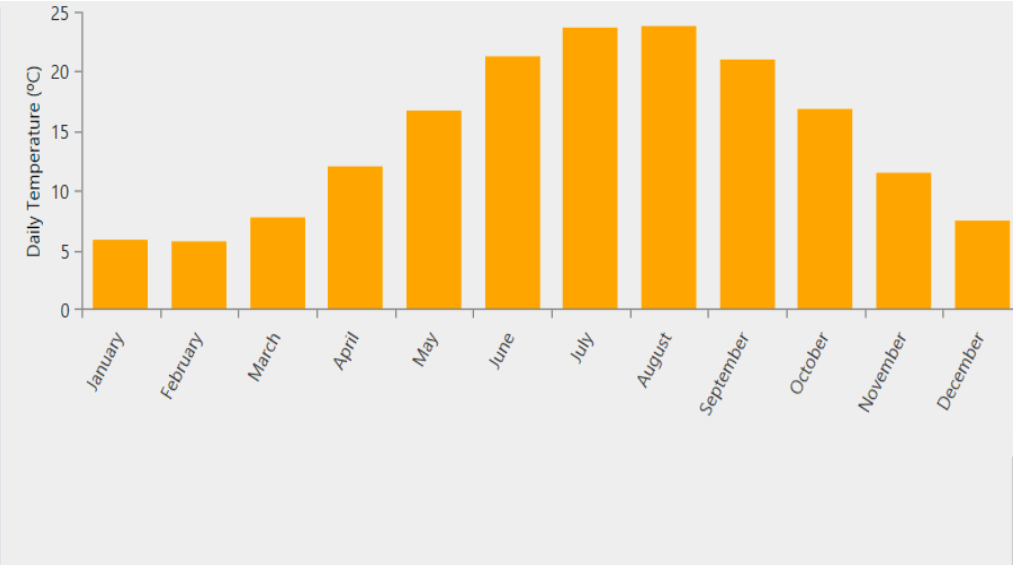

Figure 5.3 Monthly average temperature levels at the selected location

On the other hand, the minimum wind energy capacity of Turkey is determined as approximately 50,000 MW for the area which has 8.4 m/s or higher wind speed and 48,000 MW for the area which has 7 m/s or higher wind speed [52]. The wind map of Turkey is illustrated in Figure 5.4 and the operation area of this thesis is circled.

The wind speed data of the selected location is obtained from NASA Surface meteorology and Solar Energy database in order to implement in the HOMER and SAM software [51, 18]. It is illustrated in Figure 5.5. The annual average speed is 5.76 m/s.

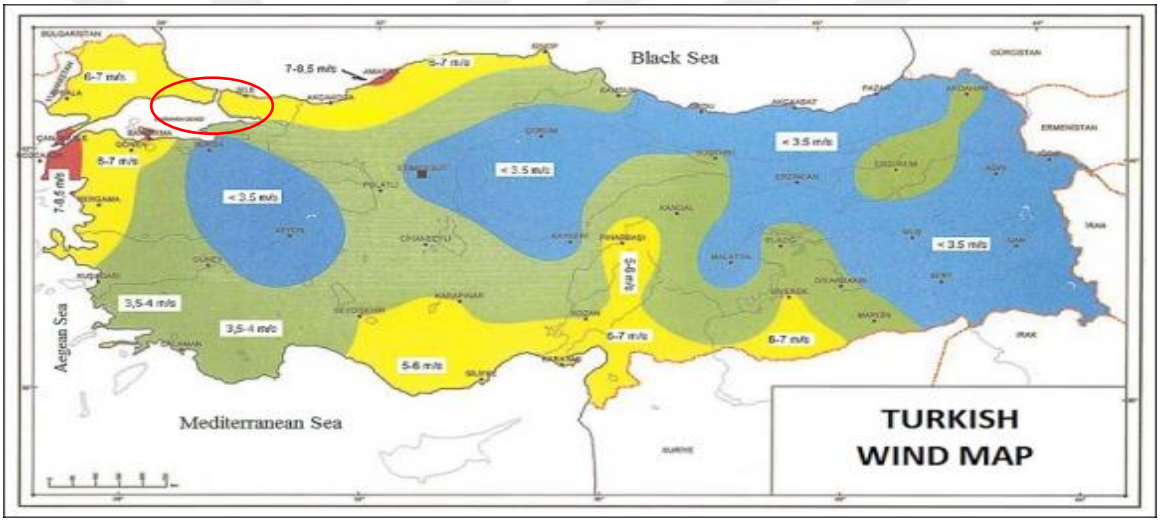

Figure 5.4 The wind speed demonstration zone by zone in Turkey [55]

Month	Average (m/s)
January	6.350
February	7.910
March	6.670
April	4.850
May	4.490
June	4.390
July	4.780
August	4.910
September	4.810
October	7.270
November	6.100
December	6.610

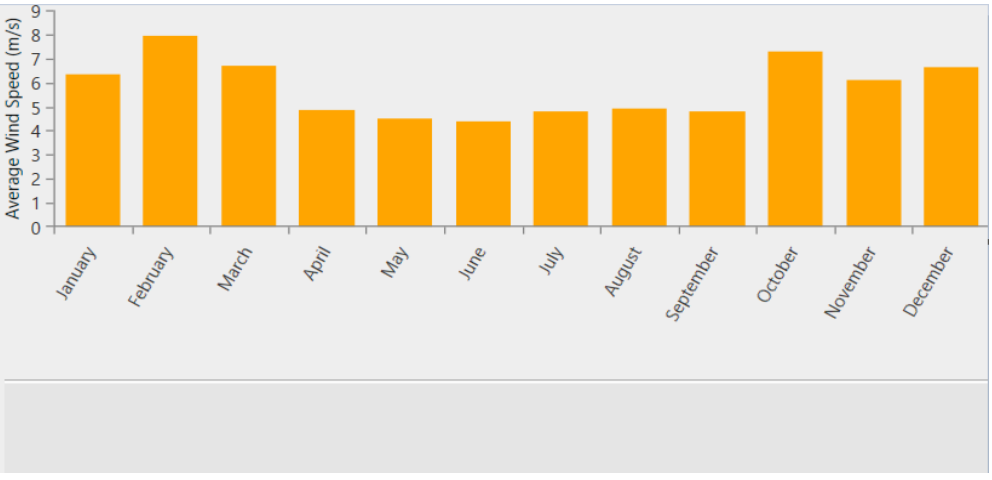

Figure 5.5 Monthly wind speed levels at the selected location

5.2 System Design and Market Analysis

Technical specification of the system components are obtained from the SAM software [18] and the system is designed in HOMER software [51] by using that specification. The grid integrated wind and solar energy are combined with battery and converter. The system's load is added as a residence which is in the selected location. The 24 hours load profile is illustrated as hour by hour in Figure 5.6.

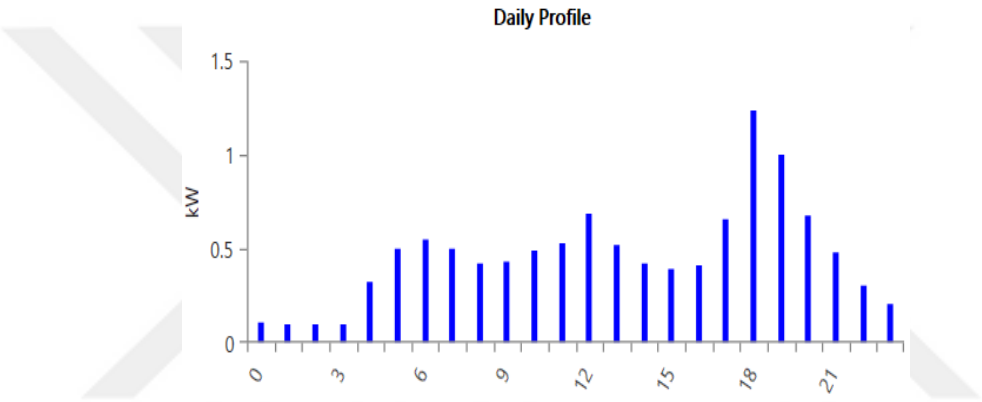

Figure 5.6 24-hours load profile as hour by hour

The scaled annual average load demand is calculated as 11.26 kWh/day. The peak demand in a day is 2.09 kW. The proposed system is designed in HOMER software with the implementation of the market products as shown in Figure 5.7.

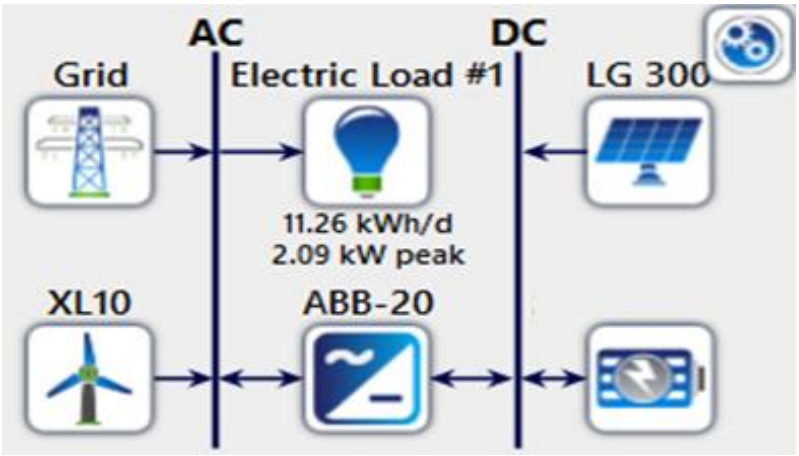

Figure 5.7 The proposed system design

Turkish Electricity Transmission Corporation (TEIAS) delivers the electricity to residences by the grid. The electricity cost is $0.122 cents/kWh which regards the rate of exchange [56]. The grid is a backup equipment which draws the surplus power. In this system, the electricity cannot sell back to grid in Turkey. However, this scenario is calculated by next section additionally. The load demand can be supplied by grid, when the renewables cannot generate the enough power.

Photovoltaic array is selected as LG300N1W-G3 [57] (flat plate) which manufactures by LG Electronics. Its life time is about 25 years and it has 13% efficiency. Initial installation cost (ICC) of that PV panel is $1,066 per 1kW. The yearly maintenance and operation cost (O&M) is assumed as zero.

Bergey Excel 10 wind turbine [58] has been used in the proposed system. It manufactures by Bergey Windpower. Its life time is about 20 years and the Initial installation cost (ICC) is $2,750 per 1kW.

The used converter/inverter is Trio-20.0 TL [59] which manufactures by ABB. It has 97.50 % efficiency and it is working with MPPT voltage input and the life time of this product is about 10 years. The capital cost for the converter is $2,800 for the 20kW capacity.

SIND 04 2145 [60] is the implemented battery in the system and it is manufactures by Trojan Battery company. There are 17 years life time of that product and it is an advanced lead-acid battery. Also, it has 2145 Ah capacity at 100 hours. The capital cost of that battery is $1,250 for two banks.

The total cost of the system components are presented in Table 5.1 with product brands, their ratings and quantities.

Table 5.1 System Equipment [57, 58, 59, 60]

Equipment	*Company Manufacturing*	*Max. Rating per item*	*Quantity*	*Total Cost USD*
Wind Turbine	Bergey Wind Power / Bergey Excel 10	10 kW	1	$27,500
PV module	LG Electronics / LG300N1W-G3	300 W	34	$10,660
Battery	Trojan / SIND 04 2145	8.879 kWh	2	$1,250
Converter	ABB / Trio-20.0 TL	20 kW	1	$1,900

5.3 Financial Presentation and Optimization Results

The system consists of different equipment which is presented in Table 5.1. There are several scenarios in this system. The wind-solar can be used together or separately with different ratings. On the other hand, the sellback is not an option in Turkey, however, it is going to be an option after 2020. This case is presented additionally.

The cost of energy which is levelized (COE) as average per kWh of the produced electrical energy by the system is one of the obtained parameters [61]. The annual producing electricity cost is divided by the total electric load served by the HOMER software. Also, the operating cost can be obtained due to all costs which are annualized other than capital costs. It is shown in Equation (5.1) [61].

$$C_{OPERATING} = C_{ANNUAL,TOT} - C_{ANNUAL,CAPITAL} \quad (5.1)$$

where:

$C_{ANNUAL,TOT}$ = the total annualized cost [$/yr]

$C_{ANNUAL,CAPITAL}$ = the total annualized capital cost [$/yr]

The system's present value of all cost should subtract from the all revenue's present value during life time in order to obtain the total net present cost (NPC) of the system [61]. That costs include the capital costs, operation and maintaining costs, and cost of the purchased energy from grid. The revenue is the grid sales. HOMER calculates the total NPC by using the annualized total cost and levelized energy cost [51, 61].

The fraction percentage is the renewables' energy contribution percentage for the system. In the different cases, the minimum COE can be obtained in order to provide the system optimization. The annualized operation cost, initial capital costs, annual production, purchased electric energy from grid and fraction percentage are given according to scenarios.

CASE 1: PV + BATTERY + CONVERTER + GRID

The different PV rating is applied with battery, converter and grid integration and system is optimized in various cases in terms of the architecture and cost of the system.

Table 5.2 System architecture and costs for 3kW PV, 1 battery bank, 10kW converter

PV	*BATTERY*	*CONVERTER*	*GRID*
			
3 kW	*8.879 kWh * 1*	*10 kW*	

COE $	*Operation Cost $/yr*	*Net Present Value $/yr*	*Initial Capital $*	*PV Capital Cost $*	*PV Annual Production kWh/yr*	*Energy Purchased kWh/yr*	*Fraction %*
0.111	167.38	6,901	4,773	3,198	3,836	1,372	71.7

Table 5.3 System architecture and costs for 10kW PV, 2 battery bank, 10kW converter

PV	*BATTERY*	*CONVERTER*	*GRID*
			
10 kW	*8.879 kWh * 2*	*10 kW*	

COE $	*Operation Cost $/yr*	*Net Present Value $/yr*	*Initial Capital $*	*PV Capital Cost $*	*PV Annual Production kWh/yr*	*Energy Purchased kWh/yr*	*Fraction %*
0.0833	23.36	13,162	12,860	10,660	12,787	191	98.4

CASE 2: WIND + BATTERY + CONVERTER + GRID

The different wind turbine rating is applied with battery, converter and grid integration and system is optimized in various cases in terms of the architecture and cost of the system.

Table 5.4 System architecture and costs for 3kW wind, 1 battery bank, 10kW converter

WIND TURBINE	*BATTERY*	*CONVERTER*	*GRID*
3 kW	*8.879 kWh * 1*	*10 kW*	

COE $	*Operation Cost $/yr*	*Net Present Value $/yr*	*Initial Capital $*	*Wind Capital Cost $*	*Wind Annual Production kWh/yr*	*Energy Purchased kWh/yr*	*Fraction %*
0.0161	77.36	10,825	9,825	8,250	51,463	634	98.8

Table 5.5 System architecture and costs for 7kW wind, 1 battery bank, 10kW converter

WIND TURBINE	*BATTERY*	*CONVERTER*	*GRID*
7 kW	*8.879 kWh * 1*	*10 kW*	

COE $	*Operation Cost $/yr*	*Net Present Value $/yr*	*Initial Capital $*	*Wind Capital Cost $*	*Wind Annual Production kWh/yr*	*Energy Purchased kWh/yr*	*Fraction %*
0.0138	55.86	21,547	20,825	8,250	120,079	458	99.6

CASE 3: PV + WIND + BATTERY + CONVERTER + GRID

The various wind turbine and PV panel rating are implemented with battery, converter and grid integration as a hybrid system and that system is optimized in various cases in terms of the architecture and cost of the system.

Table 5.6 System architecture and costs for 3kW wind, 3kW PV, 1 battery bank, 10kW converter

PV	*WIND TURBINE*	*BATTERY*	*CONVERTER*	*GRID*
 *3 kW*	 *3 kW*	 *8.879 kWh * 1*	 *10 kW*	

COE ($)	0.0183
Operation Cost ($/yr)	1.85
Net Present Value ($/yr)	13,047
Initial Capital ($)	13,023
Wind Capital Cost ($)	8,250
Wind Annual Production (kWh/yr)	51,463
PV Capital Cost ($)	3,198
PV Annual Production (kWh/yr)	3,836
Energy Purchased (kWh/yr)	15.1
Fraction %	100

Table 5.7 System architecture and costs for 7kW wind, 3kW PV, 1 battery bank, 20kW converter

PV	*WIND TURBINE*	*BATTERY*	*CONVERTER*	*GRID*
 *3 kW*	 *7 kW*	 *8.879 kWh * 1*	 *20 kW*	

COE ($)	0.0150
Operation Cost ($/yr)	0.858
Net Present Value ($/yr)	24,034
Initial Capital ($)	24,034
Wind Capital Cost ($)	19,250
Wind Annual Production (kWh/yr)	170,079
PV Capital Cost ($)	3,198
PV Annual Production (kWh/yr)	3,836
Energy Purchased (kWh/yr)	7.04
Fraction %	100

Table 5.8 System architecture and costs for 10kW wind, 3kW PV, 1 battery bank, 20kW converter

 3 kW	 10 kW	 8.879 kWh * 1	 20 kW	

COE ($)	0.0147
Operation Cost ($/yr)	0.548
Net Present Value ($/yr)	33,230
Initial Capital ($)	33,230
Wind Capital Cost ($)	27,500
Wind Annual Production (kWh/yr)	171,542
PV Capital Cost ($)	3,198
PV Annual Production (kWh/yr)	3,836
Energy Purchased (kWh/yr)	4.49
Fraction %	100

Table 5.9 System architecture and costs for 10kW wind, 10kW PV, 2 battery bank, 20kW converter

 10 kW	 10 kW	 8.879 kWh * 2	 20 kW	

COE ($)	0.0174
Operation Cost ($/yr)	0
Net Present Value ($/yr)	41,310
Initial Capital ($)	41,310
Wind Capital Cost ($)	27,500
Wind Annual Production (kWh/yr)	171,542
PV Capital Cost ($)	10,660
PV Annual Production (kWh/yr)	12,787
Energy Purchased (kWh/yr)	0
Fraction %	100
Energy Sold (kWh/yr)	179,840

If the produced energy which is more than the load demand, sellback to grid and the selling cost or sellback rate is going to be $ 0.085 cents/kWh which regards the rate of exchange. The sold energy is calculated as 179,840 kWh by HOMER for that case. As annualized total income from the sold energy is going to be $15,286 $/yr (0.085*179,840) depending on this case.

Table 5.10 System architecture and costs for 7kW wind, 10kW PV, 2 battery bank, 20kW converter

 *10 kW*	 *7 kW*	 *8.879 kWh * 2*	 *20 kW*	

COE ($)	0.0193
Operation Cost ($/yr)	0
Net Present Value ($/yr)	33,060
Initial Capital ($)	33,060
Wind Capital Cost ($)	19,250
Wind Annual Production (kWh/yr)	170,079
PV Capital Cost ($)	10,660
PV Annual Production (kWh/yr)	12,787
Energy Purchased (kWh/yr)	0
Fraction %	100
Energy Sold (kWh/yr)	171,107

The sold energy is calculated as 171,107 kWh by HOMER for that case. As annualized total income from the sold energy is going to be $14,544 $/yr (0.085*171,107) depending on this case.

CHAPTER 6

CONCLUSION AND FUTURE WORK

The grid integrated hybrid system which consists of PV, wind and battery components and they are modeled with the different MPPT methods that are fuzzy logic controller and P&O. The 10kW solar and 9kW wind energy are generated with that controller algorithms. The modeled battery system is controlled by fuzzy logic controller, while PV and wind systems are controlled by either P&O or FLC.

The proposed Fuzzy and P&O based MPPT of 10 kW PV power system has been simulated at various irradiance of 250 W/M^2 , 500 W/M^2 , 750 W/M^2 and 1000 W/M^2 respectively. The fuzzy method's performance and efficiency is better than the P&O considered to the proposed system. The Fuzzy and P&O based MPPT of wind system is simulated at various wind speed such as 5 m/s, 7 m/s, 9 m/s, 11 m/s and 12 m/s. The systems' current and RMS waveforms are presented with their output power waveforms. The fuzzy based system is more efficient than the P&O based MPPT for the proposed system. They compared either graphically or numerically in Chapter 4.

On the other hand, the specific market products are selected in order to install the hybrid system in a residence which is located Istanbul, Turkey. The weather data of that location and specification of the components which are wind, solar, battery, converter, grid and load, are transferred into HOMER software. The system is optimized economically and some different scenarios are obtained in terms of the annualized system production and costs. Solar, wind and solar-wind combined systems with different kW ratings are, either presented financially or

analyzed in order to observe the systems' efficiency in Chapter 5. Also, the sellback scenario is discussed and the sold energy (surplus to requirement) is calculated approximately.

This thesis presents the solar-wind-battery energy systems and their control mechanisms with the real case economic analysis. The system has both AC and DC loads which are grid and residential. The simulated system provides to implement different loads in this way. The power outputs and the system performance were analyzed owing to different kind of the MPPT methods which are Perturb & Observe (PO) and Fuzzy Logic Controller (FLC). The output waveforms are tracked under the different weather conditions and different variables to observe the alteration of the system. A more productive and efficient method is determined as FLC in this way.

For future work, the PV and wind rating of the simulated system can be increased in order to provide the commercial use. The different MPPT algorithms can be used for the PV and wind instead of P&O and FLC. They may be Incremental Conductance, Current Sweep, Short-Current Pulse, Constant Voltage and Neuro Fuzzy algorithms/controllers. The proposed system can be tested by using them. The system efficiency can be increased in this way. Also, the different system loads like an electric vehicle station or water pumping system can be implemented in this hybrid power system simulation. On the other hand, the system can be economically analyzed for the varied countries and locations to increase the performance and produce rating of the renewables. The presented financial scenarios may be developed owing to sellback option and additional renewables.

LIST OF REFERENCES

[1] U.S.Energy Information Administration 2016. “International Energy Outlook 2016 with Projections to 2040,” *DOE Office of the Integrated Analysis and Forecasting,* April 2016.

[2] U.S. Energy Information Administration, Analysis of the Impacts of the Clean Power Plan Washington, DC: May 2015, https://www.eia.gov/analysis/requests/powerplants/cleanplan.

[3] Renewable Energy Policy Network for the 21th Century. Renewables 2017, Global Status Report, 2017.

[4] Shen, D. and Izadian A. 2014. *“Modeling and control of a combined wind-solar microgrid"* in *IECON 2014-40th Annual Conference of the IEEE Industrial Electronics Society, pp. 2173-2179*.

[5] Wandhare, R. G. and Agarwal V. 2012. *“Novel control scheme to reduce the effect of intermittent solar radiation on the grid connected pv system power output without losing mppt,"* in 2012 *Twenty-Seventh Annual IEEE of Applied Power Electronics Conference and Exposition (APEC), pp. 79-85*.

[6] Yoshimoto, K., Nanahara, T., Koshimizu, G. 2006. *“New Control Method for Regulating State-of-Charge of a Battery in Hybrid Wind Power/Battery Energy Storage System,” IEEE Power Systems Conference and Exposition, pp. 1244-1251*.

[7] Ridzuan, M. 2009. Modeling and Simulation of Power Conditioning for Grid-Connected PV/Wind Hybrid Generation System, Faculty of Electrical Engineering, Universiti Teknologi Malaysia.

[8] Eteiba, M., El Shenawy, T., Shazly, H., and Hafez, Z. 2013. A Photovoltaic (Cell, Module, Array) Simulation and Monitoring Model using MATLAB/GUI Interface, *International Journal of Computer Applications*, 69 *(6), 14-28*.

[9] Diab, H. (2012). Intelligent Maximum Power Tracking and Inverter Hysteresis Current Control of Grid-connected PV Systems. Published in International Conference on Advances in Power Conversion and Energy Technologies, APCET- 2012, IEEE, INDIA

[10] Park, J., Kim, H., Cho, Y., Shin, C. Simple Modeling and Simulation of Photovoltaic Panels Using Matlab/Simulink. *Advanced Science and Technology Letters Vol.73 (FGCN 2014), pp.147-155*.

[11] The Electric Energy. Retrieved from “http://theelectricenergy.com/connecting-solar-cells into-an-array-or-panel/.” in October 2017.

[12] Li, C.H., Zhu, X.J., Cao, G.Y., Sui S. & Hu, M.R. 2009. Dynamic modeling and sizing optimization of stand-alone photovoltaic power systems using hybrid energy storage technology, Renewable Energy 34 (3), 815-826.

[13] Dizqah, A. M., Maheri, A., and Busawon, K. 2012. *"An Assessment of Solar Irradiance Stochastic Model for the UK,"* in *2nd International Symposium on Environment Friendly Energies and Applications (EFEA) Newcastle Upon Tyne*.

[14] Duffie, W. B. Solar Engineering of thermal processes. John Wiley and Sons, Inc., New York, 2006.

[15] Villalva, M., Gazoli, J., and Filho, E. (2009). Comprehensive Approach to Modeling and Simulation of Photovoltaic Arrays, *IEEE Transactions on Power Electronics*, 24 *(5), 1198 1208*.

[16] Wang, C. "Modeling and control of hybrid wind/photovoltaic/fuel cell distributed generation systems," 2006.

[17] Walker, G. "Evaluating MPPT converter topologies using a MATLAB PV model," *Journal of Electrical & Electronics Engineering, Australia*, vol. 21, pp. 49-56, 2001.

[18] System Advisor Model (SAM) Software by National Renewable Energy Laboratory (NREL).

[19] Haque, M. E., Muttaqi, K. M. & Negnevisky, M. “Control of a Stand-alone Variable Speed Wind Turbine with a Permanent Magnet Synchronous Generator”, IEEE Power and Energy society General Meeting – Conversion and Delivery of Electrical Energy in the 21st century, pp.1-9. 2008.

[20] Saikuma, S., Saravanan, S. and Sandip, R. V. “Modelling and Control of a Wind Turbine using Permanent Magnet Synchronous Generator”, IJEST, vol. 3, pp.2377-2384, 3 March 2011.

[21] Heier, S. "Grid Integration of Wind Energy Conversion Systems," John Wiley & Sons Ltd, 1998, ISBN 0-471-97143-X.

[22] Chander, S., Agarwa, P., and Gupta, I. “Auto-tuned, Discrete PID Controller or DC-DC Converter for fast transient response,” in *International Conference on Power Electronics*, pp.1-7, 2011.

[23] Enslin, J. H. R., Wolf, M. S., Snyman, D. B. and Sweigers, W. “Integrated photovoltaic MPPT converter,” in *IEEE Trans. Ind. Electron*, vol. 44, pp. 769-773, 1997.

[24] Mohan, N., Undeland, T. M. and Robbins, W. P. “Power Electronic: Converters, Application, and Design”, Wiley, 2002.

[25] Nejabatkhah, F., Danyali, S., Hosseini, S. H., Sabahi, and M., Niapour, S. M. “Modeling and Control of a New Three-Input DC–DC Boost Converter for Hybrid PV/FC/Battery Power System”, in *IEEE Transactions on power electronics, 27 (5), 2309-2324, 2012.*

[26] Wai, R. J. and Duan, R. Y. “High-efficiency bidirectional converter for power sources with great voltage diversity,” in *IEEE Trans. Power Electron.*, vol. 22, pp. 1986-1996, Sep. 2007.

[27] Khaligh, A. and Onar, O. C. Energy Harvesting Solar, Wind, and Ocean Energy Conversion Systems (Energy, Power Electronics, and Machines). CRC Press, London, 2009.

[28] Mukund, R. P. Wind and Solar Power Systems. CRC Press, London, 1999.

[29] Duarte, J. L., Hendrix M. and Simoes M. G. “Three-port bidirectional converter for hybrid fuel cell systems,” in *IEEE Trans. Power Electron.*, pp. 480-487, Mar. 2007.

[30] Lead-Acid Battery Model, Retrieved from SimPowerSystems of Matlab/Simulink Library and Electric Drives/Extra Sources, https://www.mathworks.com/help/physmod/sps/powersys/ref/battery.html.

[31] Prechanon, K. “Mathematical Model of the PMSG based on Wind Energy ConversionSystem” in *International Research Journal of Innovative Engineering*. *Vol. 3*(*1*), 2015. ISBN: 2395-0560.

[32] Gencer, A. “Modelling and analysis of operation PMSG based WECS under different load conditions”, *ECAI 2016 - International Conference – 8th Edition Electronics*, Computers and Artificial Intelligence. 30 June -02 July, 2016.

[33] Esram, T., Chapman, P.L. "Comparison of Photovoltaic Array Maximum Power Point Tracking Techniques," IEEE Transactions on Energy Conversion, vol. 22, no. 2, pp. 439-449, June 2007.

[34] Mohammad, N., Quamruzzaman, M., Hossain, R. T., Alam, M. R. 2013. “Parasitic Effects on the Performance of DC-DC SEPIC in Photovoltaic Maximum Power Point Tracking Applications.” Vol. 4, No. 1. Article ID: 28142.

[35] Aashoor, F. A. O. 2015. Maximum power point tracking techniques for photovoltaic water pumping system. University of Bath, Department of Electronic and Electrical Engineering.

[36] Mhusa, N. J. 2016. “Modeling and Control Of Photovoltaic-Wind Hybrid Power System using a Neuro-Fuzzy Controller.” Mechatronic Engineering, Masters Of Science. Jomo Kenyatta University of Agriculture And Technology.

[37] Shen, D. “Hybrid Wind-Solar-Storage Energy Harvesting Systems.” Master of Science in Electrical and Computer Engineering. May 2016. Purdue University, Indiana.

[38] Fuzzy Logic Controller Toolbox User's Guide. MATLAB R 2017b.

[39] Abusleme, A., Dixon, J., and Soto, D. "Improved performance of a battery powered electric car, using photovoltaic cells," IEEE Bologna PowerTech Conference, Italy, 2003.

[40] Ngan M. S., Tan C. W. A Study of Maximum Power Point Tracking Algorithms for Stand-alone Photovoltaic Systems. IEEE Applied Power Electronics Colloquium (IAPEC). 2011.

[41] Mohamed S. E., Adel M. S., Ahmed M. A., Adel S. E. PV Solar-Optimal Maximum Power Search using a Modified P&O Technique. EJERS, European Journal of Engineering Research and Science. Vol. 2, No. 5, May 2017.

[42] Iancu, I. "A Mamdani type fuzzy logic controller," *Fuzzy Logic: Controls, Concepts, Theories and Applications, InTech Croatia, Rijeka,* pp. 55-54, 2012.

[43] Bai, Y. et al., Advanced fuzzy logic technologies in industrial applications: Springer, 2007.

[44] Saranya, S. D., Sathyamoorthi, S. and Gandhiraj, R. "A Fuzzy Logic Based Energy Management System for a Microgrid." ARPN Journal of Engineering and Applied Sciences Asian Research Publishing Network (ARPN). Vol. 10, No. 6, April 2015. ISSN 1819-6608.

[45] Ozdal, O. M., Altas, I. H. "Fuzzy logic control for a wind/battery renewable energy production system." TUBITAK. Turk J Elec Eng & Comp Sci, Vol.20, No.2, 2012. doi:10.3906/elk-1104-20.

[46] Shezan, A., Khan, N. H., Anowar, T., Delwar H., Islam, D., Reduanul, H., Hasan, M. and Kabir, A. "Fuzzy Logic Implementation with MATLAB for Solar-Wind-Battery-Diesel Hybrid Energy System." *Imperial Journal of Interdisciplinary Research (IJIR).* Vol-2, Issue-5, pp.*574.* 2016 ISSN: 2454-1362.

[47] Venkateshkumar, M., Raghavan, R. "Hybrid Photovoltaic and Wind Power System with Battery Management System using Fuzzy Logic Controller", International Journal of Applied Power Engineering (IJAPE), 2016.

[48] Viorel, I., B., Istrate, M., Machidon, D. and Pantelimon, R. "A Study on Anti-Islanding Detection Algorithms for Grid-Tied Photovoltaic Systems." May 2014. DOI:10.1109/OPTIM.2014. 6850940.

[49] Saw, O. O., Lwin, Z. K. "Power Conversion Model and Simulation of Grid Connected Solar and Wind Hybrid System." American Scientific Research Journal for Engineering, Technology, and Sciences (ASRJETS). ISSN: 2313-4410.

[50] Qian, J. Li, K., Wu, H., Yang, J and Li, X. "Synergetic Control of Grid-Connected Photovoltaic Systems." Hindawi International Journal of Photoenergy. Volume 2017, Article ID: 5051489. https://doi.org/10.1155/2017/5051489.

[51] National Renewable Energy Laboratory, 2017, “NREL. HOMER User Manual”, Boulder, CO, USA.

[52] Kick, C. (2011). How is 100% Renewable Energy Possible for Turkey by 2020? Research Associate, Global Energy Network Institute (GENI). July 2011.

[53] Erdil, A, Erbiyik, H. “Renewable Energy Sources of Turkey and Assessment of Sustainability.” *11th International Strategic Management Conference*. Procedia - Social and Behavioral Sciences, *207*. 2015. *669 – 679*. doi: 10.1016/j.sbspro.2015.10.137.

[54] SolarGIS Maps and GIS data. Retrieved from http://solargis.com/products/maps-and-gis-data/ in November 2017.

[55] Akova, Ismet, “Development Potential of Wind Energy in Turkey.” EchoGeo, 2011. http://echogeo.revues.org/12457

[56] Turkey cost of electricity. Retrieved from “http://enerjienstitusu.com/elektrik-fiyatlari/.” in November 2017.

[57] LG300N1W-G3 PV panel datasheet. Retrieved from https://www.lgenergy.com.au/downloads/category/5/product-datasheets.” in November 2017.

[58] Bergey Excel 10. Retrieved from “http://bergey.com/documents/2013/10/excel-10-spec-sheet_2013.pdf.” and http://smallwindcertification.org/wp-content/uploads/2015/12/Summary-Report-10-12-2015.pdf” in November 2017.

[59] ABB TRIO 20KW SOLAR INVERTER - THREE PHASE - 2 MPPT. Retrieved from “https://library.e.abb.com/public/5125f5ed9a1044d69ef362bc209f4ca4/TRIO-20.0-27.6-Datasheet-RevH.pdf” and “https://www.cclcomponents.com/abb-trio-20kw-solar-inverter-three-phase-2-mppt.” in November 2017.

[60] Trojan SIND 04 2145 Battery bank. Retrieved from “http://www.trojanbattery.com/pdf/datasheets/SIND_04_2145_DS.pdf” and “https://www.altestore.com/store/trojan-batteries-m76/” in November 2017.

[61] HOMER software, support and user manual. Retrieved from https://www.homerenergy.com /support/docs/3.10/levelized_cost_of_energy.html.” in November 2017.

Appendix A: PV Panel Datasheet

LG300N1W-G3 PV data-sheet that is manufactured by LG electronics, is presented below [57].

LG295/300S1C-A5

LG MonoX® Plus

Mechanical Properties

Cells	6 x 10
Cell Vendor	LG
Cell Type	Monocrystalline / P-type
Cell Dimensions	161.7 x 161.7 mm
# of Busbar	4
Dimensions (L x W x H)	1686 x 1016 x 40 mm
Front Load	6000 Pa
Rear Load	5400 Pa
Weight	18.0 kg
Connector Type	Genuine MC4, IP68 (Male: PV-KST4) (Female: PV-KBT4)
Junction Box	IP68 with 3 bypass diodes
Length of Cables	2 x 1000 mm
Front cover	High transmission tempered glass
Frame	Anodised aluminum with protective black coating

Certifications and Warranty

Certifications	ISO 9001
	IEC 61215, IEC 61730-1/-2
	IEC 61701(Salt Mist Corrosion Test)
	IEC 62716 (Ammonia Corrosion Test)
Module Fire Rating	Class C
Product Warranty	12 Years
Output Warranty of Pmax (Measurement Tolerance ± 3%)	Linear Warranty[1]

[1] 1) 1st year: 98%, 2) After 1st year: 0.55%p annual degradation, 3) 84.8% for 25 years

Temperature Characteristics

NOCT	45± 3 °C
Pmax	-0.41 %/°C
Voc	-0.30 %/°C
Isc	0.03 %/°C

Electrical Properties (STC[2])

Module Type	295 W	300 W
Maximum Power Pmax (W)	295	300
MPP Voltage Vmpp (V)	31.3	31.7
MPP Current Impp (A)	9.43	9.47
Open Circuit Voltage Voc (V)	38.6	38.9
Short Circuit Current Isc (A)	10.02	10.07
Module Efficiency (%)	17.2	17.5
Operating Temperature (°C)	-40 ~ +90	
Maximum System Voltage (V)	1000	
Maximum Series Fuse Rating (A)	20	
Power Tolerance (%)	0 ~ +3	

[2] STC (Standard Test Condition): Irradiance 1000 W/m², module temperature 25 °C, AM 1.5.
The nameplate power output is measured and determined by LG Electronics at its sole and absolute discretion.

Electrical Properties (NOCT[3])

Module Type	295 W	300 W
Maximum Power Pmax (W)	216	220
MPP Voltage Vmpp (V)	28.7	29.1
MPP Current Impp (A)	7.53	7.56
Open Circuit Voltage Voc (V)	35.7	36.0
Short Circuit Current Isc (A)	8.06	8.10

[3] NOCT (Nominal Operating Cell Temperature): Irradiance 800 W/m², ambient temperature 20°C, wind speed 1 m/s

Dimensions (mm)

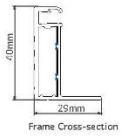

Frame Cross-section

Current – Voltage characteristics at various irradiance levels

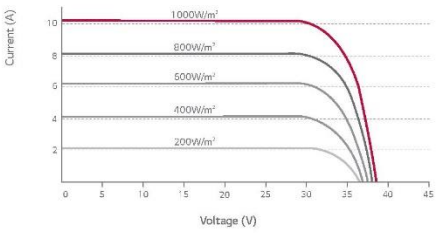

Current – Voltage characteristics at various cell temperatures

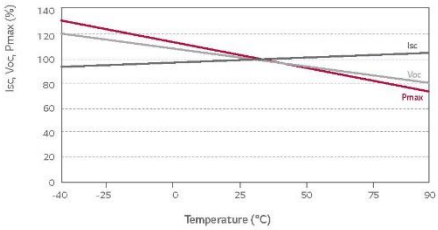

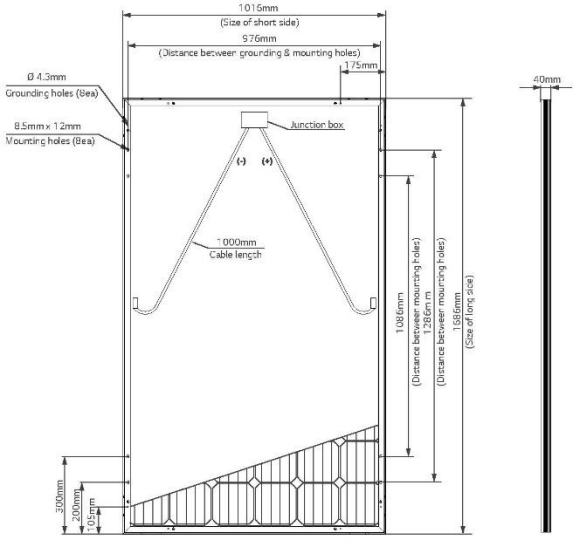

Appendix B: Wind Turbine Datasheet

Bergey Excel 10 wind turbine which manufactures by Bergey Windpower, has been used in the proposed system [58].

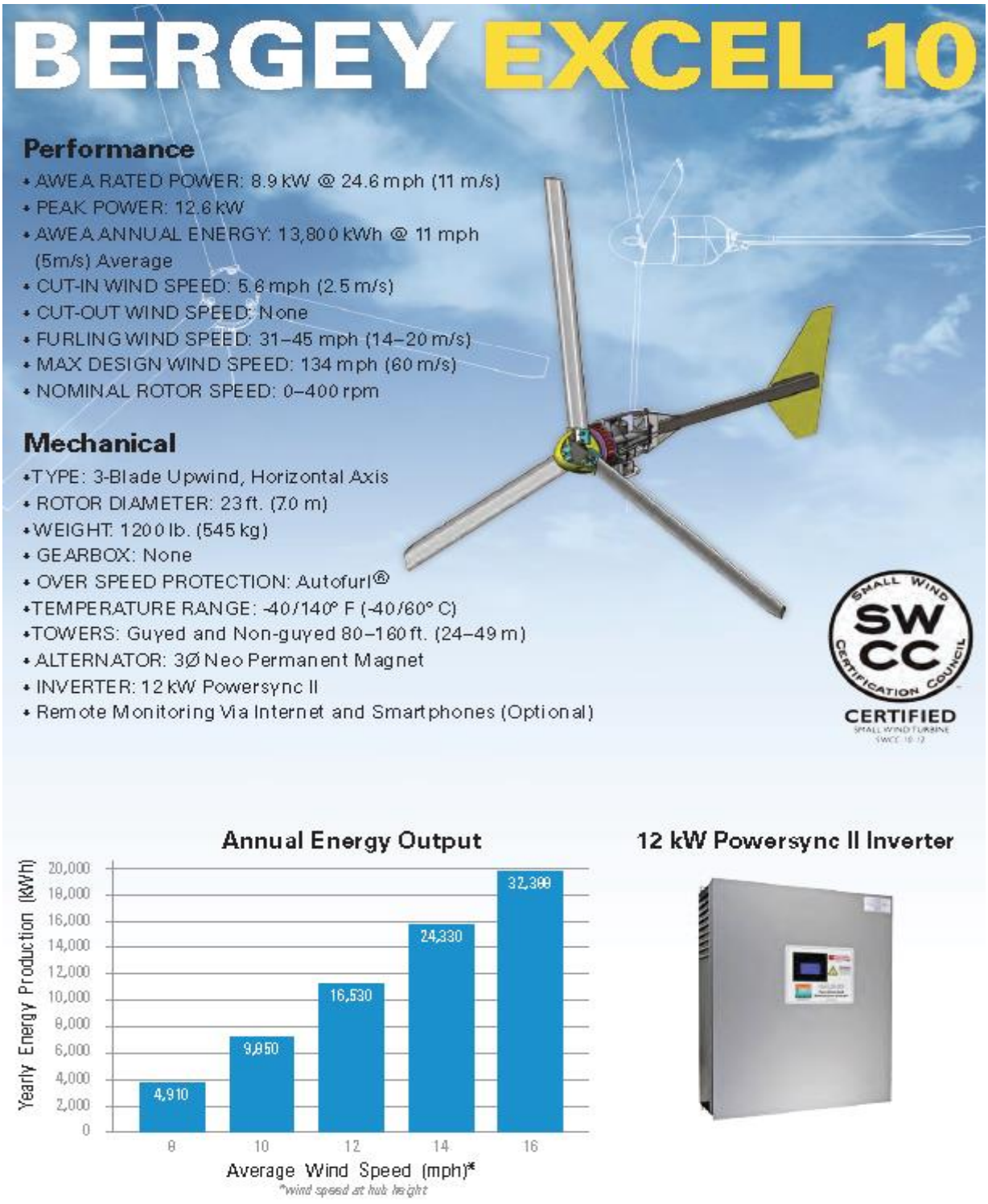

Appendix C: Converter/Inverter Datasheet

The used converter/inverter is Trio-20.0 TL which manufactures by ABB [59]. It is working with MPPT voltage input that is given its datasheet.

Additional highlights

- Integrated string combiner with different options of configuration which include DC and AC disconnect switch in compliance with international standards (S2, S1J, -S2J, -S2F and -S2X versions)
- Natural convection cooling for maximum reliability
- Outdoor enclosure for unrestricted use under any environmental conditions
- Capability to connect external sensors for monitoring environmental conditions
- Availability of auxiliary DC output voltage (24 V, 300 mA)

Technical data and types

Type code	TRIO-20.0-TL-OUTD	TRIO-27.6-TL-OUTD
Input side		
Absolute maximum DC input voltage ($V_{max,abs}$)	1000 V	
Start-up DC input voltage (V_{start})	430 V (adj. 250...500 V)	
Operating DC input voltage range (V_{dcmin}...V_{dcmax})	0.7 x V_{start}...950 V (min 200 V)	
Rated DC input voltage (V_{dcr})	620 V	
Rated DC input power (P_{dcr})	20750 W	28600 W
Number of independent MPPT	2	
Maximum DC input power for each MPPT ($P_{MPPTmax}$)	12000 W	16000 W
DC input voltage range with parallel configuration of MPPT at P_{acr}	440...800 V	500...800 V
DC power limitation with parallel configuration of MPPT	Linear derating from max to null [800 V≤V_{MPPT}≤950 V]	
DC power limitation for each MPPT with independent configuration of MPPT at P_{acr}, max unbalance example	12000 W [480 V≤V_{MPPT}≤800 V] the other channel: P_{dcr}-12000 W [350 V≤V_{MPPT}≤800 V]	16000 W [500 V≤V_{MPPT}≤800 V] the other channel: P_{dcr}-16000 W [400 V≤V_{MPPT}≤800 V]
Maximum DC input current (I_{dcmax}) / for each MPPT ($I_{MPPTmax}$)	50.0 A / 25.0 A	64.0 A / 32.0 A
Maximum input short circuit current for each MPPT	30.0 A	40.0 A
Number of DC inputs pairs for each MPPT	1 (4 in -S2X, -S2F, -S1J, -S2J versions)	1 (6 in -S2X and -S2F versions, 4 in -S1J and -S2J)
DC connection type	PV quick fit connector [3] / Screw terminal block on Standard and -S2 versions	
Input protection		
Reverse polarity protection	Yes, from limited current source	
Input over voltage protection for each MPPT - varistor	Yes, 4	
Input over voltage protection for each MPPT - plug in modular surge arrester (-S2X, -S1J and -S2J versions)	-S2X: Type 2; -S1J, -S1J: Type 1+2	
Photovoltaic array isolation control	According to local standard	
DC switch rating for each MPPT (version with DC switch)	40 A / 1000 V	
Fuse rating (versions with fuses)	15 A / 1000 V	
Output side		
AC grid connection type	Three-phase 3W+PE or 4W+PE	
Rated AC power (P_{acr} @cosϕ=1)	20000 W	27600 W
Maximum AC output power (P_{acmax} @cosϕ=1)	22000 W [4]	30000 W [5]
Maximum apparent power (S_{max})	22200 VA	30670 VA
Rated AC grid voltage (V_{acr})	400 V	
AC voltage range	320...480 V [1]	
Maximum AC output current (I_{acmax})	33.0 A	45.0 A
Contributory fault current	35.0 A	46.0 A
Rated output frequency (f)	50 Hz / 60 Hz	
Output frequency range (f_{min}...f_{max})	47...53 Hz / 57...63 Hz [2]	
Nominal power factor and adjustable range	> 0.995, adj. ± 0.9 with P_{acr}=20.0 kW, ± 0.8 with max 22.2 kVA	> 0.995, adj. ± 0.9 with P_{acr}=27.6 kW, ± 0.8 with max 30 kVA
Total current harmonic distortion	< 3%	
AC connection type	Screw terminal block, cable gland PG36	
Output protection		
Anti-islanding protection	According to local standard	
Maximum external AC overcurrent protection	50.0 A	63.0 A
Output overvoltage protection - varistor	4	
Output overvoltage protection - plug in modular surge arrester (-S2X version)	4 (Type 2)	
Operating performance		
Maximum efficiency (η_{max})	98.2%	
Weighted efficiency (EURO/CEC)	98.0% / 98.0%	
Feed in power threshold	40 W	
Night consumption	< 0.6 W	

Block diagram of TRIO-20.0/27.6-TL-OUTD

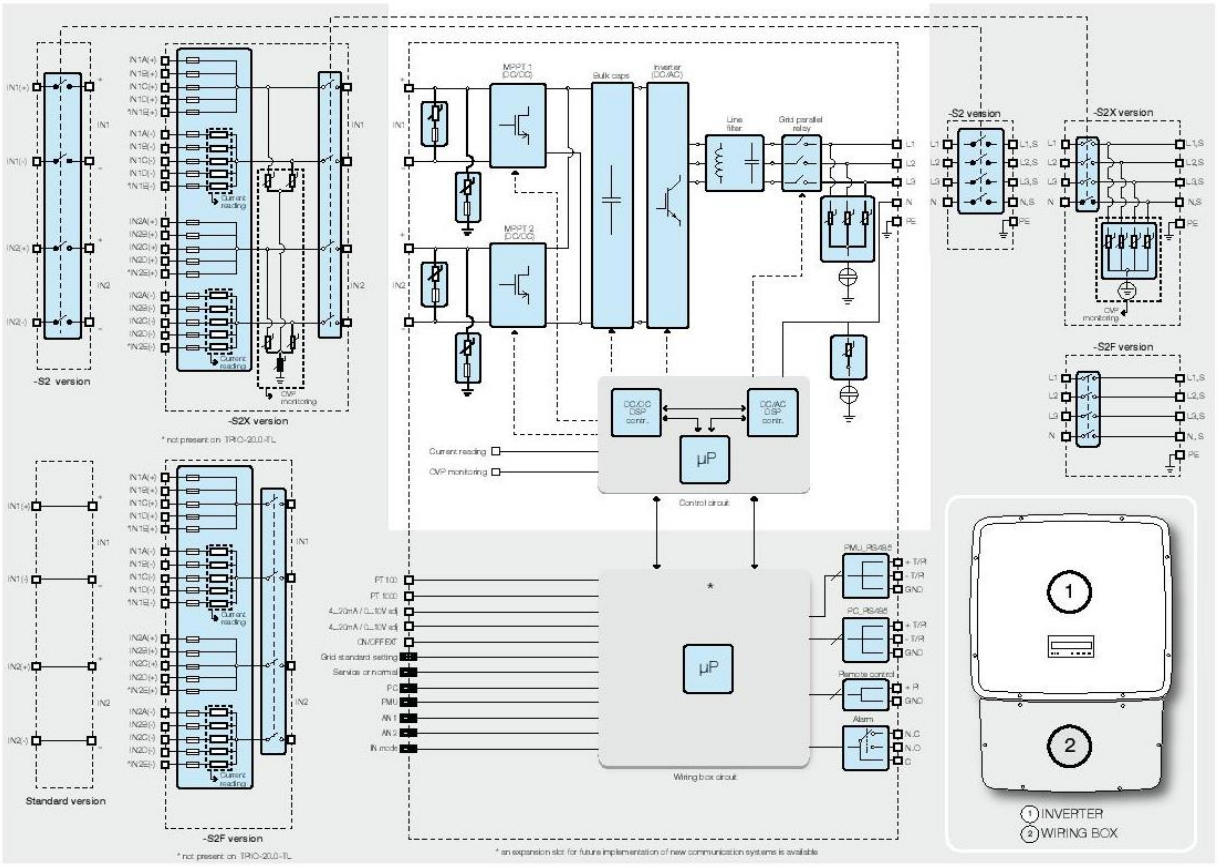

Technical data and types

Type code	TRIO-20.0-TL-OUTD	TRIO-27.6-TL-OUTD
Communication		
Wired local monitoring	PVI-USB-RS232_485 (opt.)	
Remote monitoring	VSN300 Wifi Logger Card (opt.), VSN700 Data Logger (opt.)	
Wireless local monitoring	VSN300 Wifi Logger Card (opt.)	
User interface	Graphic display	
Environmental		
Ambient temperature range	-25...+60°C /-13...140°F with derating above 45°C/113°F	
Relative humidity	0...100% condensing	
Sound pressure level, typical	50 dBA @ 1 m	
Maximum operating altitude without derating	2000 m / 6560 ft	
Physical		
Environmental protection rating	IP65	
Cooling	Natural	
Dimension (H x W x D)	1061 mm x 702 mm x 292 mm / 41.7" x 27.6" x 11.5"	
Weight	< 70.0 kg / 154.3 lbs (Standard version)	< 75.0 kg / 165.4 lbs (Standard version)
Mounting system	Wall bracket	
Safety		
Isolation level	Transformerless	
Marking	CE (50 Hz only), RCM	
Safety and EMC standard	EN 50178, IEC/EN 62109-1, IEC/EN 62109-2, AS/NZS 3100, AS/NZS 60950.1, EN 61000-6-2, EN 61000-6-3, EN 61000-3-11, EN 61000-3-12	
Grid standard (check your sales channel for availability)	CEI 0-21, CEI 0-16, DIN V VDE V 0126-1-1, VDE-AR-N 4105, G59/3, C10/11, EN 50438 (not for all national appendices), RD 1699, RD 413, RD 661, P.O. 12.3, AS 4777, BDEW, NRS-097-2-1, MEA, IEC 61727, IEC 62116, Ordinul 30/2013, VFR 2014	
Available products variants		
Standard	TRIO-20.0-TL-OUTD-400	TRIO-27.6-TL-OUTD-400
With DC+AC switch	TRIO-20.0-TL-OUTD-S2-400	TRIO-27.6-TL-OUTD-S2-400
With DC+AC switch and fuse	TRIO-20.0-TL-OUTD-S2F-400	TRIO-27.6-TL-OUTD-S2F-400
With DC+AC switch, fuse and surge arrester	TRIO-20.0-TL-OUTD-S2X-400	TRIO-27.6-TL-OUTD-S2X-400
With DC+AC switch, fuse and 1 DC surge arrester Type 1 + 2	TRIO-20.0-TL-OUTD-S1J-400	TRIO-27.6-TL-OUTD-S1J-400
With DC+AC switch, fuse and 2 DC surge arrester Type 1 + 2	TRIO-20.0-TL-OUTD-S2J-400	TRIO-27.6-TL-OUTD-S2J-400

[1] The AC voltage range may vary depending on specific country grid standard
[2] The Frequency range may vary depending on specific country grid standard
[3] Please refer to the document "String inverters – Product manual appendix" available at www.abb.com/solarinverters for information on the quick-fit connector brand and model used in the inverter
[4] Limited to 20000 W for Germany
[5] Limited to 27600 W for Germany

Remark. Features not specifically listed in the present data sheet are not included in the product

Appendix D: Battery Bank Datasheet

SIND 04 2145 is the implemented battery in the system and it is manufactures by Trojan Battery company [60].

Trojan BATTERY COMPANY

DATA SHEET

SOLAR
TRUE DEEP-CYCLE INDUSTRIAL

MODEL	**SIND 04 2145**
VOLTAGE	**4V**
CAPACITY	**2145Ah @ 100Hr**
MATERIAL	**Polypropylene** (internal cell container) **Polyethylene** (outer container)
DIMENSIONS	**Inches (mm)**
BATTERY	**Deep-Cycle Flooded/Advanced Lead Acid Battery**
COLOR	**Maroon**
WATERING	**Single-Point Watering Kit (Optional)**
PRODUCT HIGHLIGHTS	**Smart Carbon™ for Improved Performance** **17 Years Battery Life Based on IEC 61427**

PRODUCT + PHYSICAL SPECIFICATIONS

Model	Terminal Type [D]	Dimensions [B] Inches (mm)			Weight [E] Lbs. (kg)	HydroLink or SPWK	Handles
		Length	Width	Height [C]			
SIND 04 2145	14	27.22 (691)	10.44 (265)	24.01 (610))	465 (211)	SPWK	Molded

ELECTRICAL SPECIFICATIONS

Voltage	Capacity [A] Amp-Hours (Ah)					Energy (kWh)
	10-Hr	20-Hr	48-Hr	72-Hr	100-Hr	100-Hr
4V	1474	1647	1896	2030	2145	8.58

CHARGING INSTRUCTIONS

Charger Voltage Settings (at 77°F/25°C)			
System Voltage	12V	24V	48V
Maximum Charge Current (% of C_{20} Rate)*	13%		
Maximum Absorption Phase Time (hours)	4		
Absorption Voltage **	14.40	28.80	57.60
Float Voltage	13.50	27.00	54.00
Equalization Voltage	16.20	32.40	64.80

Do not install or charge batteries in a sealed or non-ventilated compartment. Constant under or overcharging will damage the battery and shorten its life as with any battery.
*If charging time is limited contact Trojan Technical Support for assistance.
**In cases where controller has a bulk voltage setting, use absorption voltage setting above.